4ème Ligne de Lumière CRG-FAME à l'ESRF

Sommaire

Résumé

Cette année a été marquée par l'audit de la ligne (BeamLine Review Panel) par un comité scientifique désignée par l'ESRF. Celui-ci a été pour nous l'occasion de faire un premier bilan de l'activité scientifique de la ligne, 3 ans après son ouverture, ainsi que des développements techniques réalisés. Un document de synthèse a été rédigé dans ce sens. Dans ses conclusions (jointes dans ce rapport), le comité souligne la qualité du nouvel appareillage, ainsi que l'importance des développements techniques en cours (micro-focalisation, cristaux analyseurs et renouvellement de l'électronique du détecteur de fluorescence).

La qualité scientifique et technique de la ligne est mise en avant par les 19 publications, 10 actes de colloques et 23 communications orales pour 2004 et 2005. La demande croissante en temps faisceau (+6% en 2005 par rapport à 2004, +44% par rapport à 2003) est également symptomatique de ce bon fonctionnement. Deux exemples scientifiques sont mis en exergue, dans le domaine des sciences de l'univers (I. Martinez et al.) domaine de recherche représentant plus de la moitié environ des activités de la ligne et de la biologie moléculaire (P. D'Angelo et al., highlight ESRF 2005).

Les demandes d'investissement pour 2006 visent toutes à continuer l'amélioration technique de la ligne et plus particulièrement la stabilité de la ligne et le mode de détection. Le remplacement d'une vanne pneumatique sur la conduite générale d'azote liquide en 2005 nous a obligés à différer deux opérations prévues: Le remplacement du bloc support du 1er

cristal du monochromateur par un pont thermique plus rigide pour améliorer encore l'amortissement des vibrations éventuelles et l'équipement d'une boite à gant. Cette dernière opération est à présent caduque, la boite à gant n'existant plus.

L'électronique analogique du détecteur nécessite des frais (réparations de cartes électroniques) et n'est pas complètement adapté pour la future station de micro-faisceau. Nous avons donc, comme l'année passée, déposé une demande de financement dans le cadre des mi-lourds CNRS-SDU, pour une électronique numérique de type XIA (identique à celles opérationnelles sur les lignes BM29, ID26, BM01 de l'ESRF et la ligne µfaisceau 10.3.2 de l'ALS).

Le projet micro-faisceau est largement dans sa phase terminale, la partie optique est terminée, il reste à finaliser l'environnement échantillon : un état des lieux du projet est présenté ici. Les premières expériences acceptées via le comité de programme CRG sont programmées mi Mars 2006.

Un autre projet nous tient particulièrement à coeur pour 2006, la réitération de l'organisation d'une formation pour les utilisateurs de la ligne, FAME+ (Formation en Absorption X pour la Maîtrise de l'Expérience et le Pilotage d'une Ligne Utilisant un Synchrotron). Un dossier a été monté dans ce sens avec la formation permanente du CNRS.

Côté personnel, Hervé Palancher post-doc du CEA/Cadarache a rejoint l'équipe en janvier 2005. Vivian Nassif (post-doc CEA/Grenoble) termine son post doc début juin 2005. Jean-Jacques Menthonnex est parti en retraite en septembre 2005. Son remplacement via un poste Noémi ne sera effectif qu'à partir de septembre 2005. Ce manque de personnel est difficile à gérer, il est impératif afin de ne pas handicaper le fonctionnement de la ligne de consolider cette équipe. L'attribution d'un post doc « récurent » (ou d'un poste permanent) serait le bien venu.

1. Statistiques

Répartition du temps de faisceau sur FAME en 2005

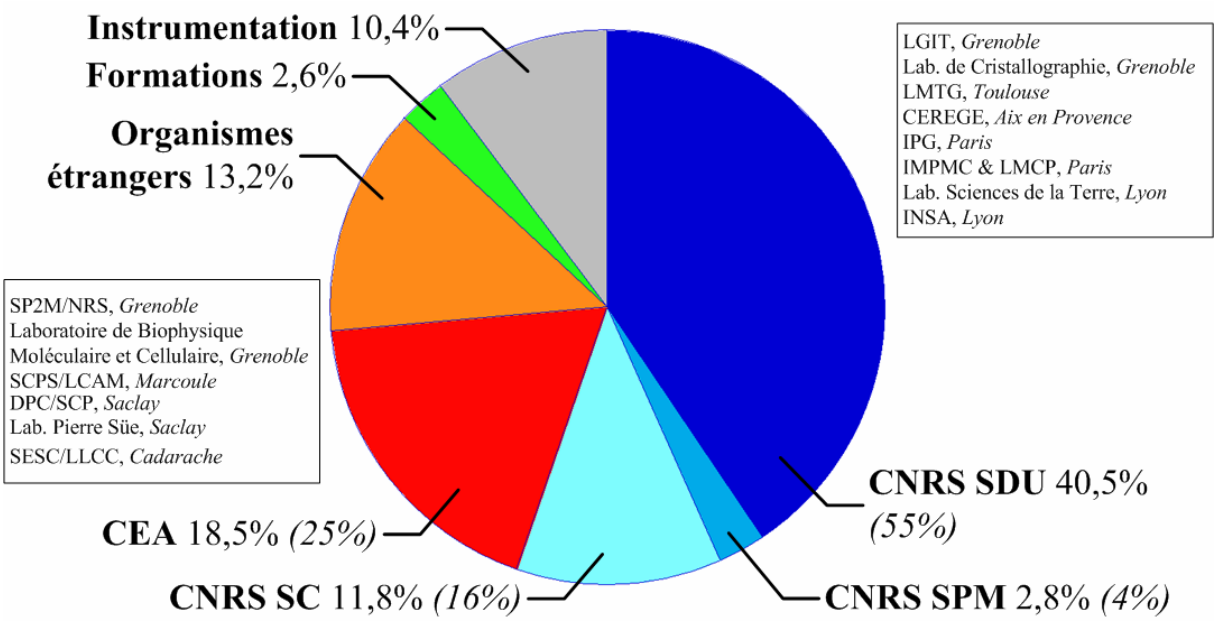

Figure 1 : Répartition du temps de faisceau sur la ligne FAME pour l'année 2005 (comités de programme CRG et ESRF, instrumentation et enseignement). En italique : répartition en ne considérant que les différents départements du CNRS et le CEA.

Evolution de l'attribution et des demandes de temps de faisceau :

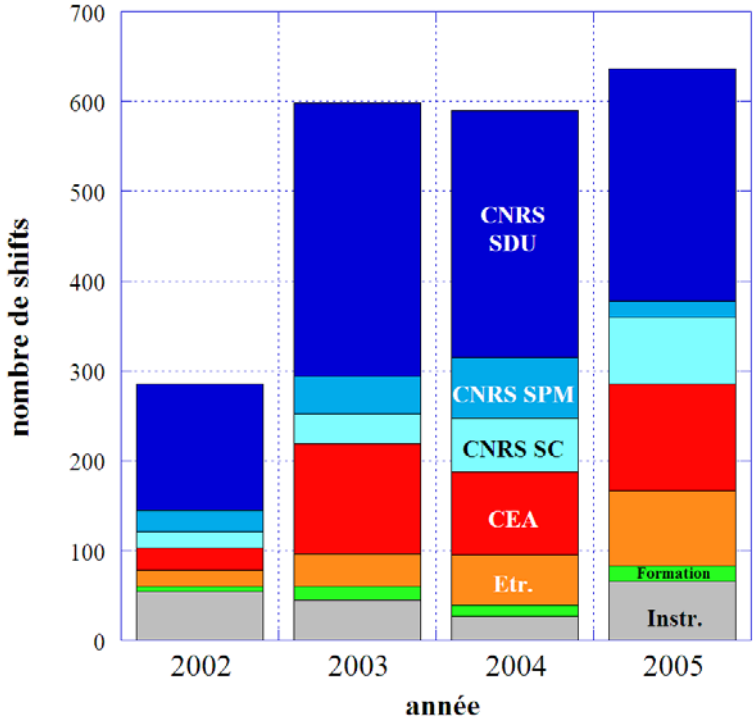

Figure 2 : Evolution de la répartition du temps de faisceau sur la ligne FAME entre 2002 et 2005 en fonction des organismes de recherche

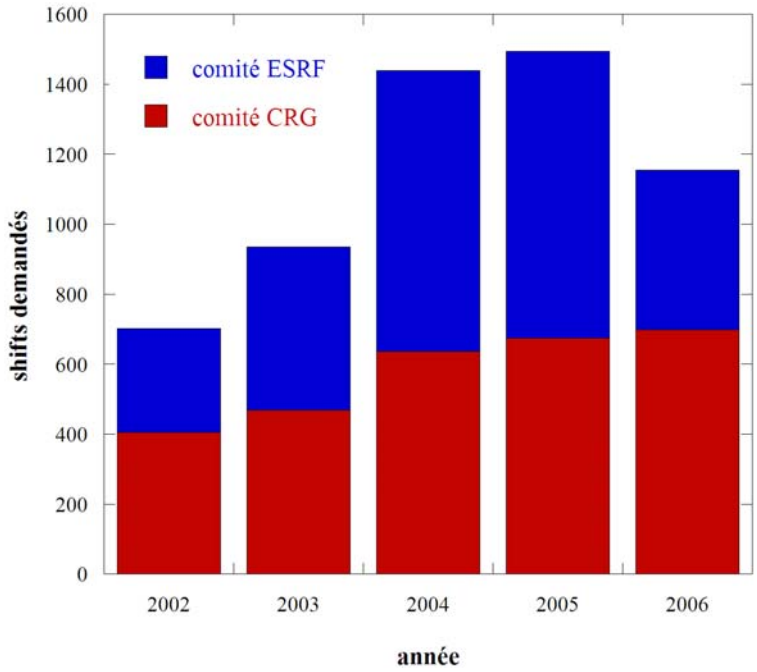

Figure 3 : Evolution des shifts demandés aux différents comités, CRG et ESRF (pour 2006, uniquement le 1er semestre)

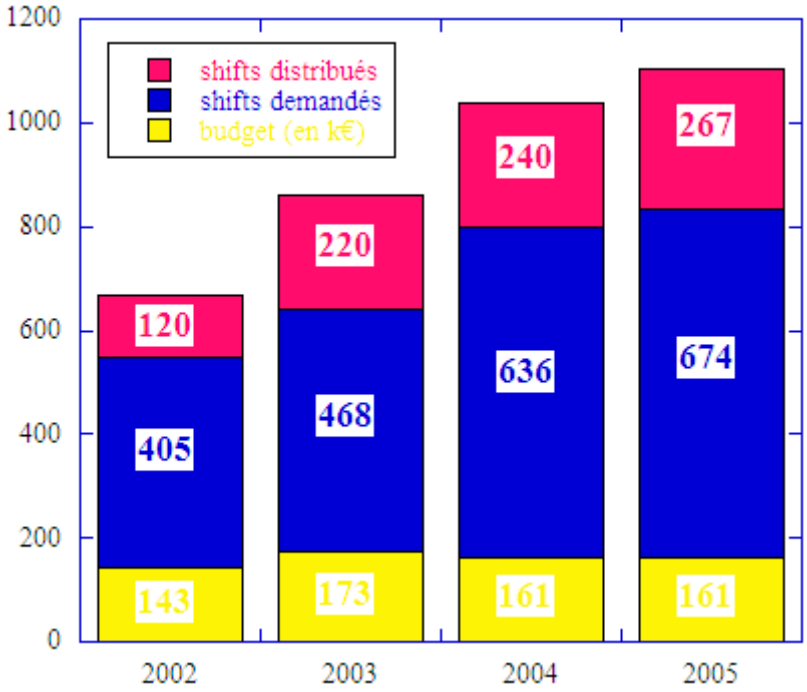

Figure 4 : Evolutions du budget (en k€) et du nombre de shifts demandés et distribués par le comité CRG français

2. Rapport du BeamLine Review Panel ESRF

Report on BM30B/FAME May 17-18, 2005

This project was started in 1999, the beamline designed, constructed and commissioned by 2002 and commenced with scheduled users in September of that year. Dedicated to EXAFS and XANES, the scientific programme on FAME has concentrated on Environmental and Earth Sciences, Physics, Catalysis and Biology during the last two and half years. During this time the support team has been set up, comprising five permanent employees and two post-doc researchers employed by CNRS and CEA. Originally the technical emphasis of FAME was directed at determining atomic environments of elements at very low concentrations in natural systems. Subsequently the beamline operations have been streamlined and made very efficient to accommodate a wide range of other measurements and versatile experiments, of which more than half now involve in situ environment stages (cryostat, HP and HT cells, catalyst rigs etc). An extensive user manual has been produced and formal training sessions for users set up. Our impression is that FAME has developed into a very reliable and user-friendly facility offering a very stable focussed beam from 4 to 22 keV, with unfocussed beams available to 40 keV. For X-ray spectroscopy this encompasses most of the periodic table relevant to environmental and biological science and with the X-ray detectors available concentrations that are realistic. Finally we note that the user community has developed from researchers mainly from the Grenoble region to now include the majority of French groups in environmental and earth science, reflecting the objectives of the original funding from CNRS, CEA and the Rhône-Alpes Region.

Research by Users

Since it was established in 2002, FAME has attracted an extensive range of science. We are particularly impressed by the work on heavy metals, their speciation, toxicity and remediation. In the process they have developed a powerful finger printing methodology for analysing complex mineralogical and biological systems from a X-ray spectroscopy data bank of model systems. This has been applied to contaminated sediments, soil-root systems, ground waters, colloids, cements, slags and ash. Across this wide portfolio there is also an imaginative integration of approaches from the molecular scale to the macroscopic level encountered in environmental hazards. We highlight the phytoremediation of metal polluted soils by Sarret (LGIT) and the microbial

sequestration of As in Bangladesh rivers and groundwaters by Rose (CEREGE), both benefiting from the very stable EXAFS conditions on FAME. The work of Arcovito (Stockholm) and Della Longa (L'Aquila) on photolyzation of myoglobin systems has exploited the ultra dilute capability of the CRG in resolving subtle conformational changes from high quality XANES spectroscopy.

Elsewhere in the areas of nuclear fuel, catalysis etc we judge that the experiments developed so far are of high standard.

Research by Staff

The panel found the work by Hazemann on supercritical liquids and the precipitation from solutions under these extreme conditions outstanding. On the one hand the engineering of HP/HT cells with spherical Be windows has resulted in reliable operation under these taxing conditions, which is typical of the high level of technical developments on FAME. On the other hand the performance of the XAFS facilities has meant that very precise analysis has been possible of density, solubility, transport properties and the extraction of metals with implications for ore deposits and pollution containment. This pioneering work has attracted groups from France (Toulouse, Lyon, Paris) and more recently Australia, a good example of the enlargement of the user base but which is currently inhibited by present staffing levels.

Overall we consider the average activity is high and that the technical developments are in many cases exceptional. Nevertheless we recommend:

- the successful technical networking established between FAME and local laboratories, including the ESRF be further developed

- with the maturation of the beamline attention be given to increasing publications from FAME which do not in our view reflect the scientific success of this attractive beamline

Technical Status of the Beamline

This new beamline has benefited from improvements in X-ray optics, detector design and beamline control. Despite this we consider that the FAME team has achieved more than best practice for a 3rd generation source and has delivered a first rate XAFS facility well-suited to the environmental and earth science community in particular. The introduction of a user training programme is applauded, as is the creation of a comprehensive user manual.

Future Technical Developments

Given that this is a new beamline with excellent performance, it is good to see a programme developing for refining the beam optics and X-ray detection to meet future scientific challenges. In particular we strongly support the following initiatives:

- incorporation of digital electronics into the 30 element Ge fluorescence detector system. This will enhance the count rate by a factor 3 and create a unique capability at the ESRF.

- development of a microfocus KB mirror assembly to perform EXAFS for energies 4 – 22 keV with a spatial resolution of 20 x 20 μm^2 which is a pre-requisite for analysis using diamond anvil cells and other HP/HT devices.

- implementation of spherically bent analyser for selection of fluorescence of minority species with an energy resolution of 20 eV, sufficient to remove unwanted Compton Scattering and fluorescence contamination from host matrix.

Future Scientific Directions

Whilst the current scientific programme is positively organised and very productive in the first 2 to 3 years of user operation, we suggest that FAME may encounter challenge in remaining leading-edge if attention is not paid to prioritisation and identification of future opportunities.

- We think that the whole field of supercritical systems is a bourgeoning area, not just for earth science applications but in enriching fundamental physics and chemistry of heterogeneous complex systems involving liquids. With the technical lead that they have established we believe that FAME is now well-placed to become a scientific reference in this field. For this they are encouraged to establish this as a new theme for FAME, in addition to environmental science. For this they will need to strengthen their collaborations and dedicated manpower in this area.

- Similar experimental arrangements and tools could also be harnessed to explore the diversity of micro organisms in extreme environments. The ability to record XAFS at very dilute levels, detect density and chemical environment in living systems, coupled with the facility of robust environment stages capable of controlling and changing pH, T, P, redox, salinity etc we believe will give FAME an international advantage in this exciting field. We also recognise that this should pay dividends in future environmental science applications.

Staff

We recognise that huge efforts have been made by the existing FAME team since 2002 but that the future success of this beamline will require some additional support.

We recommend that:

- The engineer due to retire is automatically replaced to support electronics and computing
- an additional scientist is recruited to assist in promoting the scientific potential of the FAME beamline

Summary of Recommendations

From this strong and successful initial phase of FAME we would recommend:

- they build on the environmental studies and in situ experiments to extend the visibility of FAME to a wider community
- they take the opportunity to enlarge the user community of FAME to other non-French research groups making use of the special developments made in the robust monochromator and detector design
- consideration be given to the level of in-house support. Currently there are two dedicated staff for scientific and technical assistance which we consider insufficient to fully exploit the scientific capabilities of FAME

Settimio Mobilio

Pascal Philippot

Guillaume Fiquet

Neville Greaves

G Schneider, G Fiquet, R Fourme, JP Samama, C Schulze Briese, C Nave, N Greaves, S Mobilio, P Philippot

3. Exemples scientifiques

Une présentation plus détaillée des résultats des expériences est résumée dans les rapports d'expérience joints en annexe et les articles de la ligne regroupés dans la bibliographie.

Iron speciation in high pressure high temperature H_2O-CO_2 fluids in contact with crystalline siderite and /or magnetite

Martinez I.[1], Testemale D.[2,3], Dufaud F.[1], Hazemann J.L.[2] and Guyot F.[4]

1. Institut de Physique du Globe, CNRS, Paris ; 2. Lab. de Cristallographie, CNRS, Grenoble ; 3. SNBL/ESRF ; 4. Dep. de Mineralogie, IMPMC et IPGP

Geological context

We have carried out a first series of experiments to study the reactivity of $FeCO_3$ (siderite) in water under acidic conditions up to 1000 bar and 300°C, according to reaction:

$$(1)\ FeCO_3 + 2\ H^+ \rightarrow Fe^{2+} + H_2O + CO_2$$

In deep geological storage context, the quantity of CO_2 that cannot be sequestred as carbonate is directly related to the concentration of Fe^{2+} in the fluid. We have measured, for the first time under hydrothermal conditions, the dissolution of siderite in water by monitoring *in situ* the concentration of Fe^{2+} at different pressures, temperatures and pH. First data on Fe speciation in the relevant fluids have also been recorded.

Experimental details

HP/HT XAFS spectroscopy analyses were performed at the Fe K-edge, using an X-ray cell developed at the Lab. de Cristallographie (Grenoble). A total of six experiments were performed: **(a)** $FeCl_2$ (0.05M) + HCl (0.1M), **(b)** $FeCl_2$ (0.05M) + HCl (0.1 M) + NaCl (1M), **(c)** $FeCl_2$ (0.05M) + oxalic acid (0.05 M) used as a source of CO_2 above 150°C, **(d)** siderite + HCl (0.1M), **(e)** siderite + HCl (0.1 M) + NaCl (1M), **(f)** siderite + oxalic acid (0.05 M).
In each experiment, data were obtained at different temperatures along isobars up to 300°C and 1000 bar.

Results

The experiments with $FeCl_2$ provide reference data for both Fe^{2+} concentration and speciation in solutions under HP/HT: in fig. 1, there is a clear temperature dependence of the Fe local solvation structure The presence of NaCl (1M) was shown to have no major effect on speciation.

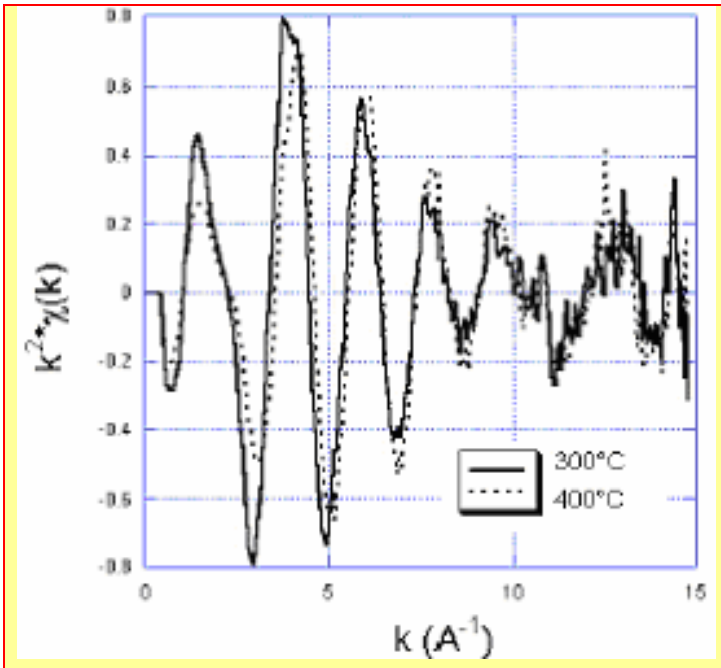

Figure 1: EXAFS oscillations of 0.05M $FeCl_2$ solutions at 300 bar (300 and 400°C).

The solubility results can be adequately fitted with available thermodynamical data, providing that the specific heats of compounds involved in reaction (1) be adjusted. Precise refinements on solubility data could further provide important constraints on thermodynamic parameters of reaction (1). In

particular, a tentative increase in solubility of siderite, unexpected for carbonates, that was measured between 100°C and 300°C (fig. 2) can be modelled with an adequate set of specific heats.

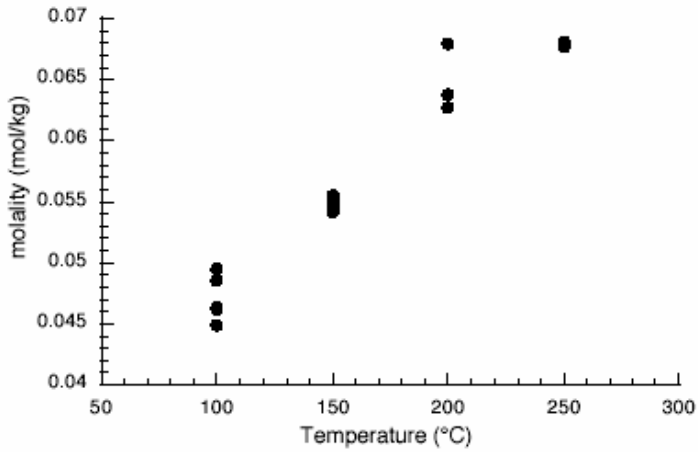

Figure 2: $FeCl_2$. Evolution of Fe^{2+} concentration in the fluid at 300bars as a function of temperature

The kinetics of siderite dissolution in HCl (0.1 M) was determined at 300 bar and 100°C. NaCl apparently decreased the dissolution of siderite, a behaviour which remains to be explained using thermodynamical parameters and a fine analysis of the spectroscopic data on Fe speciation in the fluid. In the case of dissolution of siderite in oxalic acid solutions, two regimes should be considered: (1) a low temperature regime (T<150°C,) below decomposition temperature of oxalic acid, where dissolution is lower than in HCl solutions at the same conditions (at 100°C, a concentration of 9mMol of Fe^{2+} is measured compared to 30mMol in HCl solutions); (2) a high temperature regime (T>200°C) where a decrease of solubility is observed (<4mMol at 250°C). This decrease can be attributed to the presence of CO_2 which is a weaker acid than oxalic acid.

Perspectives

These first results are encouraging. Longer acquisition time spectra would be important for determining the exact speciation of Fe^{2+} in those H_2O-CO_2-Cl fluids. It would be desirable to better control the activity of CO_2 which is a key parameter in the dissolution reaction. The use of oxalic acid decomposition as a source of CO_2 is a limiting factor because of the equivalent low partial pressure of CO_2 available (we estimate a maximum PCO_2 of 3 bar in our experiments). A direct loading of CO_2/H_2O mixtures at ambient temperature would be a good method to control and vary this parameter, essential for appropriate modelling of these reactions.

References

Martinez I., Testemale D., F. Dufaud, F. Guyot and J.L. Hazemann, “Experimental study of dissolution of siderite in high pressure high temperature H_2O-CO_2 fluids with implications for geological storage of CO_2” *European Geosciences Union*, General Assembly, Vienna, Austria, (24-29 Avril 2005), *Geophysical Research Abstracts*, 7 (2005) 09226

Testemale D., F. Dufaud, I. Martinez, F. Guyot and J.L. Hazemann, “Speciation of iron in high pressure high temperature H_2O-CO_2 fluids” *European Geosciences Union*, General Assembly, Vienna, Austria, (24-29 April 2005), *Geophysical Research Abstracts*, **7** (2005) 09447

X-ray absorption studies on the N-terminal copper-binding region of *Haemophilus ducreyi* Cu,Zn superoxide dismutase

D'Angelo P.[1], Pacello F.[2], Mancini G.[1], Proux O.[3], Hazemann J.-L.[4], Desideri A.[2,5] and Battistoni A.[2,5]

1 Dep. of Chemistry, University "La Sapienza", Rome; 2 Dep. of Biology, University of Rome Tor Vergata; 3 LGIT, CNRS-Grenoble; 4 Lab. de Cristallographie, CNRS-Grenoble; 5 INFM, University of Rome Tor Vergata

Copper is an essential element for all aerobic organisms which incorporate this metal ion in several important enzymes. One of these enzymes is Cu,Zn superoxide dismutase (Cu,ZnSOD), which protects cells from the toxic effects of reactive oxygen intermediates by converting the superoxide radical into hydrogen peroxide and molecular oxygen. In bacteria Cu,ZnSOD is located in extracytoplasmic compartments where it plays an important role in protecting microorganisms from exogenous sources of superoxide. The Cu,ZnSOD from a subset of Gram-negative pathogens possess divalent metal binding N-terminal extensions, which presumably favors the uptake of the enzyme's prosthetic metals in environments where their concentration is very low [1].

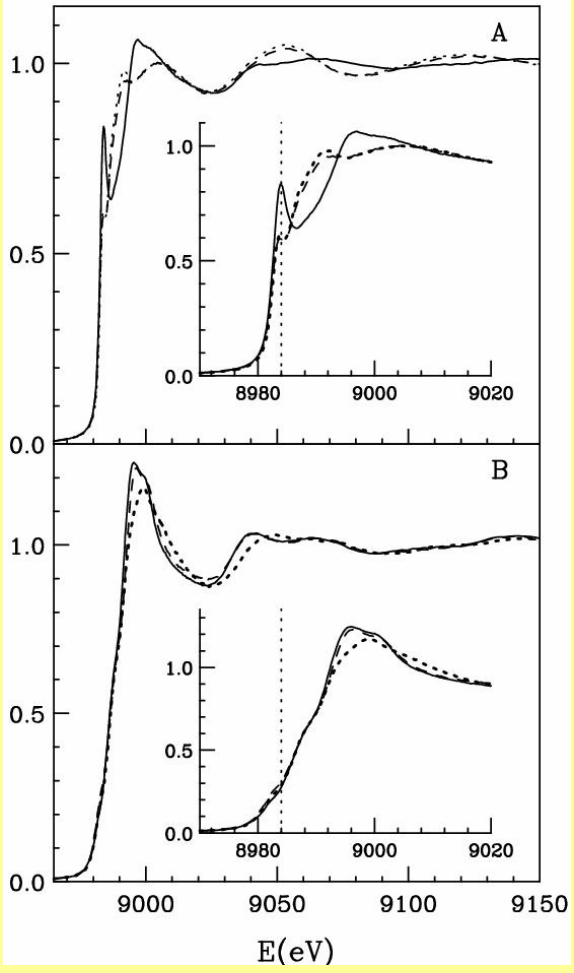

Figure 1: Cu K-edge XANES spectra of Cu(I) and Cu(II) complexes. (A) Cu(I) with Met-rich (dotted line), His-rich (solid line) and an equimolar mixture of the two peptides (dashed line) in water solution. Inset shows the 1s $\rightarrow$4p region. (B) Cu(II) with Met-rich (dotted line), His-rich (solid line) and an equimolar mixture of the two peptides (dashed line) in water solution. Inset shows the 1s $\rightarrow$3d region.

In particular, the N-terminal extension of the Cu,ZnSOD from *Haemophilus ducreyi*, the causative agent of a genital ulcerative disease known as chancroid, shows particularly interesting features (HGDHMHNHDTKMDTMSKDMMSM). The histidine-rich region at the N-terminus of the domain is very similar to the transition metal binding regions already identified in other proteins able to bind Ni, Zn or Cu(II) [1]. In contrast, the second half of the domain contains a methionine-rich sequence which resembles the Cu(I) binding domains observed in several proteins involved in copper homeostasis [2,3]. These observations suggest that the N-terminal domain of *H. ducreyi* Cu,ZnSOD could allow the efficient binding of Cu(II) and Cu(I) at the histidine-rich and methionine-rich sequences, respectively.

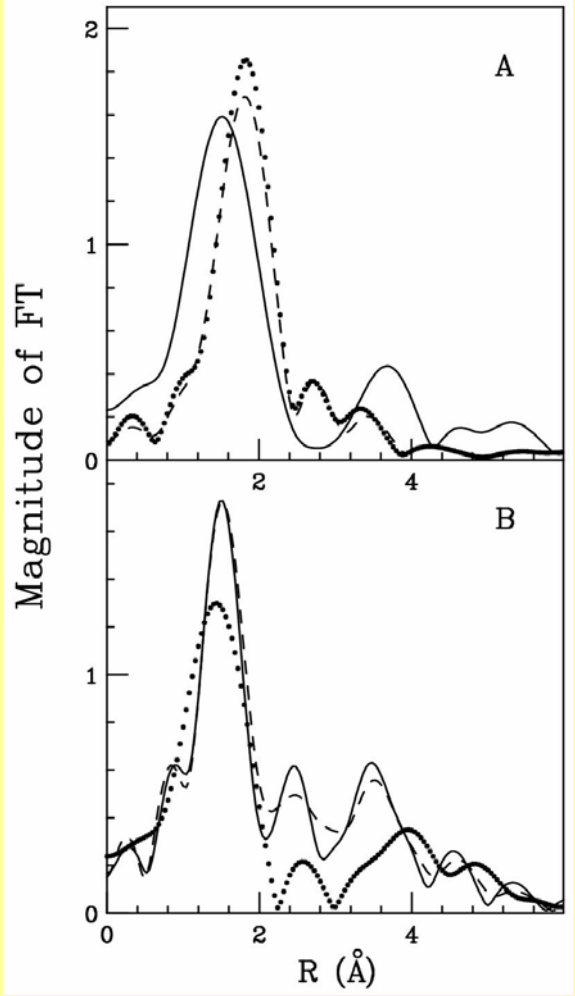

Figure 2: Fourier Transforms of the k^2-weighted EXAFS experimental data. (A) Cu(I) complexes (B) Cu(II) complexes. Data are shown as dotted lines (Met-rich peptide), solid line (His-rich peptide), and dashed line (equimolar mixture of the two peptides).

To test this hypothesis X-ray absorption spectroscopy experiments have been carried out on peptides corresponding to the two metal binding regions [4]. Cu K-edge XAS spectra were collected in fluorescence mode on samples with Cu concentrations of 2.5 and 1.25 mM. Our results indicate that both sequences can bind either Cu(II) or Cu(I) (Fig. 1). However, competition experiments demonstrate that Cu(II) is preferred by histidine residues belonging to the first half of the motif, while the methionine-rich region preferentially binds Cu(I) via the interaction with three methionine sulfur atoms (Fig. 2).
These findings demonstrate that the N-terminal domain of H. ducreyi Cu,ZnSOD is an unusual metal trapping peptide able to bind Cu(I) or Cu(II) at different sites, possibly favouring an efficient copper uptake under copper starvation. Moreover, alterations in the copper coordination environment mediated by changes in the copper redox state could play a role in favoring metal transfer from the N-terminal domain to the active site.

[1] Battistoni, A. *et al*., "A histidine-rich metal binding domain at the N terminus of Cu,Zn-superoxide dismutases from pathogenic bacteria: a novel strategy for metal chaperoning". *J. Biol. Chem*. **276**, 30315-30325 (2001)
[2] Huffman, D.L. *et al.*, "ENDOR Spectroscopy of Cu(II)-PcoC and the Multicopper Oxidase Function of PcoA, Two Essential Components of the pco Copper Resistance Operon in Escherichia coli" *Biochemistry*, **41**, 31, 10046-10055 (2002)
[3] Peariso, K., Huffman, D.L., Penner-Hahn, J.E., and O'Halloran, T.V. "The PcoC Copper Resistance Protein Coordinates Cu(I) via Novel S-Methionine Interactions" *J. Amer. Chem. Soc*, **125** n°2, 342-343 (2003)
[4] D'Angelo P., Pacello F., Mancini G., Proux O., Hazemann J.L., Desideri A. and Battistoni A., "X-ray absorption investigation of a unique protein domain able to bind both Cu(I) and Cu(II) at adjacent sites of the N-terminus of Haemophilus ducreyi Cu,Zn superoxide dismutase", *Biochemistry* **44** (2005) 13144-13150

4. Bilan du personnel impliqué dans la gestion de la ligne

Depuis décembre 2004, deux points sont à noter concernant le personnel impliqué sur FAME.

- Hervé Palancher a commencé son stage post-doctoral CEA (DES/SESC, CEA/Cadarache) début 2005. Une partie de son activité consiste à préparer et à accueillir sur FAME les expériences du groupe de Carole Valot, une autre partie consiste en sa participation au projet micro-faisceau,
- Jean-Jacques Menthonnex est en retraite depuis septembre 2005. Son remplacement via un poste NOEMI (CNRS-SDU) sera effectif en août 2006.

En juin 2006, le contrat de Vivian Nassif, post-doc CEA depuis juin 2004, arrivera à échéance, son remplacement ou la création d'un poste fixe est souhaitable.

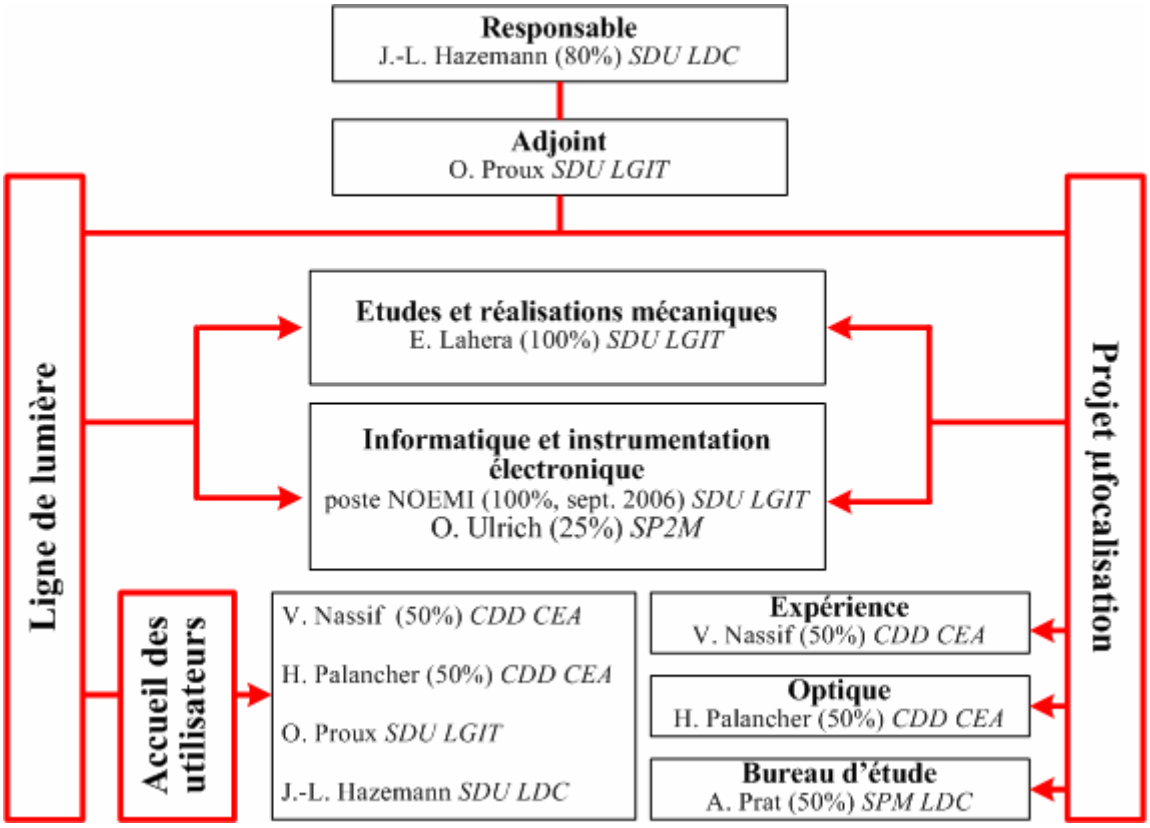

Figure: Organigramme de la ligne FAME

5. Bilan de la formation FAME+ 2005

Au total, 22 personnes ont demandé à suivre la formation. Le nombre de personnes retenues a été limité à 12, de 7 laboratoires différents. X. Cette formation s'est retrouvée programmée en même temps qu'un congrès international majeur de géochimie (*Goldschmidt*, USA) auquel bon nombre d'utilisateurs de FAME, donc de stagiaires potentiels, participaient. Un formulaire rempli par 11 stagiaires sur 12 permet de tracer quelques grandes lignes sur leur profil, leurs besoins, attentes, avis sur la formation... en complément de l'évaluation orale de celle-ci réalisée à la fin de la 2ème journée.

<table>
<tr><th></th><th>Jeudi 19 mai</th><th>Vendredi 20 mai</th><th>Samedi 21 mai</th></tr>
<tr><td>9h00-9h30</td><td colspan="2">Accueil</td><td colspan="2">PSS training</td><td rowspan="2">Calculs XANES</td><td rowspan="3">Réglage de la ligne</td></tr>
<tr><td>9h30-10h00</td><td colspan="2" rowspan="2">Généralités sur l'optique</td><td rowspan="3">Réglage de la ligne</td></tr>
<tr><td>10h00-10h30</td></tr>
<tr><td>10h30-11h00</td><td colspan="2">Pause</td><td colspan="2">Pause</td><td>Pause</td></tr>
<tr><td>11h00-11h30</td><td colspan="2">Introduction au TD XANES</td><td rowspan="3">Réglage de la ligne</td><td rowspan="3">Calculs XANES</td><td rowspan="3">Réglage de la ligne</td></tr>
<tr><td>11h30-12h00</td><td colspan="2" rowspan="2">Introduction au pilotage de la ligne</td></tr>
<tr><td>12h00-12h30</td></tr>
<tr><td>12h30-14h00</td><td colspan="2">Pause déjeuner
Salle de réception cantine H2</td><td colspan="2">Pause déjeuner
Salle de réception cantine H2</td><td>Pause déjeuner
Cantine ESRF</td></tr>
<tr><td>14h00-14h30</td><td rowspan="3">Calculs XANES</td><td>PSS training</td><td colspan="2">Choix des détecteurs</td><td rowspan="6"></td></tr>
<tr><td>14h30-15h00</td><td rowspan="3">Réglage de la ligne</td><td colspan="2" rowspan="2">Comment marche un détecteur ?</td></tr>
<tr><td>15h00-15h30</td></tr>
<tr><td>15h30-16h00</td><td colspan="2">Pause</td><td colspan="2">Evaluation de la formation</td></tr>
<tr><td>16h00-16h30</td><td rowspan="3">Calculs XANES</td><td rowspan="3">Réglage de la ligne</td><td>Réglage des détecteurs</td><td>Cryostat</td></tr>
<tr><td>16h30-17h00</td><td rowspan="2">Cryostat</td><td rowspan="2">Réglage des détecteurs</td></tr>
<tr><td>17h00-17h30</td></tr>
<tr><td>17h30-18h00</td><td colspan="2"></td><td colspan="2"></td><td></td></tr>
</table>

Leurs profils. Un seul des stagiaires avait déjà effectué des calculs XANES. 1/4 d'entre eux seulement (3 doctorants) n'avait jamais fait d'expériences d'Absorption X ; dans la suite, nous avons identifié leurs réponses sous la dénomination "débutant". Pour bon nombre d'entre eux, leur but principal est d'acquérir de l'autonomie en ce qui concerne le pilotage de la ligne, d'apprendre le fonctionnement des différents constituants d'une ligne de lumière pour mieux appréhender les expériences à venir sur la ligne.

Adéquation de la formation. La formation répond visiblement très bien aux niveaux et aux besoins des stagiaires, les débutants étant plus réservés sur leur niveau.

Cours généraux. Les stagiaires ont été en très grande majorité tout à fait intéressés par les cours généraux, jusqu'à 100% pour l'introduction aux calculs XANES. Les avis les plus partagés (toutes proportions gardées), pour le pilotage de la ligne et pour le fonctionnement des détecteurs, sont surtout le fruit des stagiaires débutants. Ces cours ont lieu avant l'approche pratique sur la ligne: ceci explique peut-être cela. La description du fonctionnement informatique et électronique des constituants de la ligne demeure en effet assez ardue, et il est sans doute plus difficile de s'y intéresser lorsque l'on ne voit pas clairement dans quel cadre cela s'insère concrètement.

Travaux pratiques. Les stagiaires ont été en très grande majorité tout à fait intéressés par les travaux pratiques, que ce soit le réglage de la ligne (100%), du détecteur de fluorescence (80%), le fonctionnement du cryostat (80%) et les calculs XANES (80%), les 20% restants étant dans le camp des "plutôt oui". Cet intérêt transparaissait effectivement pendant les travaux pratiques, les stagiaires étant dans l'ensemble dynamique, n'hésitant pas à poser des questions...

Nombre de participants. Le nombre de participants par demi-groupe (6) est jugé globalement correct, un peu élevé pour les deux travaux pratiques sur la ligne pour 20% des réponses. Il est clair que pour

la ligne, ce nombre, même s'il est globalement correct, est un maximum, autant du point de vue de l'organisation que de l'exiguïté de la salle de contrôle.

Durée idéale de la formation. A cette question, la majorité des stagiaires s'accorde à trouver la durée de la formation un peu trop courte (2,5 jours), le plus grand nombre s'accordant sur une durée idéale de 3 jours. Cette légère augmentation peut-être directement reliée aux demandes de compléments de formation formulées par les stagiaires (*cf.* les conclusions de ce bilan), compléments qui peuvent être ainsi planifiés sans augmentation du volume horaire journalier jugé correct.

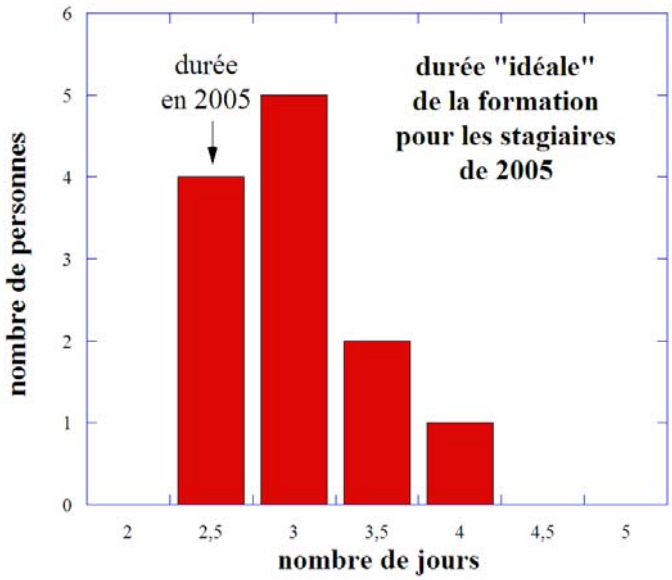

Conclusions

Points forts. L'ensemble des stagiaires a trouvé la formation très satisfaisante, les deux points qui ressortent lors de l'évaluation orale de la formation étant les travaux pratiques sur la ligne et sur les calculs XANES. D'un point de vue pratique, l'hébergement à l'ESRF est jugé idéal pour cette formation.

Il manque... Une demi-journée de plus serait nécessaire pour aborder l'analyse et les simulations EXAFS, comme cela est fait pendant la formation XAS à Montpellier ou pendant les travaux pratiques DEA et HERCULES sur la ligne. D'autres présentations d'outils expérimentaux seraient également une bonne idée, avec éventuellement des travaux pratiques. Les outils demandés sont les appareillages hautes pressions (enclumes diamants et autoclaves) et les fours.

Reconduction de la formation. Le ratio demandes sur places disponibles est proche de 2 pour la formation de 2005. FAME+ a sans problème un "vivier potentiel" pour être reconduite l'an prochain, avec quelques aménagements sur le fond pour répondre aux demandes formulées cette année par les stagiaires et sur la forme pour gommer les petits ratés dans l'organisation en amont (inscriptions non centralisées).

6. Micro-focalisation sur FAME

De plus en plus d'applications nécessitent d'avoir une taille de faisceau sur l'échantillon la plus faible possible. Actuellement, cette taille est de 300 µm en horizontal (focalisation par le 2nd cristal du monochromateur) et de 100 µm en vertical (focalisation par le 2nd miroir). Cette taille peut être malgré tout trop importante dans de nombreux cas. FAME a donc été conçue de manière à intégrer un système optique permettant d'obtenir un « micro-faisceau », soit de 20×20 µm^2, soit de 10x10 µm^2. Des expériences d'absorption X pourront être ainsi réalisées sur de nouveaux types d'échantillons:

- échantillons inhomogènes, nodules, échantillons météoritiques, roches magmatiques et métamorphiques…,
- échantillons très petits, monocristaux « micrométriques », cellules végétales…,
- échantillons dans un environnement spécifique, dans une enclume diamant par exemple (plus la taille du faisceau est petite, plus on peut se permettre de diminuer la taille de diamants au niveau du point d'impact et donc se permettre d'atteindre des pressions élevées).

Les rapports d'expérience, les demandes spécifiques des utilisateurs et l'audit de la ligne réalisé par l'ESRF soulignent la nécessité de cette évolution qui cohabitera avec le montage actuel. Une réorganisation de la cabane d'expérience est prévue à cet effet pour limiter au maximum le temps de réglage.
Le personnel permanent de la ligne (cf. organigramme) est fortement impliqué dans le développement de la micro-focalisation sur FAME. Deux post-doctorants (CEA) ont été recrutés pour permettre l'aboutissement de ce projet, prévu début 2006.

Dans ce rapport, les études de faisabilité technique, le montage développé et finalement le budget de ce projet seront successivement développés.

Validation optique des caractéristiques d'installation d'un système micro-focalisant

Deux séries de tests ont permis de démontrer la faisabilité d'obtenir un micro-faisceau sur FAME :

- en utilisant deux miroirs KB optimisés pour la ligne D15 du LURE, une taille minimale de 19×19µm^2 a été obtenue sans collimater le faisceau incident (en collaboration avec S. Lequien (Lab. Pierre Süe, CEA-Saclay)),
- en utilisant un seul miroir (ID30, ESRF) et en focalisant verticalement la nappe. Pour une ouverture des fentes de 50 µm (50% du flux), la taille obtenue est de 5,8 µm. Pour une ouverture des fentes de 10 µm (10% du flux) la taille chute à 3,6 µm

Ces différentes données nous ont, de plus, permis de définir les conditions d'implantation des miroirs KB et de choisir la divergence interceptée par les miroirs, de manière à garder une taille des éléments optiques raisonnable.

Première expérience EXAFS sur FAME en micro-faisceau

En mai 2005, une série de mesure EXAFS a été effectuée au seuil K du Molybdène (20,0 keV) et L_{III} de l'Uranium (17,166 keV) en focalisant verticalement le faisceau dans les conditions de la 2ème série de tests. Le but de cette expérience test était de se rendre compte si la stabilité de l'optique de la ligne était suffisante pour pouvoir étudier un échantillon fortement inhomogène en micro-faisceau.

Conditions expérimentales

Le montage expérimental (figure 1) intègre, en plus du miroir focalisant précédemment utilisé:

- un microscope optique pour positionner l'échantillon
- le détecteur de fluorescence Canberra 30-éléments
- un porte-échantillon motorisé (X,Z)

Le tableau 1 récapitule les ouvertures des fentes lors de l'expérience. La limitation de l'ouverture horizontale de 50 à 10mm a été dictée par l'importance de la fluorescence L□ de l'Uranium au seuil K du Molybdène. La limitation verticale a quand à elle été imposée par l'acceptance du miroir micro-focalisant. La taille du faisceau ainsi obtenu est de 300×18 µm^2 (HxV, FWHM, fig. 2).

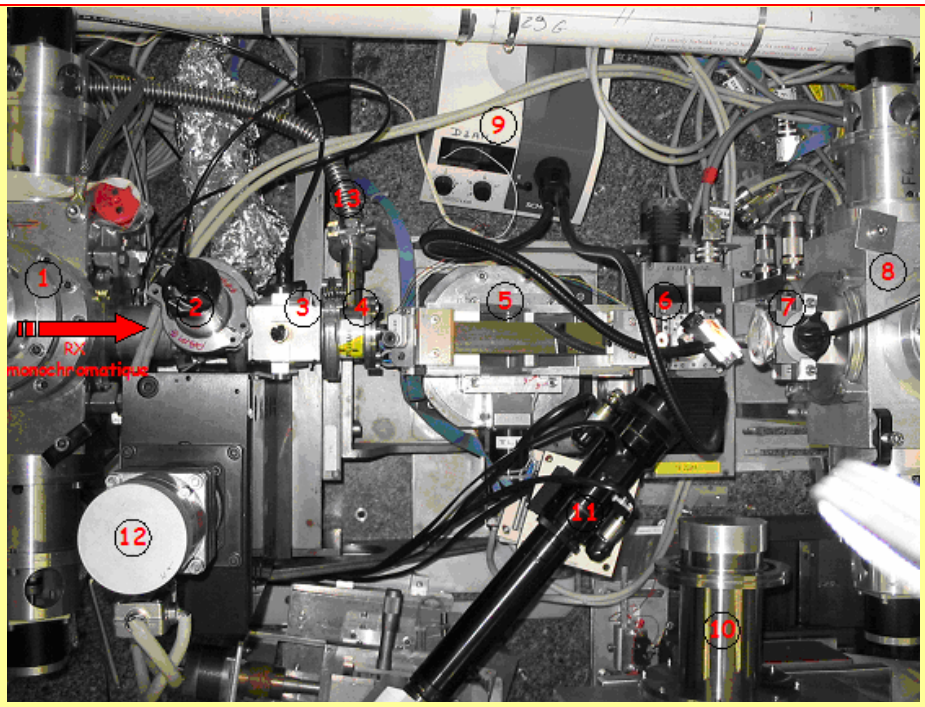

Figure 1: Montage de micro-focalisation verticale sur la table EXAFS[1]. **1** : Fentes 5. **2** : Shutter expérimental. **3** : Diodes en Silicium (I_0). **4** : Fenêtre en Béryllium. **5** : Miroir expérimental, monté sur la tête goniométrique. **6** : Système porte-échantillon. **7** : Diodes en Silicium (I_1). **8** : Fentes 6. **9** : Fibres optiques pour éclairer l'échantillon. **10** : Détecteur Canberra 30 éléments. **11** : Caméra « microscope ». **12** : Motorisation (X,Z) des mouvements du miroir. **13** : Tuyau de pompage du vide.

Direction	Horizontale	Verticale
Ouverture des fentes (mm)	10	0,7
Ouverture maximales des fentes (mm)	50	2,1
Taille de la source secondaire (µm)	300	80
Taille du faisceau sur l'échantillon (µm)	300	18

Tableau 1: paramètres du faisceau

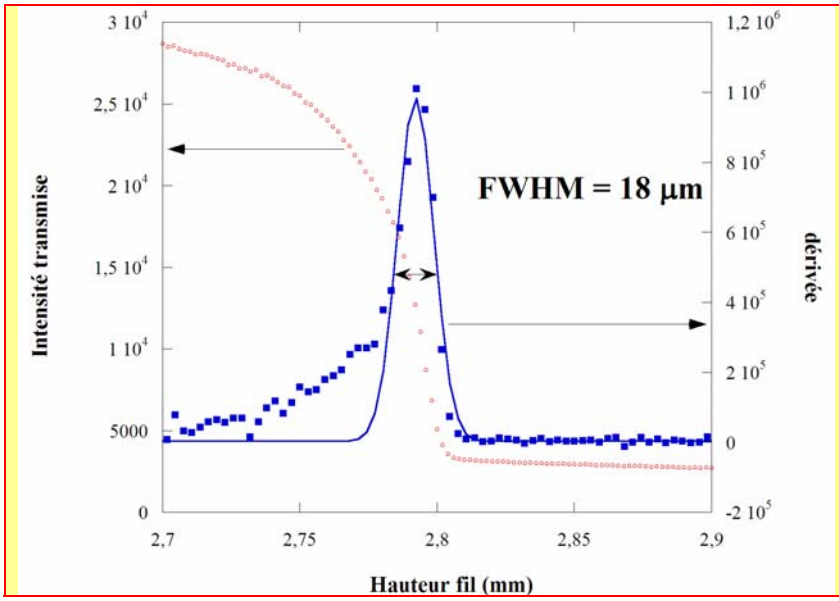

Figure 2: Détermination de la taille verticale du faisceau au niveau de l'échantillon

Positionnement de l'échantillon

[1] Maxime Argoud, "Développement et test d'un micro-faisceau", rapport de stage de fin de 2nde année, DUT Mesures Physiques de Toulouse, Juin 2005

L'optimisation du positionnement vertical de l'échantillon a été effectuée en couplant les images de la caméra microscope aux évolutions des intensités transmise et de fluorescence en fonction de la position (fig. 3).

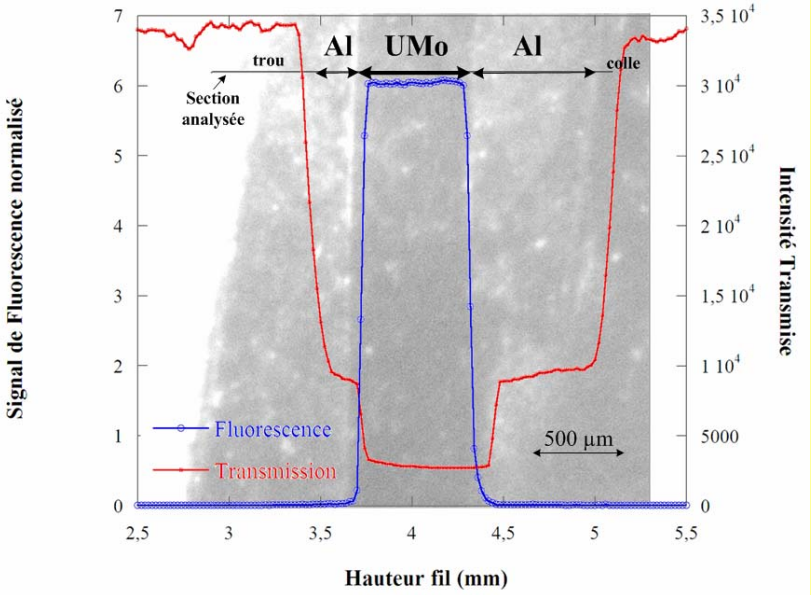

Figure 3: Optimisation de la position verticale de l'échantillon. Comparaison image microscope / profils des signaux mesurés. Echantillon: coupe transverse "sandwich" Al/UMo/Al

Mesures EXAFS

Des coupes transverses de « sandwich » de diffusion ont été étudiées. Dans ces échantillons, une plaque d'alliage Uranium-Molybdène est maintenue entre deux plaques d'aluminium lors d'un recuit qui favorise la croissance d'une couche d'interdiffusion UMo/Al. Dans l'un des sandwichs analysés, deux plaques d'aluminium différentes ont été utilisées (Al A5 et Al 6061). Ainsi, les couches d'inter-diffusion UMo/Al A5 et UMo/Al 6061 pouvaient présenter des compositions différentes.

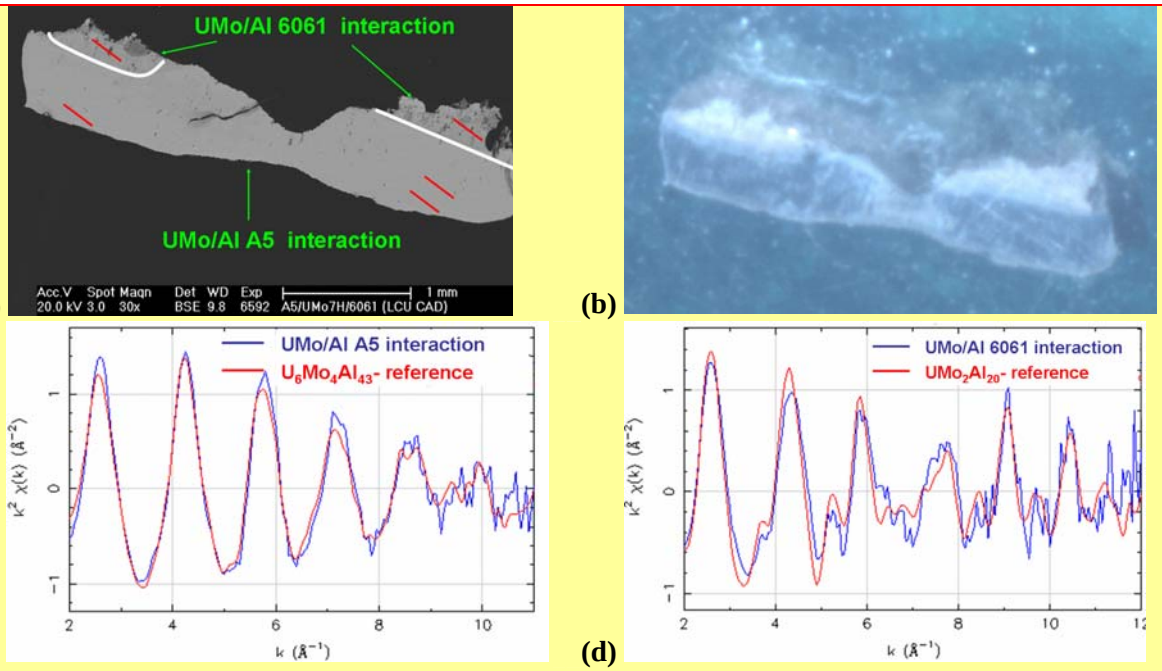

Figure 4. Analyse EXAFS d'un échantillon hétérogène UMo/Al au seuil K du Molybdène. **(a)** Cliché MEB de la coupe transverse et position du faisceau pour les mesures (traits rouges). **(b)** Image obtenue à l'aide du microscope. **(c)** et **(d)** Spectres EXAFS obtenus sur l'échantillon et comparés à ceux de références. La durée totale d'acquisition pour les 2 zones de l'échantillon est d'environ 4 heures (6 spectres).

Ces deux zones ont donc été analysées par µ-EXAFS.[2] La qualité des données obtenues est un élément de plus montrant la stabilité du faisceau sur la ligne. Comme le montre les superpositions des spectres obtenus (figures 4c et d), l'environnement du Molybdène dans la couche d'interdiffusion UMo/Al est fortement influencé par la composition chimique de la plaque d'aluminium. Dans les deux cas, le Molybdène est localisé dans une phase ternaire UMoAl:

- $U_6Mo_4Al_{43}$ proche de l'interface UMo/Al A5,
- UMo_2Al_{20} proche de l'interface UMo/Al 6061.

Test du monochromateur en mode "sortie fixe"

A basse énergie (<14keV), la position verticale du faisceau évolue au cours de l'acquisition d'un spectre EXAFS ("sortie variable", le gap entre les deux cristaux du monochromateur est constant). Dans la configuration EXAFS "classique", cette variation n'est pas pénalisante. Elle est en effet compensée par un mouvement vertical très précis de la table d'expérience. Ce choix n'est cependant plus adapté à la table d'expérience "micro-faisceau" puisque celle-ci doit, à terme, supporter les éléments optiques micro-focalisant en plus du porte-échantillon.
Les propriétés de la translation du gap entre les deux cristaux du monochromateur ont donc été testées. En effet, la variation de ce gap (g) au cours du spectre en énergie peut permettre également d'assurer une sortie fixe du faisceau au niveau du monochromateur (à hauteur H), et par là-même une position verticale constante de ce faisceau sur l'échantillon. On peut écrire:

$$H=2g\cos(\theta_{Bragg}) \quad (1)$$

Pour que H soit constant entre 2 énergies E_0 et E_1, on doit donc avoir:

$$g(E_1)\cos(\theta_{Bragg}(E_1)) = g(E_0)\cos(\theta_{Bragg}(E_0)) \quad (2)$$

soit une variation relative $\Delta g/g$ égale à

$$\Delta g/g = [g(E_1) - g(E_0)] / g(E_0) = \cos(\theta_{Bragg}(E_0)) / \cos(\theta_{Bragg}(E_1)) - 1 \quad (3)$$

La figure 5.a illustre les évolutions théoriques absolues (équ. 1) et relatives (équ. 3) du gap.

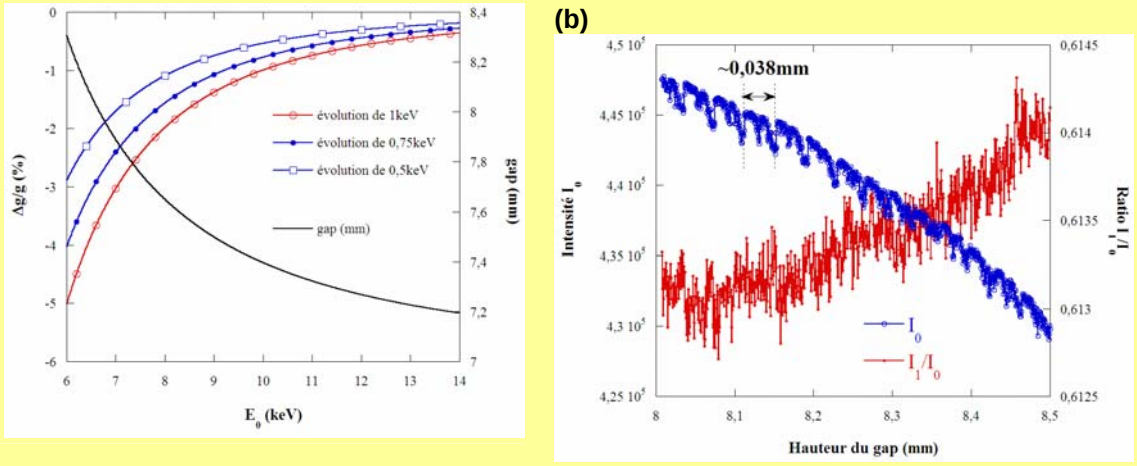

Figure 5. **(a)** Evolutions théoriques de la variation relative du gap $\Delta g/g$ (en %) en fonction de l'énergie initiale E_0, pour des variations E_1-E_0 égales à 0,5, 0,75 et 1 keV, et de la valeur absolue du gap pour une sortie fixe correspondant à H=14mm. **(b)** Evolutions expérimentales de l'intensité du faisceau I_0 et du ratio I_1/I_0 en fonction du gap (variation relative de 6,25%); ajustement automatique de l'angle entre les cristaux pendant le déplacement.[3]

Expérimentalement, nous avons suivi l'évolution de l'intensité du faisceau monochromatique (I_0) en fonction du gap (fig. 5b, courbe bleue). La perte de flux pour un déplacement de gap de plus de 6% est de l'ordre de 4%. Cette diminution est très vraisemblablement due au déplacement du faisceau sur le 2nd cristal et donc à une perte d'optimisation de la focalisation horizontale. Les accidents périodiques (tous les 0,038mm environ) doivent être causés par les défauts de la vis qui assure la translation. Toutefois, malgré ces défauts, la compensation entre les détecteurs est très correcte: le

[2] Palancher H. *et al*., "Study of UMo/Al Interaction Layer by XRD and XAS with Micro-Focused X-Ray Beam", *2005 International Reduced Enrichment for Research and Test Reactors Meeting*, Boston, USA (6-10Novembre 2005)
[3] Proux O. *et al.*, "Feedback system of a liquid nitrogen cooled double-crystal monochromator: design and performances", *Journal of Synchrotron Radiation* **13** (2006) 59-68

bruit global sur le ratio I_1/I_0 est de 0,03% sur l'ensemble du déplacement (1s par point). Le fonctionnement du monochromateur en mode "sortie fixe" est donc faisable.

Développement des miroirs focalisants

Les principes généraux mis en oeuvre pour la conception des courbeurs sont identiques à ceux utilisés pour le courbeur du 2nd cristal du monochromateur de FAME, à savoir:

- mouvements angulaires décorrélés par l'utilisation de charnières de type "points faibles",
- forme des miroirs en U de manière à les fixer sur les mâchoires des courbeurs à l'aide d'un alliage métallique (alliage de French), de manière à limiter au maximum les contraintes sur le miroir dues à leur fixation,
- utilisation de vérins pas-à-pas spéciaux, conçus et validés sur le monochromateur, associés à des piezo-électriques pour les mouvements les plus précis (courbures des miroirs).

Le projet a largement évolué depuis 2004 : l'étude technique est aujourd'hui achevée (cf. Fig. 6).

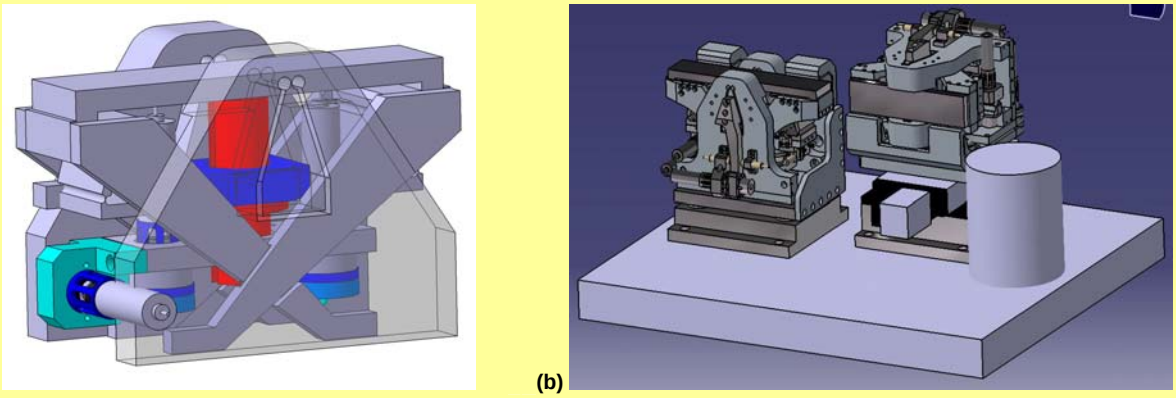

Figure 6. Vue 3D du 1er courbeur **(a)** et représentation schématique de la disposition des deux miroirs dans la géométrie Kirkpatrick-Baez **(b)**. Dans la figure b, le cylindre bleu clair apposé à droite du 2nd courbeur matérialise le volume disponible pour l'environnement échantillon.

Les 2 miroirs ont été commandés à la Société Européenne de Systèmes Optiques (SESO, Aix en Provence). Leur nature, en Silicium recouvert de Rhodium, est identique à celle des deux autres miroirs de la ligne, de manière à couvrir le domaine [4-22 keV]. Leur recette a été réalisée chez SESO fin octobre 2005. Le montage des courbeurs va maintenant débuter.

Budget

A ce jour, les 81000 € dépensés couvrent principalement l'achat (cf. tableau 1) :

- de l'ensemble des éléments nécessaires au montage du système micro-focalisant (courbeurs et miroirs),
- d'un microscope qui permet de visualiser l'échantillon avec une résolution maximale de 1 µm.

Articles		**Montant (€)**
Mécanique (totalité du montage)		14 986
Electronique	*(commande des mouvements générés par les piezo-électriques)*	22 708
	(codeur)	2 130
Miroirs		19 000
Microscope		11 790
Autres (billes, jauges, limites, platine, vérins, …)		10 399
Total		**81 103**

Tableau 2. Détail des dépenses engagées au 15 octobre 2005 dans le cadre du projet micro-faisceau.

Les futures dépenses (cf. tableau 3) doivent permettre l'aménagement d'un dispositif expérimental indépendant du montage actuel, les deux montages co-existant. Ce choix garantit un passage simple et rapide d'un faisceau micro-focalisé (20×20 µm²), à un faisceau de taille conventionnelle (150×80 µm²).

Pour couvrir une partie de ces dépenses, une demande « équipements mi-lourds CNRS-INSU » associée à l'électronique numérique du détecteur de fluorescence a été effectuée pour un montant de 85420 €. Cette nouvelle électronique est nécessaire pour analyser plusieurs raies de fluorescence simultanément, fonction indispensable lorsque l'on effectue une cartographie en fluorescence X, mais

elle permettra également un remplacement de l'électronique analogique actuelle du détecteur qui commence à devenir vieillissante (2 cartes sur les 30 sont réparées en moyenne tous les ans) et peut-être un peu moins compétitive pour les mesures EXAFS classiques.

Articles	**Montant (€)**
Table	50 000
Porte-échantillon	9 000
Nouvelle Détection (diode et électronique)	10 000
Electronique numérique pour détecteur de fluorescence multi éléments résolu en énergie	85 423
Total	**154 423**

Tableau 3. Détail des dépenses à effectuer pour finaliser le projet micro-faisceau.

Conclusions

L'implantation d'un micro-faisceau sur FAME est un projet :

- solide techniquement comme le montrent les différents tests effectués à ce jours et ambitieux puisqu'il a nécessité, par exemple, le développement de nouveaux courbeurs,
- qui répond à une demande émanant des utilisateurs et soutenue par l'ESRF,
- qui complète le montage existant en élargissant le type d'échantillon pouvant être étudié par EXAFS sur cette ligne.

Le projet est à ce jour très avancé : les premiers tests sous faisceau de l'optique de micro-focalisation sont prévus début 2006.

7. Tests de cristaux analyseurs sur FAME

Cristal analyseur en mode transmission

En décembre 2003, une série de mesures a été réalisée sur la ligne en collaboration avec A. Manceau (LGIT, Grenoble) de manière à tester les cristaux analyseurs courbes (Bent Crystal Laue Analyzers, BCLA) développés par G. Bunker (APS, Chicago).[4] L'échantillon était composé de goethite contenant une faible quantité de zinc, étudié au seuil K du Zn. La géométrie d'analyse était en transmission (fig. 1 gauche), les faisceaux diffractés par le cristal étant collectés grâce au détecteur Canberra 30 éléments (fig. 1 droite), en mode MCA (pour vérifier la sélectivité du BCLA) ou SCA, avec une fenêtre (ROI) centrée sur les raies de fluorescence Kα1 et Kα2 du Zn.

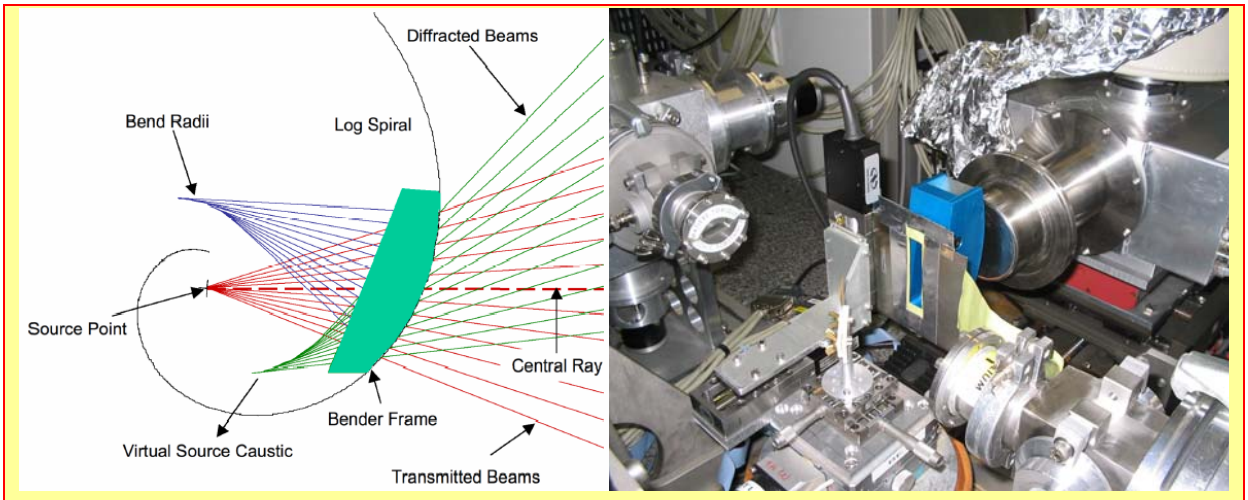

Figure 1: Gauche: design en spirale du BLCA: point source, source virtuelle, faisceaux diffractés et transmis, rayons de courbure. Droite: montage sur FAME

Sans l'analyseur, le signal de fluorescence est complètement saturé par la fluorescence Kα du Fe (pic autour du canal 600, fig. 2 gauche). En conditions optimales (fig. 2 droite, l'angle de Bragg du BCLA corresponds exactement à la fluorescence Kα du Zn), la fluorescence Kα du Fe est toujours présente mais la raie correspondant à la fluorescence Kα du Zn (zone grisée) devient prépondérante.

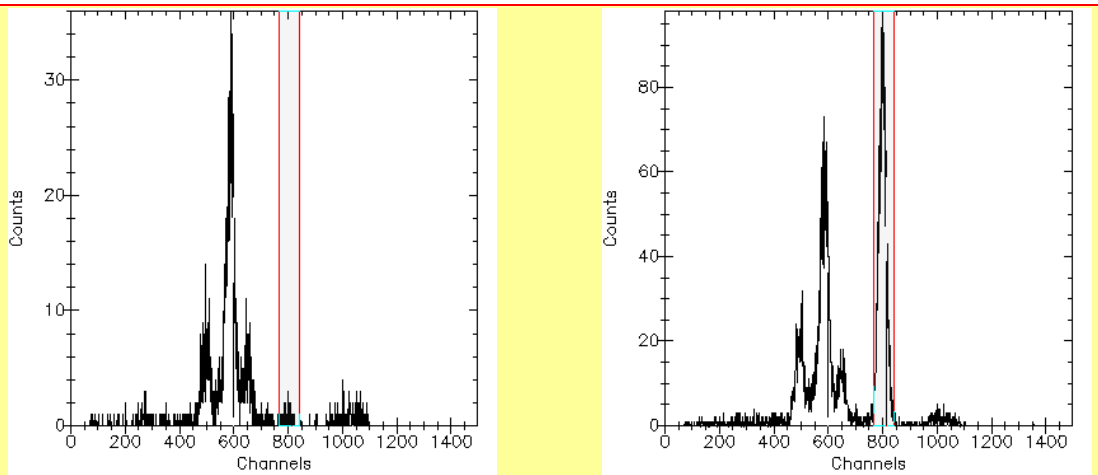

Figure 2: Signaux de Fluorescence mesurés aves le BCLA mal aligné (gauche) et optimisé (droite)

Cependant, aucune amélioration significative du taux de comptage n'est apportée par ce système par rapport au détecteur solide Germanium, peut-être à cause de l'absorption du wafer de silicium, et la sensibilité du système au niveau du réglage reste assez grande. Le fait d'être en transmission et non en réflexion limite l'utilisation de ce type d'analyseur plutôt aux hautes énergies, où l'absorption du Si est beaucoup plus faible, où aux lignes ayant plus de flux sur l'échantillon, typiquement sur un

[4] A. J. Kropf, J. A. Fortner, R. J. Finch, J. C. Cunnane, C. Karanfil, "A Bent Silicon Crystal in the Laue Geometry to Resolve Actinide X-Ray Fluorescence for X-Ray Absorption Spectroscopy", *Physica Scripta* **115** (2005) 918

onduleur ou wiggler. Compte-tenu des taux de réflectivité des monocristaux, il paraît donc plus judicieux dans ce contexte de travailler en mode réflexion.

Cristal analyseur en mode réflexion

Deux séries d'expérience ont été effectuées en septembre et novembre 2005 pour tester des cristaux analyseurs courbés sphériquement fonctionnant en mode réflexion (développés par Emilie Collart pendant sa thèse sous la direction d'Abhay Shukla, LMCP-Paris) et conçus pour des analyses hautes résolutions[5]. Dans cette configuration, le faisceau diffracté par le cristal est focalisé sur un système avec un fort taux de comptage. Avec un rayon de courbure de 2m, une résolution en énergie des cristaux inférieure à 300meV a été obtenue au seuil K du Cu (8.979keV). Avec un rayon plus petit, la résolution se dégrade, le but étant d'avoir:

- une résolution suffisante pour bien pouvoir discriminer des raies de fluorescence proche,
- une acceptance angulaire plus grande et donc un taux de comptage potentiellement plus important.

Conditions de mesure

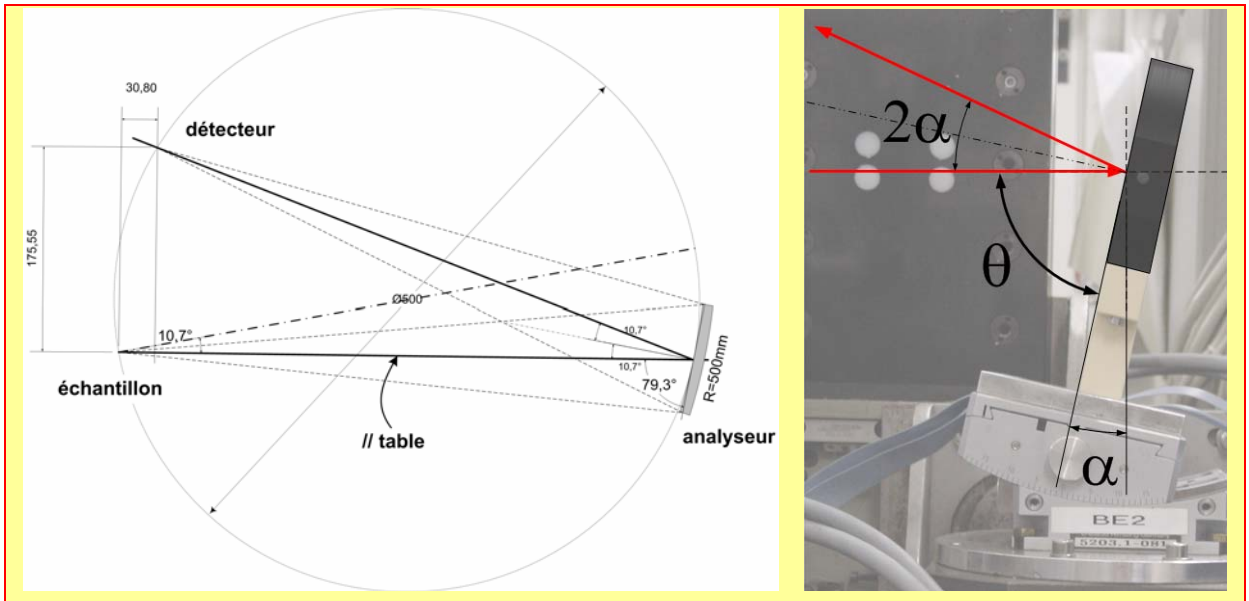

Figure 3: Géométrie du montage en cristal courbe. L'échantillon, le cristal et le détecteur sont sur le cercle de Rowland. θ est l'angle de Bragg de diffraction des photons provenant de l'échantillon. Conception et réalisation du montage de l'analyseur: Eric Lahera.

Cristal analyseur Si(444), distance interplanaire: d=0,78383Å,
Rayon de courbure: 0,5m
Détecteur utilisé: 1 élément du détecteur 30-éléments Canberra résolu en énergie, shaping time 125ns.
Domaine angulaire centré autours de θ=79,3°, ce qui correspond à une énergie diffractée de 8keV.

[5] Collart E., Shukla A. et al., "Spherically bent analyzers for resonant inelastic X-ray scattering with intrinsic resolution below 200 meV", *J. Sync. Rad.* **12** (2005) 473-478

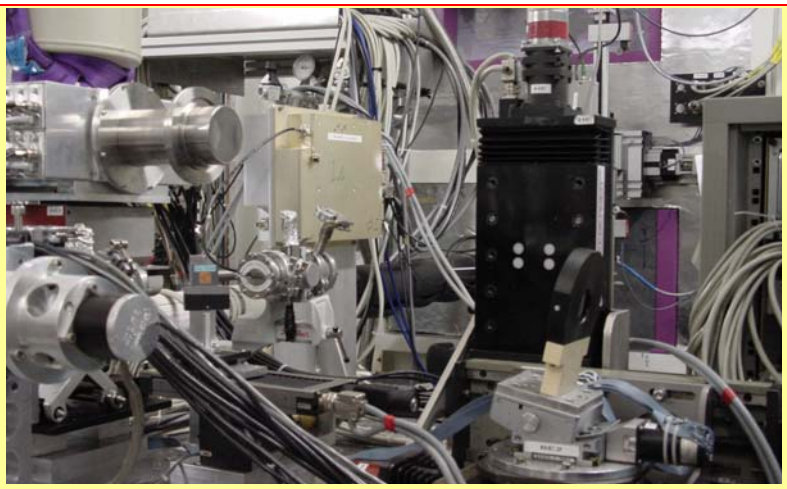

Figure 4: Photo du montage

Résolution en énergie

La résolution en énergie des cristaux a été estimée de deux façons:
- à angle fixe, en fonction de l'énergie du faisceau incident (mesure du pic élastique, fig. 5),
- à énergie fixe, en fonction de l'angle du cristal analyseur (mesure des pics de fluorescence, fig. 6).

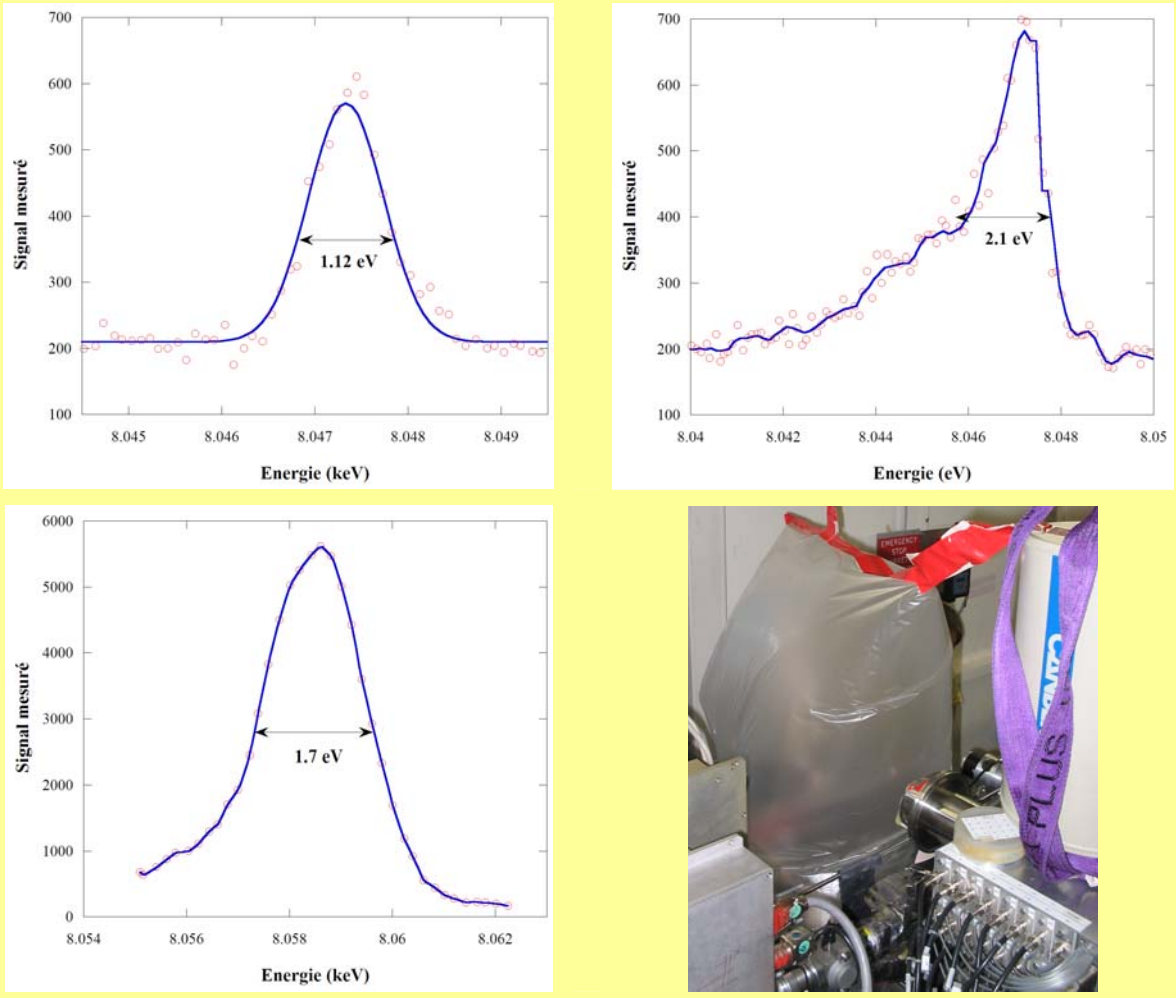

Figure 5: pic élastique à 8.04778 keV mesuré en utilisant le centre (haut - gauche) et l'ensemble du cristal (haut - droite) sous air. Pic élastique à 8.0586 keV mesuré sous hélium avec l'ensemble du cristal (bas - gauche). Montage avec l'"helium bag" en polyéthylène (bas - droite)

Le premier type de mesure a permis de se rendre compte de l'influence de la diffusion par l'air. En masquant à l'aide de plomb certaine partie de l'analyseur, nous avons déterminé que la résolution est meilleure lorsque l'on utilise le faisceau diffracté par le centre du cristal (~1.1eV, fig. 5 haut gauche) que lorsque l'ensemble du cristal est utilisé (~2.1eV, fig. 5 haut droite). En effet, dans le second cas, le pic mesuré est asymétrique vers les basses énergies: l'épaulement correspond au faisceau diffusé inélastiquement (Compton). Si l'on ne sélectionne que la partie centrale du cristal, on limite l'effet du diffusé (minimum à 90°).
Il est possible de limiter l'importance du diffusé en travaillant soit sous vide (avec les contraintes que cela implique) soit sous atmosphère d'hélium (beaucoup plus simple à mettre en œuvre).
En prenant en compte la résolution du monochromateur (0.46eV), la résolution de l'analyseur "plein champ" est de l'ordre de 1.6-1.7 eV à l'air, 1.2-1.3 eV lorsque l'on limite les faisceaux diffusés en mettant l'ensemble des trajets sous hélium.

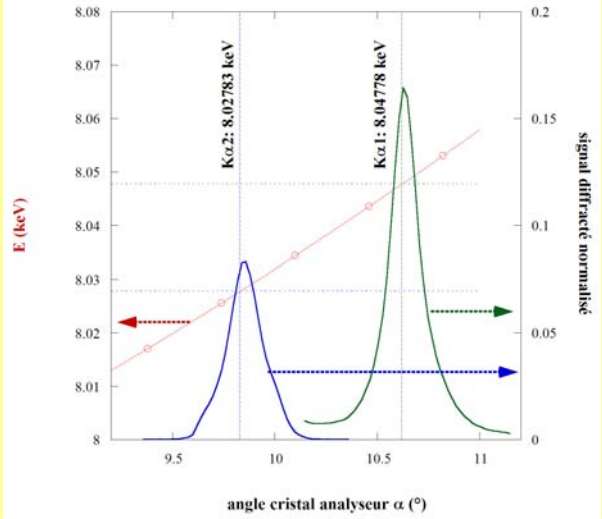

Figure 6: Pics de fluorescence Kα1 et Kα2 du Cu mesuré avec le cristal entier, à l'air.

Le second type de mesure a été effectué en utilisant l'ensemble du cristal. Le tableau 1 rapporte les principales valeurs déduites des pics mesurés (figure 6). Le principal enseignement de cette mesure est tout d'abord que l'on arrive très bien à discriminer les 2 raies de fluorescence. Quantitativement, le ratio I(Kα2)/I(Kα1) est trouvé égal à 0.5 (0.51 dans la littérature).
A partir de la largeur des pics, il est possible d'estimer la résolution du cristal, en supposant Lorentzien les profils des pics et en considérant l'élargissement dû 1) à la largeur naturelle de l'émission, 2) à la résolution du faisceau incident et 3) au cristal analyseur. La valeur trouvée, identique pour les deux raies de fluorescence (1.46±0,05eV), est similaire à celle trouvée par la première méthode à la barre d'erreur près.

Raie sélectionnée	**Cu Kα1**	**Cu Kα2**
Energie	8047.78 eV	8027.83 eV
Largeur du pic (L_p)	4,2±0,05 eV	4,7±0,05 eV
Largeur naturelle théorique de l'émission de fluorescence[6]	2,11 eV	2,17 eV
Largeur naturelle mesurée de l'émission de fluorescence[7] *(L_n)*	2,28±0,05eV	2,78±0,05eV
Résolution intrinsèque du monochromateur (R_{mono})	0,46 eV	0,46 eV
Résolution mesurée du cristal analyseur (L_p-L_n-R_{mono})	1,46±0,1 eV	1,46±0,1 eV

Tableau 1: Principales valeurs déduites de l'analyse des raies Cu Kα1 et Kα2

[6] M.O. Krause and J.H. Oliver "Natural widths of atomic K and L levels, X-ray emission lines" *J. Phys. Chem. Ref. Data* **8** (1979) 329-338
[7] H Sorum "The Kα1,2 X-ray spectra of the 3d transition metals Cr, Fe, Co, Ni and Cu", *J. Phys. F* **17** (1987) 417-425

Spectres d'absorption X en fluorescence

Une mesure EXAFS a été effectuée sur un échantillon de $CuSO_4$ en solution aqueuse ([Cu]=1% massique). La mesure a été effectuée en transmission (saut de seuil: 0,5) et en fluorescence, en mesurant l'intensité des raies Kα1 puis Kα2 (Partial Fluorescence Yield EXAFS, fig. 7). Les différences les plus notables entre les différents spectres sont au niveau du pre-pic, beaucoup plus marqué pour les spectres de fluorescence que pour le spectre en transmission. De plus, un fond montant sous le pre-pic est clairement visible pour la mesure avec la raie Cu Kα2. Ce fond n'est pas un artefact de normalisation car l'avant seuil avant 8980 eV est dans les deux cas (Kα1 et Kα2) clairement nul.
D'un point de vue expérimental, les mesures avec ce dispositif (une fois optimisé) n'ont pas présenté de problèmes, la tolérance de ces cristaux à un positionnement imparfait étant peut-être plus grande que les BCLA. Il est toutefois difficile de conclure car la stabilité de la ligne est bien meilleure maintenant qu'en 2003.

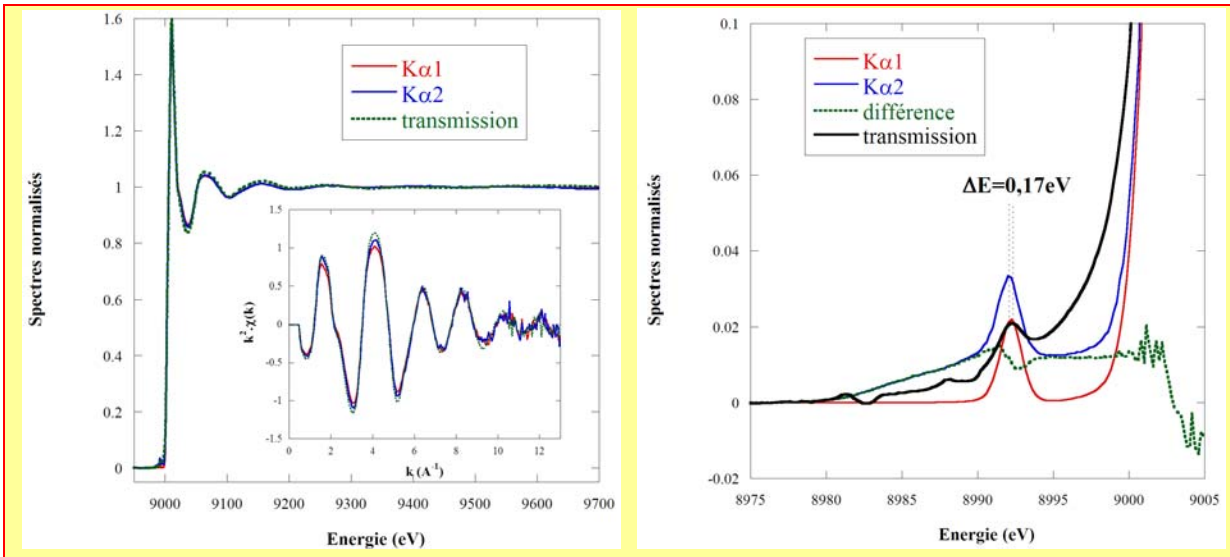

Figure 7: Spectres EXAFS mesurés en enregistrant en mode transmission et en mode fluorescence en enregistrant les évolutions des intensités des raies Cu Kα1 et Cu Kα2. Temps d'acquisition global par spectre: 6h

Raie sélectionnée	**Cu Kα1**	**Cu Kα2**
Transition électronique sondée, 1s vers	2p3/2	2p1/2
Nombre de coup de fluorescence avant-seuil (/s)	<10	<10
Nb de coup de fluorescence sur la raie blanche (/s), sous air	~70 000	~40 000
Nb de coup de fluorescence après-seuil (/s), sous air	~40 000	~25 000
Nb de coup de fluorescence sur la raie blanche (/s), sous He	~180 000	
Nb de coup de fluorescence après-seuil (/s), sous He	~105 000	

Tableau 2: Conditions de mesure des spectres de fluorescence. [Cu] = 1% massique. Capillaire: 2mm. Paroi: 10μm. Les mesures sous hélium on été fait avec un sac en polyéthylène, cf fig. 8

Spectres d'absorption X en diffusion Raman inélastique (XRS)

Une mesure XRS a été effectuée sur un échantillon d'eau pure en conditions ambiantes. Les conditions expérimentales sont restées inchangées par rapport aux mesures de fluorescence. L'angle de 90° entre le faisceau incident et l'analyseur est dans ce cas fortement défavorable, l'intensité diffusée, élastiquement et inélastiquement, étant alors minimum.
Par rapport à la mesure faite à APS, (spectre (d), figure 8 droite), on peut noter que la statistique de mesure est dans notre cas beaucoup plus faible ainsi que la résolution en énergie qui ne permet pas bien de discerner l'épaulement dans le seuil et l'asymétrie de la raie blanche. Il faut rapporter ça à la source (un élément d'insertion contre un aimant de courbure), à la géométrie (angle de diffusion de

55,8° contre 90°), au nombre de cristaux analyseurs (2) et à la résolution en énergie de l'expérience (1eV à l'APS contre ~1,7eV ici). Pour le dernier point, le gain en résolution peut provenir du monochromateur utilisé (Si 400 contre Si 220), avec une résolution intrinsèque $\Delta E/E$ de 1.4 10^{-5} contre 6.6 10^{-5}.

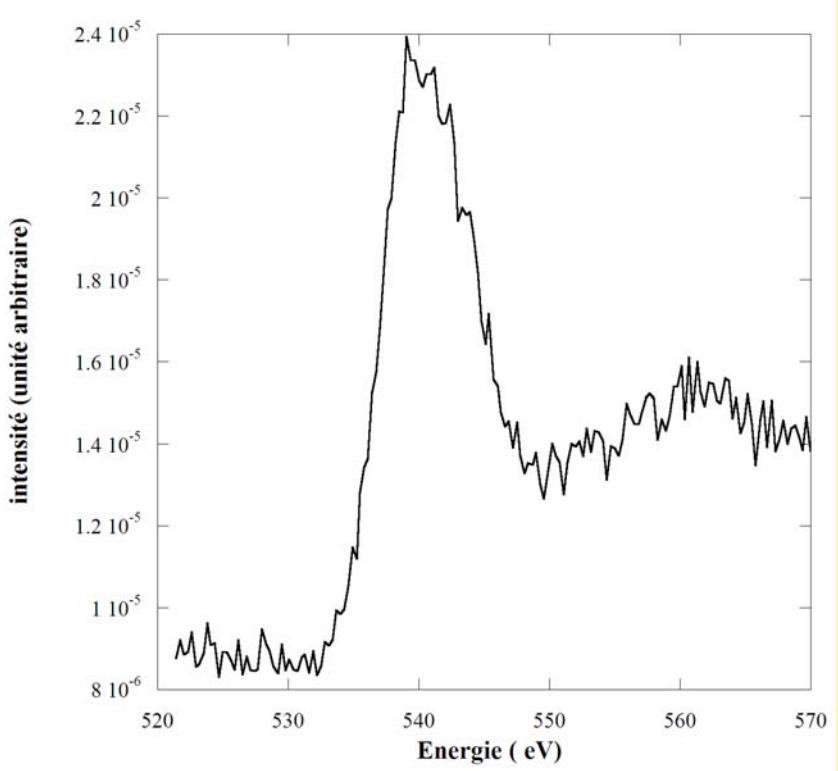

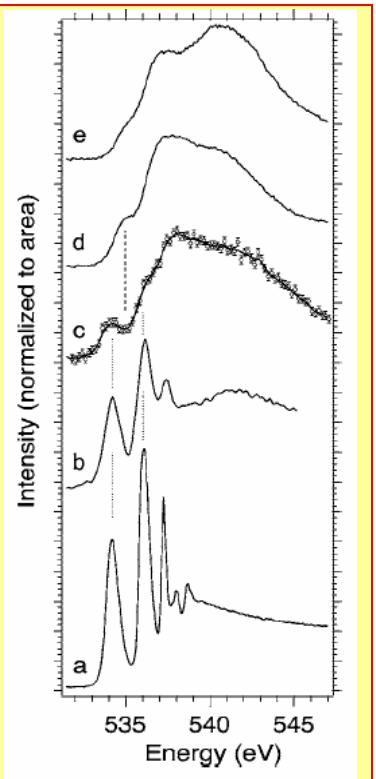

Figure 8: Seuil K de l'Oxygène de l'eau en conditions ambiantes, mesuré en diffusion Raman inélastique, en enregistrant le pic élastique à 8058,6eV (figure de gauche). Temps de comptage: 360 s par point (temps total de 16h48). Capillaire de 2mm, paroi de 0,01mm. Cristal analyseur à 90° du faisceau incident. Trajet des faisceaux dans l'hélium (photo fig. 5). Comparaison avec des spectres obtenus à APS[8] (résolution: ~1eV): (a) eau en phase gaz, (b) surface de l'eau, (c) eau supercritique, (d) eau en conditions ambiantes, (e) glace

Conclusions

Quels types de cristaux pour FAME?

Au vue des tests effectuées sur la ligne, le meilleur choix pour les cristaux analyseurs et le modèle en mode "réflexion". Les principaux avantages que l'on y voit:

- plus grande facilité de réglage,

- pas de perte de flux dû à l'absorption par le wafer de Silicium lorsque l'on travaille en Laüe,

- focalisation du faisceau sur un détecteur, et non dispersion: le détecteur que collecte le faisceau "analysé" par le cristal peut être de taille beaucoup plus réduite.

Quels apports?

Spectroscopie EXAFS sur des échantillons particuliers

Première possibilité offerte par les cristaux analyseurs : pouvoir étudier l'évolution d'une raie de fluorescence en fonction de l'énergie et ce sans que le détecteur ne sature à cause d'autres raies de fluorescence. La très bonne sélectivité des cristaux (aucun signal parasite, comme l'atteste l'absence de signal avant-seuil) fait que des études sur de l'ordre local d'éléments (numéro atomique Z) dilués dans des matrices contenant un (ou des) éléments plus légers (Z-1, Z-2...) sont possibles. Même si le nombre de photons de fluorescence collecté est faible, la statistique de mesure ne portera que sur des "bons" photons.

[8] Ph. Wernet, D. Testemale, *et al.* "Spectroscopic characterization of microscopic hydrogen-bonding disparities in supercritical water", *J. Chem. Phys*. **123** (2005)154503

La très bonne discrimination en énergie des cristaux peut également autoriser une sélectivité de site dans certains cas particuliers où deux atomes identiques dans deux sites différents n'ont pas la même valence, ce qui va affecter les positions des raies de fluorescence relatives à chacun de ces atomes.[9]

Spectroscopie XANES mieux résolue

Autre possibilité: pouvoir faire des études XANES beaucoup mieux résolues. En effet, les mesures en "PFY-XAFS" permettent quasiment de s'affranchir des largeurs de trous profonds des niveaux sondés lorsque la résolution des analyseurs est largement inférieure à ceux-ci.[10] Dans le cas des tests, la résolution des analyseurs n'est inférieure que d'1/3 environ au trou profond du Cu, mais les améliorations sur les pré-pics observés sont manifestes. Cette amélioration est d'autant plus importante que les études XANES quantitatives sont amenées à se multiplier, les programmes permettant de faire ce genre de calculs devenant plus simples d'utilisation.

Spectres d'absorption X en diffusion Raman inélastique (XRS)

Dernière possibilité: pouvoir faire des mesures de Diffusion Raman Inélastique. Le test est prometteur, reste à voir 1) si la statistique est suffisante pour des temps de comptage raisonnable, ainsi que 2) la résolution en énergie.

Quel montage?

Les cristaux

Chaque cristal permet de sonder un domaine en énergie d'environ 2keV pour un déplacement angulaire en θ de ~90° à 48°, d'environ 1keV si l'on restreint le domaine angulaire de ~90° à 60°. D'une manière générale, plus l'angle de Bragg sera proche de 90°, meilleure sera la résolution en énergie. Au vue des domaines en énergie couverts par les différents types de cristaux (Fig. 9 et Tab. 3), deux cristaux en silicium d'orientation 111 et 110 permettent d'analyser les raies de fluorescence depuis 5.95keV jusqu'à environ 14keV ou bien, en terme de seuil d'absorption:

- depuis Z=26 (Fe) jusqu'à Z=37 (Rb) au seuil K,
- depuis Z=64 (Gd) jusqu'à Z=92 (U) au seuil L_{III}.

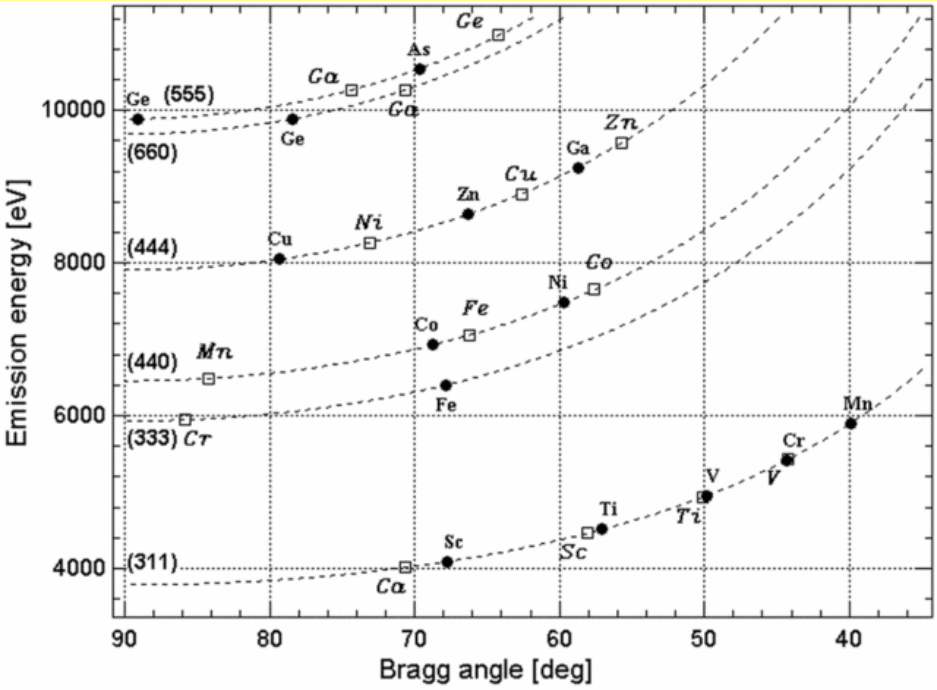

Figure 9: Energies d'emission Kα (cercles noirs) and Kβ (carrés blancs) de différents éléments en fonction de l'angle de Bragg de l'analyseur, d'après Welter *et al*.[11]

[9] Glatzel P., Jacquamet L. et al., "Site-Selective EXAFS in Mixed-Valence Compounds Using High-Resolution Fluorescence Detection: A Study of Iron in Prussian Blue", *Inorganic Chemistry* **41** (2002) 3121-3127

[10] Hämäläinen K., Siddons D.P., Hastings J.B. and Berman L.E., "Elimination of the Inner-Shell Lifetime Broadening in X-ray Absorption Spectroscopy", *Phys. Rev. Lett*. **67** (1991) 2850-2853, Hayashi H. *et al.,* "Lifetime-broadening-suppressed/free XANES spectroscopy by high-resolution resonant inelastic x-ray scattering", *Phys. Rev. B* **68** (2003) 045122

[11] Welter E. et al., "A new X-ray spectrometer with large focusing crystal analyzer", *J. Sync. Rad.* **12** (2005) 448-454

cristal			énergie (keV) sélectionnée pour un angle de		
plans	**d (Å)**	**$\Delta E/E$[12]**	**85°**	**65°**	**45°**
Si(311)	*1.6374*	*1.31 10^{-4}*	3.801	4.178	5.355
Si(333)	*1.0451*	*5.77 10^{-5}*	5.955	6.546	8.390
Si(440)	*0.96000*	*2.77 10^{-5}*	6.483	7.126	9.133
Si(444)	*0.78382*	*8.91 10^{-5}*	7.940	8.728	11.19
Si(660)	*0.64000*	*9.99 10^{-5}*	9.725	10.69	13.70
Si(555)	*0.62706*	*5.50 10^{-5}*	9.925	10.91	13.98

Tableau 3: énergies analysées en fonction des cristaux analyseurs choisis

Le montage

Le cristal doit avoir au minimum 3 mouvements permettant de régler:

- l'angle $\theta_{cristal}$ (domaine angulaire:45-85°)
- sa hauteur $z_{cristal}$, (domaine de déplacement: de -5 à +5mm)
- sa distance à l'échantillon, fonction de son rayon de courbure (~0,5m), $x_{cristal}$ (domaine de déplacement: de -5 à +5mm)

Le détecteur doit posséder les mêmes mouvements permettant de choisir:

- son angle dans le plan de travail, $\omega_{détecteur}$ (domaine angulaire de -45 à +45°),
- sa hauteur $z_{détecteur}$ (domaine de déplacement: de 0 à +50 cm par rapport à la hauteur du faisceau, pour un angle $\theta_{cristal}$ variant de 90 à 45° et pour un rayon de courbure de 50 cm)
- sa distance au cristal $x_{détecteur}$ (domaine de déplacement: de 0 à +50 cm par rapport à la position horizontale du faisceau, pour un angle $\theta_{cristal}$ variant de 90 à 45° et pour un rayon de courbure de 50 cm).

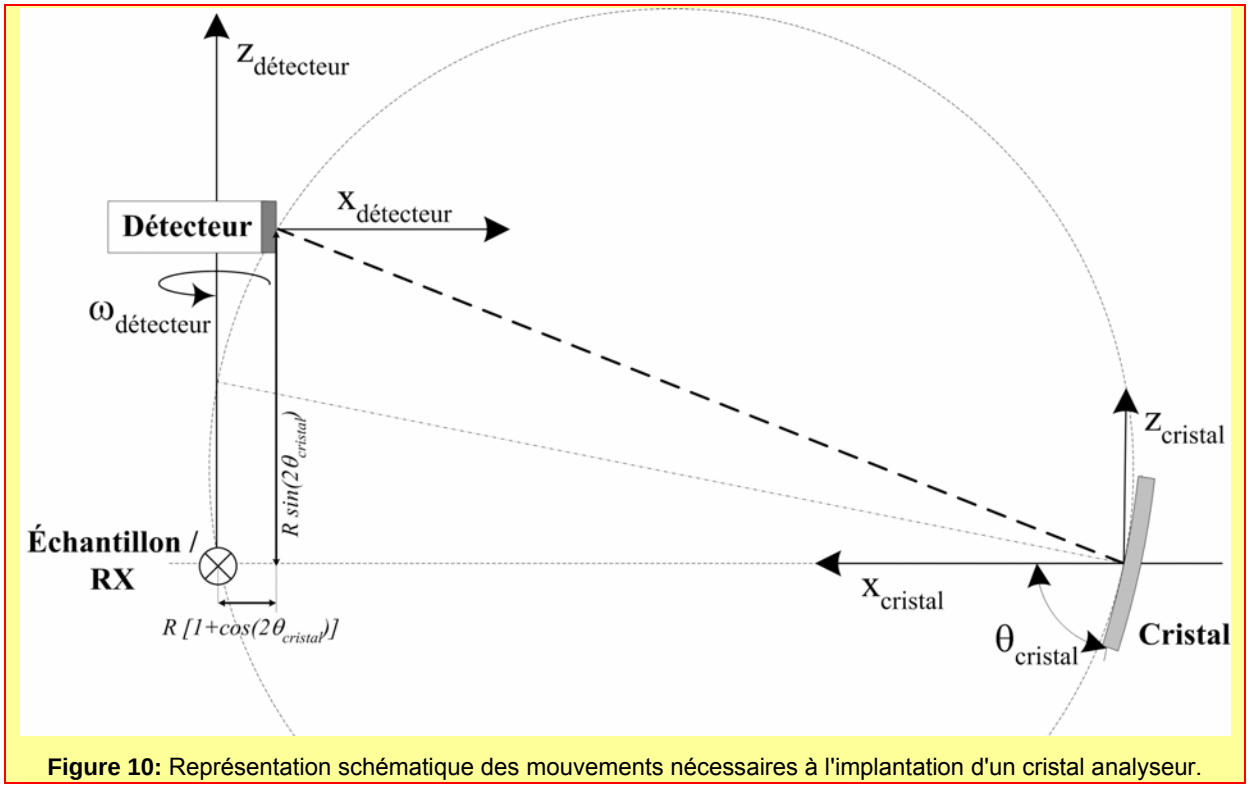

Figure 10: Représentation schématique des mouvements nécessaires à l'implantation d'un cristal analyseur.

[12] $\Delta E/E=\Delta\theta/\theta=\text{cotan}\theta\ \Delta\theta$, $\Delta\theta=\omega_{Darwin}$ = $[2r_e\lambda^2C|F(hkl)|e^{-M}]/[V\pi\sin(2\theta)]$, $\lambda = 2d_{hkl}\sin\theta$, au final $\Delta E/E=2.2428\ 10^{-7}\ d_{hkl}^2|F(hkl)|$. $|F(hkl)|$ est obtenu à partir des facteurs de diffusion atomiques f_{hkl} (International tables for X-ray cristallography, vol. IV, p74, f_{hkl} en fonction de $\sin\theta/\lambda=1/2d_{hkl}$), $|F(hkl)|=M\ f_{hkl}$ où M=8 si hkl est pair et h+k+l=4n, $M=4*2^{1/2}$ si hkl impair, M=0 sinon.

Budget et mise en œuvre

Le coût d'un cristal courbe seul est d'environ 3k€. Notre objectif est de concevoir un montage le plus simple possible, mettant en oeuvre par exemple des systèmes de charnière par point faible (comme pour le courbeur du second cristal du monochromateur) pour optimiser les angles à la place de berceaux goniométriques (onéreux). Le but est alors de pouvoir multiplier le nombre de cristaux opérationnels pendant une même acquisition pour améliorer par exemple la statistique de comptage, ou bien régler le 1er cristal sur la raie Kα1, le 2nd sur la raie Kβ1...

Au vue des évolutions des énergies d'émission analysées en fonction de l'angle de Bragg (figure 9 et tableau 3), il apparaît qu'avec 2 types de cristaux (Si(111) et Si(110)) il est possible d'analyser des raies de fluorescence depuis 6keV jusqu'à environ 14keV, en fonction de l'ordre de la réflection choisie. Un jeu de 2 cristaux de chaque type serait donc à envisager dans un premier temps, avec les déplacements correspondants.

- 4 cristaux courbes de rayon 0,5m *12 k€*
- 2 manipulateurs pour les cristaux, 3 axes (θ, x, z) motorisés *10 k€*
- 1 support pour le détecteur de fluorescence, 3 axes (ω, x, z), manuels *5 k€*

Ce développement instrumental sera mené par Eric Lahera. Il sera secondé par un stagiaire en 3ème année d'école d'ingénieur (Ecole Nationale Supérieure de Mécanique et des Microtechniques de Besançon), Aurélien Braillard.

10. Liste des publications (11/2004 – 03/2006)

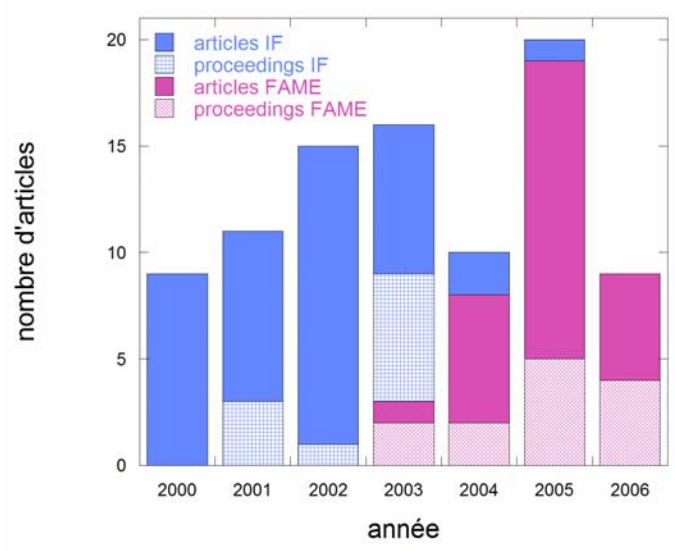

Figure : Nombres d'articles et de proceedings portant sur des expériences effectuées sur l'expérience EXAFS, sur IF et sur FAME (ouverture de la ligne en septembre 2002)

Articles

2006

2006-1 Guiné V., Spadini L., Sarret G., Muris M., Delolme C., Gaudet J.-P. and Martins J. M. F., "Zinc Sorption to Three Gram-Negative Bacteria: Combined Titration, Modeling, and EXAFS Study", *Environmental, Science and Technology* (2006) sous presse

2006-2 Proux O., Nassif V., Prat A., Ulrich O., Lahera E., Biquard X., Menthonnex J.-J. and Hazemann J.-L., "Feedback system of a liquid nitrogen cooled double-crystal monochromator: design and performances", *Journal of Synchrotron Radiation* **13** (2006) 59-68

2006-3 Schlegel M. and Manceau A., "Evidence for the nucleation and epitaxial growth of Zn phyllosilicate on montmorillonite", *Geochimica et Cosmochimica Acta* **70** (2006) 901-917

2006-4 Strobel P., Darie C., Thiéry F., Bacia M., Proux O., Ibarra-Palos A., Soupart J.B., "New nanocrystalline manganese oxides as cathode materials for lithium batteries: electron microscopy, electrochemical and X-ray absorption studies", *Solid State Ionics* **177** (2006) 523-533

2006-5 Strobel P., Darie C., Thiéry F., Ibarra-Palos A., Bacia M., Proux O., Soupart J.B., "Electrochemical lithium intercalation in nanosized manganese oxides", *Journal of Physics and Chemistry of Solids* (2006) sous presse

2005

2005-1 Andreev T., Y. Hori, X. Biquard, E. Monroy, D. Jalabert ,A. Farchi , M. Tanaka, O. Oda, L Si Dang and B. Daudin, "Optical and morphological properties of GaN quantum dots doped with Tm", *Physical Review B* **71** (2005) 115310

2005-2 D'Angelo P., Pacello F., Mancini G., Proux O., Hazemann J.L., Desideri A. and Battistoni A., "X-ray absorption investigation of a unique protein domain able to bind both Cu(I) and Cu(II) at adjacent sites of the N-terminus of Haemophilus ducreyi Cu,Zn superoxide dismutase", *Biochemistry* **44** (2005) 13144-13150

2005-3 Arcovito A., Lamb Don C, Nienhaus G. U., Hazemann J.-L., Benfatto M. and Della Longa S., "Light-Induced Relaxation of Photolyzed Carbonmonoxy Myoglobin: A Temperature-Dependent X-ray Absorption Near Edge Structure (XANES) Study", *Biophysical Journal* **88** (2005) 2954-2964

2005-4 Cancès B., Juillot F., Morin G., Laperche V., Alvarez L., Proux O., Hazemann J-L., Brown Jr. G. E., Calas G., "XAS evidence of As(V) association with iron oxyhydroxides in a

contaminated soil at a former arsenical insecticide processing plant", *Environmental, Science and Technology* **39** (2005) 9398-9405

2005-5 Casiot C., Lebrun S., Morin G., Bruneel O., Personné J.C. and Elbaz-Poulichet F., "Sorption and redox processes controlling arsenic fate and transport in a stream impacted by acid mine drainage", *Science of The Total Environment* **347** (2005) 122-130

2005-6 Coulet M.-V., Testemale D., Hazemann J.-L., Gaspard J.-P. and Bichara C., "A Reverse Monte-Carlo analysis of the local order in liquid $Ge_{0.15}Te_{0.85}$ alloys combining Neutron Scattering and X-ray Absorption Spectroscopy", *Physical Review B* **72** (2005) 174209

2005-7 Gouget B., Avoscan L., Sarret G., Collins R., Carrière M., "Resistance, accumulation and transformation of selenium by the cyanobacterium Synechocystis sp. PCC 6803 after exposure to inorganic Se^{VI} or Se^{IV}", *Radiochimica Acta* **93** (2005) 683-690

2005-8 Isaure M.P., Manceau A., Geoffroy N., Laboudigue A., Tamura N., Marcus M.A., "Zinc mobility and speciation in soil covered by contaminated dredged sediment using micrometer-scale and bulk-averaging X-ray fluorescence, absorption and diffraction techniques", *Geochimica et Cosmochimica Acta* **69** (2005) 1173-1198

2005-9 Manceau A., Tommaseo C., Rihs S., Geoffroy N., Chateigner D., Schlegel M., Tisserand D., Marcus M.A., Tamura N., Chen Z.S. "Natural speciation of Mn, Ni and Zn at the micrometer scale in a clayey paddy soil using X-ray fluorescence, absorption, and diffraction", *Geochimica et Cosmochimica Acta* **69** (2005) 4007-4034

2005-10 Maret M., Bley F., Meneghini C., Albrecht M., Köhler J., Bucher E. and Hazemann J.-L., "The Cr local structure in epitaxial $CrPt_3$(111) films probed using Polarized X-ray Absorption Fine Structure", *Journal of Physics: Condensed Matter* **17** (2005) 2529–2541

2005-11 Panfili F., Manceau A., Sarret G., Spadini L., Kirpichtchikova T., Bert V., Laboudigue A., Marcus M.A., Ahamdach N., Libert M.F., "The effect of phytostabilization on Zn speciation in a dredged contaminated sediment using scanning electron microscopy, X-ray fluorescence, EXAFS spectroscopy and principal components analysis", *Geochimica et Cosmochimica Acta* **69** (2005) 2265-2284

2005-12 Sarret G., Avoscan L., Carrière M., Collins R., Geoffroy N., Carrot F., Covès J., Gouget B. "Chemical forms of selenium in the metal-resistant bacterium Ralstonia metallidurans CH34 exposed to selenite and selenate" *Applied Environmental Microbiology* **71** (2005) 2331-2337

2005-13 Strobel P., Thiéry F., Darie C., Proux O., Ibarra-Palos A. Bacia M., and Soupart J.B., "Structural and electrochemical properties of new nanospherical manganese oxides for lithium batteries", *Journal of Materials Chemistry* **15** (2005) 4799-4808

2005-14 Testemale D., Argoud R., Geaymond O., Hazemann J.L., "A high-pressure/high-temperature cell for x-ray absorption and scattering techniques", *Review of Scientific Instruments* **76** (2005) 043905

2005-15 Titov A., Biquard X., Halley D., Kuroda S., Bellet-Amalric E., Mariette H., Cibert J., Merad A. E., Merad G., Kanoun M. B., Kulatov E. and Uspenskii Yu. A., "X-ray absorption near-edge structure and valence state of Mn in (Ga,Mn)N", *Physical Review B* **72** (2005) 115209

2004

2004-1 Pokrovsky O.S., Pokrovski G.S. and Schott J., "Gallium(III) adsorption on carbonates and oxides: X-ray absorption fine structure spectroscopy study and surface complexation modeling", *Journal of Colloid and Interface Science*, **279** (2004) 314-315

Highlights

2006

2006-1 D'Angelo P., F. Pacello, G. Mancini, O. Proux, J.-L. Hazemann, A. Desideri, A. Battistoni, " X-ray Absorption Studies on the N-terminal Copper-binding Region of Haemophilus ducreyi Cu,Zn Superoxide Dismutase", *ESRF Highlights 2005* (2006) 102-103

2005

2005-1 Vahé Ter Minassian, "L'heure de gloire pour FAME", *Le Journal du CNRS*, **181** (2005)

2005-2 Testemale D., Hazemann J.L., Pokrovski G., Joly Y., Roux J., "Structural and electronic evolution of $As(OH)_3$ molecule in high temperature and high pressure aqueous solutions by X-ray spectroscopy", *ESRF Highlights 2004* (2005) 87-88

Actes de colloques

2006

2006-1 Chaurand P., Rose J., Domas J. and Bottero J.-Y., "Speciation of Cr and V within BOF steel slag reused in road constructions", *7th Symposium on the Geochemistry of the Earth's Surface*, Aix-en-Provence (23-27 Août 2005), *J. of Geochemical Exploration* **88** (2006) 10-14

2006-2 Garcia P., Martin P., Carlot G., Castelier E., Ripert M., Sabathier C., Valot C., D'Acapito F., Hazemann J-L., Proux O., Nassif V., "The Effect of highly pressurised intra-granular bubbles on the mobility and release to grain boundaries of diffusing rare gas atoms in uranium dioxide", *E-MRS 2005 Spring Meeting*, Strasbourg (31 Mai – 3 Juin 2005), *J. of Nuclear Materials* (2006), accepté

2006-3 Magnien V., Neuville D.R., Cormier L., Roux J., Pinet O. and Richet P., "Kinetics of iron redox reactions: A high-temperature X-ray Absorption and Raman spectroscopy study", *E-MRS 2005 Spring Meeting*, Strasbourg (31 Mai – 3 Juin 2005), *J. of Nuclear Materials* (2006), accepté

2006-4 Sammut M.L., Noack Y. and Rose J., "Zinc speciation in steel plant atmospheric emissions: A multi-technical approach", *7th Symposium on the Geochemistry of the Earth's Surface*, Aix-en-Provence, (23-27 Août 2005), *Journal of Geochemical Exploration* **88** (2006) 239-242

2005

2005-1 Bellet E., Biquard X., Cibert J., Bougerol C., Ferrand D., Giraud R., Halley D., Kulatov E., Kuroda S., Marcet S., Mariette H., Titov A., "Properties of Ga1-xMnxN epilayers grown by molecular beam epitaxy", *27th International Conference on the Physics of Semiconductors*, Flagstaff, Arizona, EU, (26-30 juillet 2004), *AIP Conference Proceedings* **772** (2005) 365-366

2005-2 Hori Y, Andreev T, Biquard X, Monroy E, Jalabert Dang LS, D, Tanaka M, Oda O, Daudin B, "Rare-earth doped GaN and InGaN quantum dots grown by plasma assisted MBE", *International Workshop on Nitride Semiconductors (IWN 2004)*, Pittsburgh, Pennsylvania (19-23 Juillet 2004), *Physica Status Solidi C,* **2 issue 7** (2005) 2373-2376

2005-3 Manceau A. "Unlocking metal sequestration in soil nanoparticles" , *13th International Clay Conference*, Tokyo (August 21-27 2005), *Clay Science* **12** (2005) 61-63

2005-4 Marcet S., Bellet E., Biquard X., Cibert J., Bougerol C., Ferrand D., Giraud R., Halley D., Kulatov E., Kuroda S., Mariette H., Titov A., "Properties of $Ga_{1-x}Mn_xN$ epilayers grown by molecular beam epitaxy", *27th International Conference on the Physics of Semiconductors*, Flagstaff, Arizona (26-30 juillet 2004), *AIP Conference Proceedings* **772** (2005) 365-366

2005-5 Proux O., X. Biquard, E. Lahera, J.-J. Menthonnex, A. Prat, O. Ulrich, Y. Soldo, P. Trévisson, G. Kapoujvan, G. Perroux, P. Taunier, D. Grand, P. Jeantet, M. Deleglise, J.-P. Roux and J.-L. Hazemann, "FAME: A new beamline for X-ray absorption investigations of very-diluted systems of environmental, material and biological interests", XAFS XII Sweden (Juin 2003), *Physica Scripta* **115** (2005) 970-973

2004

2004-1 Andreev T., Hori Y., Biquard X., Jalabert D., Monroy E., Tanaka M., Oda O., Le Si Dang and Daudin B., "Optical and Structural Properties of Rare Earth Doped GaN Quantum Dots", *E-MRS 2004 Spring Conference*, France, (24-28 Mai 2004), *Superlattices and Microstructures* **36** (2004) 707-712

Communications orales

2006

2006-1 Manceau A., "Probing the structure of natural nanoparticles with micrometer-sized X-ray beams", *Winter Meeting of the Mineralogical Society of Great Britain*, Bath, UK, (January 5-6 2006) (**Conférence pleinière**)

2005

2005-1 Da Silva C., O. Proux, D. Testemale, O. Geaymond, R. Argoud and J.-L. Hazemann, "Solvation Properties of Zinc Bromide in Supercritical Solutions : Characterisation by X-ray Absorption Spectroscopy", Journées Société Espagnole de Minéralogie (SEM) et Société Française de Minéralogie et Cristallographie (SFMC), *1er meeting Hydrothermalisme, Solutions Aqueuses et Minéralogie*, Biarritz (3-4 novembre 2005)

2005-2 Froideval, A., Del Nero, M., Gaillard, C., Barillon, R., Rossini, I., Hommet, J., Hazemann, J.-L., "Spectroscopic investigations of uranyl sorption on aluminium hydroxide", Uranium Mining and Hydrogeology International Conference, Freiberg, Germany, (September 11 - 16, 2005)

2005-3 Garcia P., Martin P., Carlot G., Castelier E., Ripert M., Sabathier C., Valot C., D'Acapito F., Hazemann J-L., Proux O., Nassif V., "The Effect of highly pressurised intra-granular bubbles on the mobility and release to grain boundaries of diffusing rare gas atoms in uranium dioxide", E-MRS 2005 Spring Meeting, Strasbourg (May 31 to June 3 2005)

2005-4 Hazemann J.L., "Local structures in supercritical solutions: an in situ investigation by X ray radiation", Journées Société Espagnole de Minéralogie (SEM) et Société Française de Minéralogie et Cristallographie (SFMC), *1er meeting Hydrothermalisme, Solutions Aqueuses et Minéralogie*, Biarritz (3 et 4 novembre 2005) (**Conférence invitée**)

2005-5 Hazemann J.L., "Local structures in supercritical solutions: an in situ investigation by X ray radiation", *EMLG/JMLG* (European/Japanese Molecular Liquids Group) Annual Meeting 2005, Prague (4-8 septembre 2005) (**Conférence pleinière**)

2005-6 Lanson B. et Manceau A., "Structure determination of natural and synthetic nanocrystalline phyllomanganates", *13th International Clay Conference*, Tokyo (August 21-27 2005) (**Conférence pleinière**)

2005-7 Manceau A., "Unlocking metal sequestration in soil nanoparticles", *13th International Clay Conference*, Tokyo (August 21-27 2005) (**Conférence pleinière**)

2005-8 Manceau A., "Illuminating the complex world of environmental materials with bright synchrotron light", *2005 UK Synchrotron Radiation User Meeting.* Daresbury (September 13-14 2005) (**Conférence pleinière**)

2005-9 Manceau A., "Unlocking metal sequestration in soil nanoparticles", Symposium on 'Application of Synchrotron Science to Environmental Chemistry', *Canadian Chemistry Conference Annual Meeting*, Saskatoon (28 mai - 1er juin 2005) (**Conférence invitée**)

2005-10 Manceau A., "Bridging the gap between fundamental and applied research in environmental science at 3rd generation synchrotrons", Symposium on ' The Birth of a Dream: A Synchrotron Light Source in Canada. A Symposium in Honour of G. M. Bancroft', *Canadian Chemistry Conference Annual Meeting*, Saskatoon, Canada (28 mai - 1er juin 2005) (**Conférence invitée**)

2005-11 Manceau A., "Utilisation du rayonnement synchrotron pour l'étude de la spéciation des éléments traces (Ni, Zn, Pb...) dans le milieu naturel", *Colloque du Groupe Français des Argiles*, Paris, (18-19 Mai 2005) (**Conférence invitée**)

2005-12 Manceau A., Schlegel M.L. Rihs S. and Marcus M.A. "Natural speciation of Mn, Ni and Zn at the micrometer scale in a clayey paddy soil using X-ray fluorescence, absorption, and diffraction", *15th Annual Goldschmidt Conference Moscow*, Idaho, USA, (20 - 25 Mai 2005) , *Geochimica et Cosmochimica Acta* **69** issue 10 (2005) A612 (abstract)

2005-13 Martinez I., Testemale D., F. Dufaud, F. Guyot and J.L. Hazemann, "Experimental study of dissolution of siderite in high pressure high temperature H_2O-CO_2 fluids with implications for geological storage of CO_2" *European Geosciences Union*, General Assembly, Vienna, Austria, (24-29 Avril 2005), *Geophysical Research Abstracts*, **7** (2005) 09226

2005-14 Palancher H., Martin P., Ripert M., Dubois S., Valot C., Proyne C. and Mazaudier F., "Study of UMo/Al Interaction Layer by XRD and XAS with Micro-Focused X-Ray Beam", *2005 International Reduced Enrichment for Research and Test Reactors Meeting*, Boston, USA (6-10 Novembre 2005)

2005-15 Pokrovski G.S., Hazemann J-L., Testemale D., Roux J., Tella M., "Transport of metalloids by low-density hydrothermal fluids: Insights from X-ray absorption spectroscopy" , *15th Annual Goldschmidt Conference Moscow*, Idaho, USA, (20 - 25 Mai 2005), *Geochimica et Cosmochimica Acta* **69** issue 10 (2005) A734 (abstract)

2005-16 Sarret G., Willems, G., Manceau A., Marcus M.A., Saumitou-Laprade P., "Relationships between zinc tolerance and hyperaccumulation and zinc localization and speciation in Arabidopsis halleri", 8th International Conference on the Biogeochemistry of Trace Elements (ICOBTE), Adelaïde, Australia (3-7 Avril 2005)

2005-17 Schlegel M.L. and Manceau A. "Nucleation and epitaxial growth of Zn phyllosilicate on montmorillonite", *15th Annual Goldschmidt Conference Moscow*, Idaho, USA, (20 - 25 Mai 2005), *Geochimica et Cosmochimica Acta* **69** issue 10 (2005) A611 (abstract)

2005-18 Strobel P., C. Darie, F. Thiery, A. Ibarra-Palos, O. Proux, M. Bacia and J.-B. Soupart, "Electrochemical Lithium Intercalation in New Nanometric Cu- and Co-Doped Manganese Oxides Prepared by Thermal Decomposition of Carbonates", *2005 MRS Fall Meeting*, Boston (28 novembre - 2 décembre 2005)

2005-19 Strobel P., "Electrochemical lithium intercalation in nanosized manganese oxides", *13th International Symposium on Intercalation Compounds*, Clermont-Ferrand, (6-9 juin 2005)

2005-20 Testemale D., F. Dufaud, I. Martinez, F. Guyot and J.L. Hazemann, "Speciation of iron in high pressure high temperature H_2O-CO_2 fluids" *European Geosciences Union*, Vienna, Austria, (24-29 Avril 2005), *Geophysical Research Abstracts*, **7** (2005) 09447

2005-21 Thoral S., Rose J., Van Geen L., Garnier J.M., Chapon V., Hazemann J.L., Heulin T. and Bottero J.Y. "Oxidation of natural groundwater from Bangladesh: Arsenic speciation evolution assessed by XAS", *15th Annual Goldschmidt Conference Moscow*, Idaho, USA, (20 - 25 Mai 2005), *Geochimica et Cosmochimica Acta* **69** issue 10 (2005) A615 (abstract)

Communications par affiche

2006

2006-1 Laulhé C., F. Hippert, J. Kreisel, M. Maglione, A. Simon, J.L. Hazemann and V. Nassif, "Local structure of the relaxor ferroelectric $BaTi_{1-x}Zr_xO_3$", *Fundamental Physics of Ferroelectricity - 2006*, Williamsburg, USA (12 - 15 Février 2006)

2006-2 Palancher H., P.Martin, M.Ripert, C. Proye, F. Mazaudier, C. Valot, V. Nassif, O. Proux, A. Prat, M. Argoud, J.L. Hazemann, R. Tucoulou, "Study of UMo/Al interaction layer by μXRD and μEXAFS on ID18F and FAME at the ESRF", *1st User's Meeting Soleil*, Orsay (18-19 Janvier 2006)

2005

2005-1 Auffan M., Rose J. and Bottero J.Y. "Effects of maghemite (γ-Fe_2O_3) nanoparticles on the toxicity of arsenic within cultured human fibroblasts", *15th Annual Goldschmidt Conference Moscow*, Idaho, USA, (20 - 25 Mai 2005), *Geochimica et Cosmochimica Acta* **69** issue 10 (2005) A366 (abstract)

2005-2 Chaurand P., Rose J., Bottero J.-Y. and Domas J., "Environmental impact of BOF steel slag reused in road construction: a crystallographic approach", *2005 International Conference on Engineering for Waste Treatment* (WastEng05), Albi (17-19 mai 2005)

2005-3 Panfili F., Manceau A., Sarret G., Laboudigue A., Bert V. and Marcus M.A., "Changes in Zn speciation in the rhizosphere of graminaceous plants induced by phytostabilization of a contaminated sediment", *15th Annual Goldschmidt Conference Moscow*, Idaho, USA, (20 - 25 Mai 2005), *Geochimica et Cosmochimica Acta* **69** issue 10 (2005) A626 (abstract)

2005-4 Rose J., Benard A., Susini J., Borschneck D., Hazemann J.-L., Cheylan P., Vichot A. and Bottero J.-Y., "First insight of Cr speciation in leached Portland cement using X-ray spectromicroscopy", *2005 International Conference on Engineering for Waste Treatment* (WastEng05), Albi (17-19 mai 2005)

2005-5 Rihs S., Gaillard C., Manceau A.: Interaction of U(VI) with birnessite: a solution chemistry and EXAFS study. *15th Annual Goldschmidt Conference*, Moscow, Idaho, USA, (20 - 25 Mai 2005), *Geochimica et Cosmochimica Acta* **69** issue 10 (2005) A627 (abstract)

Thèses et Habilitations à Diriger les Recherches

2005

2005-1 Chen T.-H., "Etudes physico-chimiques des jades chinois", *Thèse de l'Université de Versailles / Saint Quentin en Yvelines spécialité Chimie et Sciences des Matériaux (2005)*

2005-2 Darie C., "Elaboration de composés oxydes à propriétés spécifiques", *Habilitation à Diriger des Recherches de l'Université Joseph Fourier de Grenoble* (2005)

2005-3 Lebrun S., "Minéralogie des précipités hydratés Fe-As dans un drainage minier acide: rôle des micro-organismes acidophiles"

2005-4 Magnien V., "Etude cinétique des réactions d'oxydoréduction dans les silicates",

2005-5 Poger D., Structure, dynamique moléculaire et sélectivité à métallochaperones à cuivre et à mercure, *Thèse de l'Université Joseph Fourier de Grenoble (2005)*

11. Rapports d'expériences ligne CRG-FAME 2004-2005

ESRF

ESRF	**Experiment title: High pressure XAS investigation of a relaxor ferroelectric: $PbMg_{1/3}Nb_{2/3}O_3$**	**Experiment number**: 30 02 665
Beamline: BM30B **Shifts:** 18	**Date of experiment**: from: 28-04-2004 to: 03-05-2004 and from: 08-09-2004 to: 13-09-2004 (test-time experiment) **Local contact(s)**: J.L. Hazemann	**Date of report**: 31-08-05 *Received at ESRF:* *06-09-05*

Names and affiliations of applicants (* indicates experimentalists):

F. Hippert*, J. Kreisel*, C. Laulhé*

LMGP, ENSPG

P. Bouvier*

LEPMI, ENSIEG

Report:

It is of primary importance to analyse the local structure of relaxor ferroelectrics, and especially the cations shifts, which are at the origin of the outstanding properties of these materials. The aim of the proposed experiment was to perform EXAFS experiments under high pressure at the Pb L_{III}-edge (13keV) and at the Nb K-edge (19 keV) in $PbMg_{1/3}Nb_{2/3}O_3$ (PMN), which is a canonical example of relaxor, widely studied by other techniques. In this compound, both the X-ray diffuse scattering and the Raman spectra are strongly affected by the application of high pressure [1].

We had planned to use a diamond anvil cell to apply the pressure, like in a previous experiment on another relaxor compound $Na_{0.5}Bi_{0.5}TiO_3$ (NBT), where we succeeded in collecting meaningful EXAFS data at the Bi L_{III}-edge (13.4 keV) up to 11.9 GPa[2]. It is known that diffraction processes within the two diamonds may spoil the EXAFS signal and that an adequate orientation of the cell has to be found, in order to minimize the amplitude of the glitches in the in the energy range of interest. With the diamonds used for the experiment on NBT, we could find such an orientation and collect EXAFS data in the range [13.3-13.9 keV]. However in the present case, we could not find adequate experimental conditions neither at the Pb- L_{III}-edge nor at the Nb K-edge. At the Pb L_{III}-edge, which occurs at nearly the same energy as the Bi L_{III}-edge, such a failure was rather unexpected. At the Nb K-edge, at 19 keV, the difficulties are still larger because the number of glitches increases with increasing energy, as it gets easier to meet diffraction conditions within the diamonds. After eliminating all causes of non-reproducibility linked with possible differences in the beam optics in the two experiments, it seems that the crystalline quality of the two diamonds or their relative crystallographic orientations are the key parameters to analyze. We tried several pairs of diamond without getting any noticeable improvement.

The remaining beam time has been used to study the EXAFS oscillations at the Zr K-edge in the $BaTi_{1-x}Zr_xO_3$ (BTZ_x) system. The BTZ_x relaxors ($0.25 = x < 0.50$) crystallize at any temperature in a cubic Pm-3m perovskite structure. Such an average structure cannot explain their observed outstanding properties. Moreover, contrary to the other relaxors which are compounds of fixed composition, BTZ_x forms a solid solution from $x = 0$ up to $x = 0.50$. In the low substitution regime ($x < 0.25$), classical ferroelectric properties are reported. The EXAFS experiments were performed at room temperature in the transmission mode on 2 ferroelectric BTZ_x samples ($x = 0.05$ and 0.20) and on 4 relaxors ($x = 0.25$, 0.30, 0.35, 0.40), in the transmission mode. In addition, $BaTi_{1-x}Zr_xO_3$ EXAFS spectra were also measured at 11 K for BaZrO3 and at 11K, 90 K and 150 K for BTZ35. The energy range [17.799–19.511 keV] was covered, using a Si(220) single crystal monochromator.

We performed the EXAFS data analysis in the R-range [1.15-4.52 Å], i.e. up to the fourth neighbours of Zr atoms, taking into account the multiple scattering paths which strongly contribute to the Fourier transform of the EXAFS signal between 3.0 and 4.0 Å. The quality of fits can be appreciated in Figure 1 for $BTZ_{0.35}$ at 10 K. The main results [3] are that, for all samples and at all temperatures, the Zr^{4+} cations are located at the centre of the octahedra formed by their six oxygen first neighbours. Furthermore, the obtained Zr-O distance (2.099 Å) is very close to its value in $BaZrO_3$ and independent of the Zr/Ti ratio (x), while the average cubic lattice parameter increases linearly with x, as expected for a solid solution. Zr atoms thus tend to reproduce the same first neighbour environment as in $BaZrO_3$, which is not polar. In the relaxor samples, the analysis of the further neighbours' contribution reveal departures from a perfect cubic structure. The oxygen atoms are ex-centred with respect to Zr-Zr bonds, but Zr, O, and Ti atoms are aligned. The shape of the ZrO_6 octahedra is thus affected by its chemical environment. A large distribution of Zr-Ba distances is observed. From these results, we can conclude that the origin of the relaxor behaviour in $BaTi_{1-x}Zr_xO_3$ is not linked with the ZrO_6 octahedron and must instead be linked to Ti^{4+} or Ba^{2+} displacements.

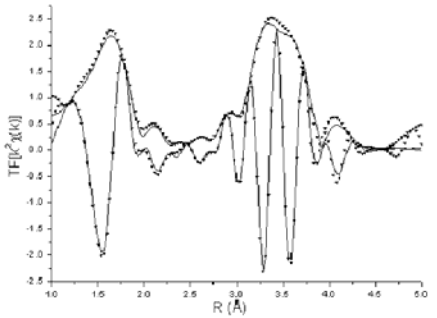

Fig.1: Imaginary and modulus of the Fourier Transform of the EXAFS signal for $BaTi_{1-x}Zr_xO_3$ at 10 K : experimental data (triangular dots) and fits (solid lines).

[1] J. Kreisel et al, Phys. Rev. B **65**, 172101 (2002) ; Phys. Rev. Lett **90**, 257601 (2003).
[2] ESRF experiment report HS2115.
[3] A publication on these results is written and should be submitted in a near future.

ESRF

ESRF	**Experiment title:** In-situ QEXAFS of the reactivity of bimetallic PtPd supported catalysts towards H2S : support effect and thioresistance.	**Experiment number:** SI 1106
Beamline:	**Date of experiment:** from: 29/096/04 to: 05/10/04	**Date of report:** 15/01/05
Shifts:	**Local contact(s):** Y. Soldo	*Received at ESRF:*

Names and affiliations of applicants (* indicates experimentalists):

Dr. Christophe GEANTET DR CNRS

Dr Pavel AFANASIEV CR CNRS

PhD student Nabil NAHAS

Dr. Herve PALANCHER postdoc

Dr Christophe PICHON Researcher IFP

Report:

Unfortunately the fluorescence detector required for the experiment was not available (the Canberra detector was expected to be back from the factory in GB after reparation). So, we had to modify our scheduled experiment and had to work in transmission mode. Two main studies were performed.

Activation of CoMo on alumina catalysts impreganted with triethyleneglycol.

We studied the activation of hydrotreating catalysts (CoMo on alumina) at both Co K-edge and Mo K-edge. We followed by QEXAFS the activation (transformation of the oxidic state into a sulfided state) under in-situ condions. the objective of the experiment was to compare the kinetic of sulfidation of a CoMo catalysts unpromoted and promoted with an organic compound : the triethyleneglycol TEG). The presence of such additive on the catalyst in the oxidic state enhances the catalytic performances. the origin of this promoting effect is not yet clarified and subject to many assumptions. One of them concerns the fact that the organic compound delays the sulfidation of the active phases and allows the formation of more active systems by this way. In the present study, we attempted by QXAS to follow during in situ sulfidation of CoMo on alumina catalysts containing various contents of TEG and a non promoted catalyst. The fist figures reflects this transformation during which Mo-O bonds are transformed into Mo-S bonds i.e. a contribution at higher distance in the FT. For the reference catalysts this nex contribution is clearly seen in the green curve corresponding to a temperature treatment of 140°C (series of FT on the left, arrow), by contrats with the TEG treated catalyst Mo-S contribution appears only à 200°C (yellow FT on the right, arrow).

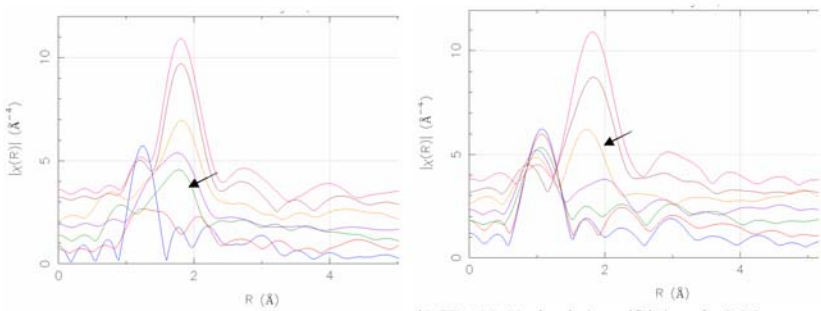

a) FT at Mo K edge during sulfidation of a CoMo on alumina reference catalysts .

b) FT at Mo K edge during sulfidation of a CoMo on alumina catalysts promoted with TEG.

A similar effect was obtained at Co K edge, indicating that the sulfidation of both elements is slowed down due to the presence of TEG.

Mo and Nb site occupancy in the $Nb_2Mo_3O_{14}$ oxide.

As recently established, mixed oxide $Mo_3Nb_2O_{14}$ has the Mo_5O_{14} – type structure eminently important for catalysis (Fig1). This compound, which can be considered as a generic host for the mixed oxide catalysts, demonstrates an original property of being partially auto-reduced independently on the preparation conditions. To explain this unusual finding, substitutional disorder between Nb and Mo was suggested which induce instability of O15 atom to the second order Jan Teller distortion and further internal redox rearrangement. The closeness of Nb and Mo masses prevents from determination of occupational distribution between Nb and Mo. EXAFS is the only technique able to provide information on the site occupancy in this system. As clearly demonstrates comparison of the EXAFS spectra, Nb and Mo in this solid have different coordination (Fig2).

Double edge fit reveals a strong tendency of Nb to occupy pentagonal bipyramids, whereas molybdenum has preference for distorded octahedral, containing abundant double bonds. Distinguishing the preferential occupation of sites by Nb and Mo is crucial for the understanding of this newly observed phenomenon of the mixed oxide structurally –induced auto-reduction.

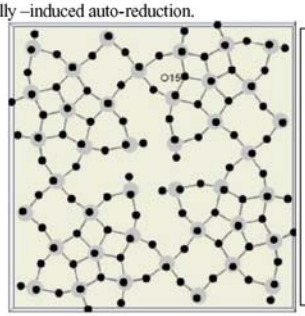

Fig.1 Mo5O14 structure with the O15 atom marked

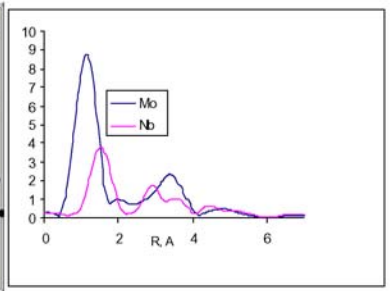

Fig.2. FT module of Nb and Mo K edge spectra

ESRF	Experiment title: **A XAFS spectroscopy study of antimony speciation and the solubility of Sb-bearing minerals in high-temperature geological fluids: Implications for metal-solvent interactions at critical conditions, and Sb transport in hydrothermal environments**	**Experiment number**: 30-02-644
Beamline: BM30B	**Date of experiment**: from: 28 October 2004 to: 02 November 2004	**Date of report**: 21 January 2005
Shifts: 15	**Local contact(s)**: Dr. Jean-Louis Hazemann, FAME, ESRF	*Received at ESRF:*

Names and affiliations of applicants (* indicates experimentalists):

***Gleb Pokrovski**, Experimental Geochemistry and Biochemistry Group, LMTG-UMR5563, Toulouse, France
***Marie Tella**, same address
***Jacques Roux**, Physique des Minéraux et des Magmas, IPGP-UMR7047, Paris, France
***Jean-Louis Hazemann**, Laboratoire de Cristallographie & SNBL/ESRF, Grenoble, France

Report:

Experimental: Dissolution of natural senarmontite (Sb_2O_3, cubic) and local atomic structure around Sb(III) in pure water and NaCl-HCl aqueous solutions were characterized by *in situ* XAFS spectroscopy at Sb K-edge (~30.5 keV) at temperatures to 500°C and pressures to 600 bar, using a new X-ray cell [1]. This cell allows simultaneous measurement of the absolute concentration of the absorbing element in the fluid (from edge-step height in transmission mode, fluid density and absorption cross-section of the element), and atomic environment around the absorber (from analysis of XANES and EXAFS spectra in fluorescence and transmission modes). Details about the cell operation, spectra analysis and solubility determination can be found elsewhere [2]. The new sample-holder design consists of a vertically oriented glassy-carbon tube with two mobile sapphire pistons inside fitted with Viton seals. This allows controlled changes of the cell internal volume with temperature and pressure. The new construction avoids solute precipitation in the colder parts of the cell and permits acquisition of high-quality spectra on dilute systems because of the low X-ray absorption of the glassy carbon.

Results on Sb local atomic structure in the fluid: Four different experiments were performed. Spectra of aqueous Sb in pure water in equilibrium with Sb_2O_3 from 250 to 400°C at 600 bar (Experiment 1) exhibit a single-shell contribution from 3±0.3 oxygens at 1.97±0.01 Å, consistent with the $Sb(OH)_3$ complex, similar to $As(OH)_3$ [3,4]. Spectra of a 0.1m Sb(III) - 3.1m HCl aqueous solution (Experiment 5) show a single Sb-Cl shell with average number of Cl atoms increasing from 2 to 3 and Sb-Cl distances decreasing from 2.43 to 2.38 Å when temperature changes from 30 to 400°C at 600 bar. This is consistent with the formation of Sb chloride complexes, in agreement with previous EXAFS studies [5]. In a 2.0m NaCl - 0.1m HCl solution in equilibrium with senarmontite at 600 bar (Experiment 2), Sb exhibits two nearest-shell contributions arising from 2.4±0.3 O at 1.97±0.01 Å and ~0.4±0.2 Cl at distances decreasing from 2.45 to 2.37 Å when temperature raises from 200 to 450°C (Fig. 1). In addition, a fourth experiment was performed in the same system at the vapor-liquid equilibrium at 400°C and 320-270 bar (Experiment 3/4, Fig. 3A). Sb atomic environment in the liquid phase is identical to that of Experiment 2, implying same mixed OH-Cl complexes. Although the poor statistics of the vapor-phase spectrum does not allow quantitative treatment, their XANES part is close to that of the liquid-phase spectra, thus suggesting the formation of analogous species (Fig. 3B).

Results on Sb_2O_3 solubility and vapor-liquid partitioning in high-temperature fluids: Monitoring the amplitude of absorption edge of transmission spectra as a function of time shows that senarmontite-solution equilibrium in Experiments 1, 2 and 3/4 was attained within an hour at temperatures above 200°C. The derived Sb equilibrium concentrations in pure water (Fig. 2) are in excellent agreement with previous predictions based on batch-reactor measurements which were interpreted by the formation of a neutral hydroxide $Sb(OH)_3$ [6]. In the presence of chloride (Experiment 2), senarmontite solubility is ~3 times higher in the range 200-450°C, demonstrating the formation of other Sb complexes (Fig. 1, 2). Combining the measured solubility increase with the average numbers of O and Cl neighbors around Sb derived from the EXAFS analysis above, we conclude that $Sb(OH)_3°$, $Sb(OH)_2^+$ and $Sb(OH)_2Cl°$ contribute almost in equal proportions to the solubility in the NaCl-HCl solution studied. Thus, contrary to previous expectations [6], mixed hydroxide-chloride species may play a major role in Sb transport in acid saline ore-forming fluids. This new finding is also supported by our preliminary batch-reactor measurements (unpublished).

Our X-ray cell allowed the first *in situ* measurement of vapor-brine fractionation in a water-salt-acid system (Experiment 3/4, Fig. 3A,B). The Sb vapor-liquid partition coefficient derived at 400°C/270 bar with ~0.1m HCl, K_{Sb}=0.092±0.030, is about 2 times higher than that measured using a batch reactor at the same conditions in HCl-poor

system (<0.01m HCl) where Sb vapor- and liquid-phase speciation is dominated by $Sb(OH)_3$, K_{Sb}=~0.045 [7]. This is the first demonstration that mixed Cl-OH species can significantly contribute to antimony volatility in boiling acid salt-rich natural fluids.

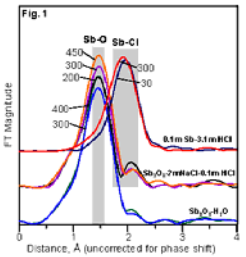

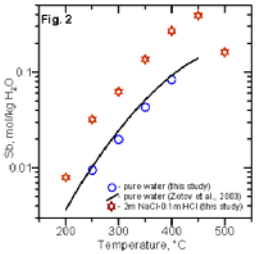

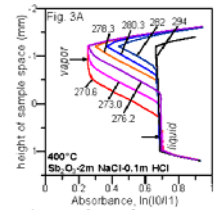

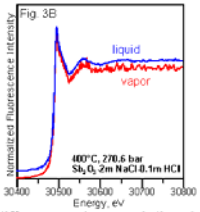

Fig. 1 Fourier Transforms of EXAFS spectra of 3 different experiments at indicated temperatures. Sb-O and SbCl contributions are indicated by the shaded regions.
Fig. 2 Senarmontite solubility in water and NaCl-HCl solutions at 600 bar.
Fig. 3 Demixtion experiment 3/4. **(A)** Absorbance measured at beam energy 30.57 keV by scanning the height of the cell at indicated pressures. Appearance of the low-density vapor phase is manifested by lower absorbance in the upper part of the cell with decreasing pressure. **(B)** Normalized XANES spectra of the coexisting phases recorded at 400°C/270.6 bar by subsequently positioning the cell at the beam passage heights indicated by arrows in Fig. 3A. Spectra are shifted along the Y-axis for clarity.

Conclusion and perspectives: This experiment demonstrated the capabilities of the XAFS technique for *in situ* measuring of mineral solubilities and, for the first time, vapor-liquid partitioning in high-temperature/pressure near-critical solutions. Our study provides new data about Sb speciation, stability and structure in acid saline fluids typical of natural hydrothermal-magmatic systems. Work is currently in progress to combine these results with batch-reactor solubility data to provide a consistent set of thermodynamic properties of Sb-OH-Cl complexes allowing prediction of Sb transport by crustal fluids. Our near-future projects are intended to better explore by XAFS spectroscopy the role of chloride and sulfide, the major natural ligands, in the transport and vapor-liquid distribution of noble metals, Ag and Au, using this new promising cell design.

References:

1. Testemale D., Argoud R., Geaymond O., Hazemann J-L. A high pressure/high temperature cell for X-ray absorption and scattering techniques. *Rev. Sci. Instruments (submitted).*
2. Pokrovski G.S., Roux J., Hazemann JL., Testemale D. (2005) An X-ray Absorption spectroscopy study of argutite solubility and aqueous Ge(IV) speciation in hydrothermal fluids to 500°C and 400 bar. *Chem. Geology (in press).*
3.Pokrovski G.S., Zakirov I.V., Roux J., Testemale D., Hazemann JL., Bychkov A.Y., Golikova G.V. (2002) Experimental study of arsenic speciation in vapor phase to 500°C: Implications for As transport and fractionation in low-density crustal fluids and volcanic gases. *Geochim. Cosmochim. Acta* **66**, 3453-3480.
4.Testemale D., Hazemann JL., Pokrovski G.S., Joli Y., Roux J., Argoud R. & Geaymond O. (2004) Structural and electronic evolution of the $As(OH)_3$ molecule in high-temperature aqueous solutions: an X-ray absorption investigation. *J. Chem. Phys.* **121**, 8973-8982.
5. Oelkers E.H., Sherman D.M., Ragnarsdottir V.K., Collins C. (1998) An EXAFS spectroscopic study of aqueous antimony(III)-chloride complexation at temperatures from 25 to 250°C. *Chem. Geology* **151**, 21-27.
6.Zotov A.V., Shikina N.D., Akinfiev N.N. (2003) Thermodynamic properties of the Sb(III) hydroxide complex $Sb(OH)_3$(aq) at hydrothermal conditions. *Geochim. Cosmochim. Acta* **67**, 1821-1836.
7.Pokrovski G.S., Roux J., & Harrichoury J-C. Fluid density control on vapor-liquid partitioning of metals in hydrothermal systems. *Geology (submitted).*

Gleb Pokrovski (Octobre 2005) *Experiment title: A XAFS spectroscopy study of antimony speciation and the solubility of Sb-bearing minerals in high-temperature geological fluids: Implications for metal-solvent interactions at critical conditions, and Sb transport in hydrothermal environments*

ESRF	**Experiment title:** **Local order and nanostructure in Al-Y-Fe amorphous alloy**	**Experiment number:** ME973
Beamline: BM30B	**Date of experiment:** from:03/11/2004 to: 09/11/2004	**Date of report:**
Shifts:	**Local contact(s):** Vivian Nassif, Olivier Proux, Jean-Louis Hazemann	*Received at ESRF:*

Names and affiliations of applicants (* indicates experimentalists):

A. Sadoc [1]*, O. Heckmann[1]*, L.Q. Xing [2], K.F. Kelton [2]

[1]LPMS, Université de Cergy-Pontoise, Neuville sur Oise, 95031 Cergy-Pontoise, Cedex, France
[2] Department of Physics, Washington University, St. Louis, MO 63130, USA.

Preliminary report:

Amorphous AlYFe alloys doped either with titanium or vanadium have been studied by EXAFS in order to determine the local structure around the doping element and to compare it to the short range order obtained previously around the major constituents. Amorphous ribbons of $Al_{87.5}Y_7Fe_5Ti_{0.5}$, $Al_{86}Y_7Fe_5Ti_2$, $Al_{87.5}Y_7Fe_5V_{0.5}$ and $Al_{87.35}Y_7Fe_5V_{0.65}$, prepared in Washington University [1,2], were investigated on the BM30B beam line. The X-ray absorption spectra at the Ti (4964 eV) and V (5463 eV) K edges were recorded with a Si (220) monochromator in the fluorescence mode. A 32-elements fluorescence detector was used. The data were collected at room temperature and, with a liquid helium cryostat, at low temperature (16 K). The ribbons were only 1mmm wide and the well focused X-ray beam available on BM30B was essential for these experiments. Moreover, the use of the fluorescence detector was also determining since the signal to noise ratio was very small for these dilute samples with low concentration (0,5 to 2%). The spectra are given in figure 1 for the different samples and the two different temperatures.

1 - , L.Q. Xing, S.Y. Tao and K. F. Kelton, 2002, Appl. Phys. Lett., **81**, 3371

2 - L.Q. Xing, Anindita Mukhopadhyay, William E. Buhro, and K. F. Kelton, 2004, Phil. Mag. Let. 84, 293.

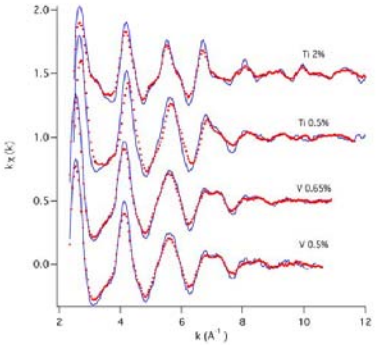

Figure 1: The EXAFS spectra, $k\,\chi(k)$, of the samples (red dots: room temperature, blue solid curve: 16K) studied for the Ti and V K edges and for the different concentrations: Ti: 2 and 0.5 %, V: 0.65 and 0.5 %.

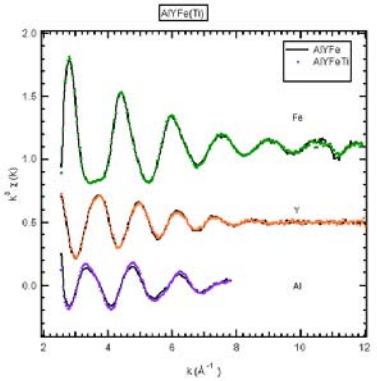

Figure 2: EXAFS spectra for the Al, Y and Fe and K absorption edges of $Al_{88}Y_7Fe_5$ (solid curve) and $Al_{87.5}Y_7Fe_5Ti_{0.5}$(dots).

The spectra become a little more intense with decreasing temperature and, consequently, decreasing dynamic disorder. They are very similar for the two vanadium concentrations, 0.5 and 0.65 %. The spectra obtained for the two titanium concentrations, 0.5 and 2 %, show similarities. They are, however, more structured for the highest concentration, in particular near 5 and 7 $Å^{-1}$. Nevertheless, all these spectra appear structured, the effect being more evident for titanium than for vanadium, and for the highest titanium concentration. The important point is that these spectra look different from those obtained for the Al, Y and Fe K edges in the same amorphous samples with or without titanium (figure 2). Likewise, the Fourier transforms of the spectra clearly show peaks of second neighbours around Ti and V atoms, while they do not around the major constituents of the samples. Consequently the local order should be different.

This is confirmed by preliminary calculations using the program feffit. The spectra for the Al, Y and Fe edges can be reconstructed using one shell of 12 Al first neighbours at a distance from the absorbing atom between 2.70 and 3.12 Å, depending of the central element. However, it is not possible to reconstruct the experimental spectra for the Ti and V edges with only one shell of Al neighbours. Second Al nearest neighbours are necessary (Al atoms at about 4.3 Å), which is the fingerprint of intermediate-range order.

Therefore, titanium and vanadium may change, enhance local ordering in these amorphous alloys.

Rapport d'expérimentation

Etude des jades chinois par XAFS janvier 2005

Des jades chinois ont été analysés par spectrométrie d'absorption des rayons X sur la ligne BM30B à l'ESRF. Cette expérimentation a visé à étudier l'effet du chauffage sur les jades ainsi que l'origine de leur couleur. Le jade-néphrite ($Ca_2(Mg, Fe^{2+})_5[Si_8O_{22}](OH, F)_2$) est formé d'agrégats minéraux d'actinote-trémolite appartenant au groupe des amphiboles. Le degré d'oxydation du fer et la géométrie des sites sont censés être les clés pour répondre aux questions posées. Pourtant, sachant que dans les échantillons mis en jeu, la teneur en fer est relativement faible (< 1 wt %), il est difficile de mesurer l'état d'oxydation du fer par des techniques analytiques telle que les spectrométries Mössbauer ou Raman en raison de leur limite de sensibilité. La spectrométrie d'absorption des rayons X au seuil K de fer est donc une méthode idéale pour cette étude.

Analyse de jades chinois du Musée Guimet à Paris

Sept objets en jade, datant du Néolithique (c. 3200 -2000 av. J. -C.) aux dynasties *Song* (960 – 1279 apr. J. -C.), du Musée Guimet à Paris ont été analysés. La Figure 3 présente un pendentif en forme de dragon de la dynastie des *Han* occidentaux. Ce jade vert-jaune en néphrite contient une partie marron dont l'origine reste à élucider. Dans les spectres XANES (Figure 4), les pré-pics de la zone vert clair et de la zone brune sont similaires, le changement de la couleur n'est donc probablement pas lié au degré d'oxydation du fer. Par contre, une légère différence a été remarquée dans les épaulements du seuil d'absorption qui montre que les géométries des sites de ces deux zones ne sont pas identiques et qu'elles peuvent avoir une relation avec la modification de couleur.

Figure 1. Un jade chinois *Cong* (Culture de Qijia, env. 2000 av. J.-C.) du Musée Guimet sur la ligne BM30B à l'ESRF

Figure 2. Pendentif en forme d'oiseau, néphrite, Royaumes Combattants (475 – 221 av. J.-C.)

Figure 3. Pendentif évidé en forme de dragon, néphrite, *Han* occidentaux, 206 av. J.-C. - 9 apr. J.-C.

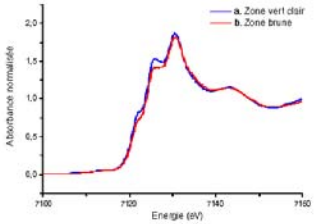

Figure 4. Spectres XANES du pendentif a. zone vert clair; b. zone brune.

Effet du chauffage

Trois séries de jades de référence préalablement chauffés à des températures différentes pendant 24 heures ont été étudiées par XAFS à la température ambiante ainsi qu'à 11K afin de mieux comprendre l'effet du chauffage sur les jades. Les jades changent de couleur à partir de certaines températures de chauffe. Sans transformation de phase au-dessous de 800°C, il s'agit de la modification de l'état d'oxydation (Fe^{2+} ? Fe^{3+}) et de la géométrie des sites.

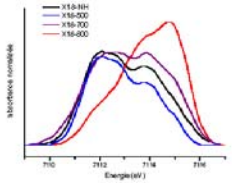

Figure 5. Pré-pics de la série X18

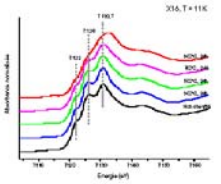

Figure 6. Spectres XANES de la série X18

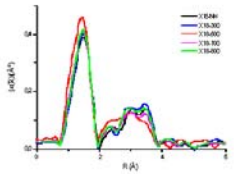

Figure 7. Transformée de Fourier des spectres EXAFS de la série X18

Effet du faisceau

Pendant l'expérimentation, un délicat effet du faisceau sur les échantillons a été observé. Plus précisément, les rayons X réagissent légèrement avec les échantillons durant l'analyse et une évolution entre les spectres mesurés consécutivement sur la même zone d'un échantillon a été remarquée. Les épaulements et les crêtes du seuil d'absorption décroissent en fonction du temps (Figure 8). Le temps d'acquisition de chaque spectre XANES de la figure 8

était de 3 minutes. Si le temps de mesure augmente, les spectres sont plus décalés en intensité. La figure 9 montre une mesure cinétique à l'énergie 7126,2eV à 11K sur un même point de l'échantillon X22-NH. L'intensité détectée décroît d'une manière exponentielle de second ordre en fonction du temps.

Ce phénomène ne résulte pas d'un changement de phase, il s'agirait plutôt de l'échange des cations dans les sites M1, M2 et M3 qui sont occupés par Fe et Mg. En conséquence, la géométrie des sites est plus ou moins modifiée et les spectres sont un peu différents.

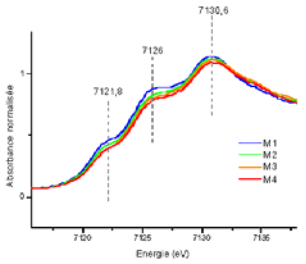

Figure 8. Spectres XANES de l'échantillon X22-NH (néphrite). Quarte mesures (M1, M2, M3 et M4) consécutives effectuées à la température ambiante sur une même zone.

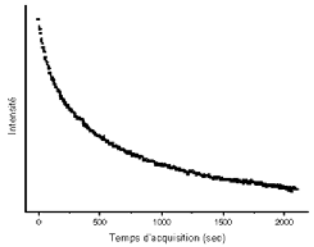

Figure 9. Mesure cinétique à l'énergie 7126,2eV à 11 K sur l'échantillon X22-NH.

Conclusion

La spectrométrie XAFS par synchrotron est une technique idéale pour analyser les objets du patrimoine, en l'occurrence les jades chinois, d'une manière non-destructive, en fournissant des informations sur l'environnement structural de l'atome ciblé (ici le fer), ainsi que son état d'oxydation. Malgré l'effet du faisceau, un phénomène qui mérite d'être étudié plus profondément, les résultats obtenus dans cette étude donnent des informations complémentaires pour explorer l'origine de la couleur et l'effet du chauffage.

ESRF	**Experiment title:** **Iron speciation in high pressure high temperature H_2O-CO_2 fluids in contact with crystalline siderite and /or magnetite**	**Experiment number**: HS 2628
Beamline: BM30b	**Date of experiment**: from: 8/12/2004 to: 15/12/2004	**Date of report**: 25/02/05
Shifts: 21	**Local contact(s)**: Olivier PROUX	*Received at ESRF:*

Names and affiliations of applicants (* indicates experimentalists):

D. Testemale*, SNBL/ESRF;

I.Martinez*, F. Dufaud*, IPGP, Paris.

F. Guyot*, LMCP, Université ParisVI.

J. L. Hazemann, CNRS-Laboratoire de Cristallographie, Grenoble.

Geological context

We have carried out a first series of experiments to study the reactivity of $FeCO_3$ siderite in water under acidic conditions up to 1000 bar and 300°C, according to reaction:

(1) $FeCO_3 + 2\,H^+ \rightarrow Fe^{2+} + H_2O + CO_2$

In deep geological storage context, the quantity of CO_2 that cannot be sequestred as carbonate is directly related to the concentration of Fe^{2+} in the fluid. We have measured, for the first time under hydrothermal conditions, the dissolution of siderite in water by monitoring *in situ* the concentration of Fe^{2+} at different pressures, temperatures and pH. First data on speciation of Fe in the relevant fluids have also been recorded.

Experimental details

High pressure-high temperature XAFS spectroscopy analyses were performed at the Fe K-edge, using an X-ray cell developped at the Laboratoire de Cristallographie (Grenoble). A total of six experiments were performed: (a) $FeCl_2$ (0.05M) + HCl (0.1M), (b) $FeCl_2$ (0.05M) + HCl (0.1 M) + NaCl (1M); (c) $FeCl_2$ (0.05M) + oxalic acid (0.05 M) used as a source of CO_2 above 150°C; (d) siderite + HCl (0.1M); (e) siderite + HCl (0.1 M) + NaCl (1M); (f) siderite + oxalic acid (0.05 M). In each experiment, data were obtained at different temperatures along isobars up to 300°C and 1000 bar.

Results

The experiments with $FeCl_2$ provide reference data for both Fe^{2+} concentration and speciation in solutions under high pressure and high temperature: in figure 1, there is a clear temperature dependence of the Fe local solvation structure The presence of NaCl (1M) was shown to have no major effect on speciation.

The solubility results can be adequately fitted with available thermodynamical data, provided that the specific heats of compounds involved in reaction (1) be adjusted. Precise refinments on solubility data could further provide important constraints on thermodynamic parameters of reaction (1). In particular, a tentative increase in solubility of siderite, unexpected for carbonates, that was measured between 100°C and 300°C (figure 2, left) can be modelled with an adequate set of specific heats.

The kinetics of siderite dissolution in HCl (0.1 M) was determined at 300 bar and 100°C (figure 2, right). NaCl apparently decreased the dissolution of siderite, a behaviour which remains to be explained using thermodynamical parameters and a fine analysis of the spectroscopic data on Fe speciation in the fluid. In the case of dissolution of siderite in oxalic acid solutions, two regimes should be considered: (1) a low temperature regime (T<150°C,) below decomposition temperature of oxalic acid, where dissolution is lower than in HCl solutions at the same conditions (at 100°C, a concentration of 9mmol of Fe^{2+} is measured compared to 30mmol in HCl solutions); 2) a high temperature regime (T>200°C) where a decrease of solubility is observed (<4mmol at 250°C). This decrease can be attributed to the presence of carbon dioxide which is a weaker acid than oxalic acid.

Perspectives

These first results are encouraging; a publication is in preparation. Longer acquisition time spectra would be important for determining the exact speciation of Fe2+ in those H2O-CO2-Cl fluids. It would be desirable to better control the activity of CO_2 which is a key parameter in the dissolution reaction. The use of oxalic acid decomposition as a source of CO_2 is a limiting factor because of the equivalent low partial pressure of CO_2 available (we estimate a maximum PCO_2 of 3 bar in our experiments). A direct loading of CO_2/H_2O mixtures at ambient temperature would be a good method to control and vary this parameter, essential for appropriate modelling of these reactions.

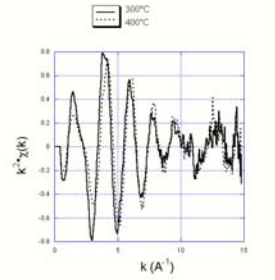

Figure 1: EXAFS oscillations of 0.05M FeCl2 solutions at 300 bar (300 and 400°C).

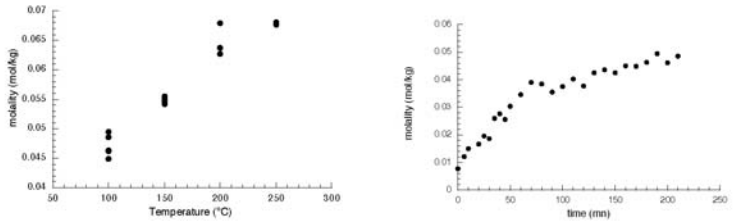

Figure 2: Left: Evolution of Fe^{2+} concentration in the fluid at 300bars as a function of temperature. Right: Concentration of Fe^{2+} (in mol/kg) at 300bar-100°C as a function of time.

ESRF	Experiment title: **Arsenic oxidation and accumulation by *Euglena mutabilis* in acid mine drainage : XAS imaging of arsenic speciation.**	**Experiment number**: ME 978
Beamline:	**Date of experiment**: 28/01/2005 at 8:00 to 04/02/2005 at 8:00	**Date of report**: 18/03/2004
Shifts:	**Local contact(s)**: Olivier Proux, Jean-Louis Hazemann	*Received at ESRF:*

Names and affiliations of applicants (* indicates experimentalists):

Guillaume MORIN*, Prof. François GUYOT* , Jennyfer MIOT * / IMPMC UMR7590 - Paris6&7 – IPGP, 140 rue de Lourmel 75015 Paris

Corinne CASIOT, Jean-Christian PERSONNÉ, Françoise ELBAZ -POULICHET / HYDROSCIENCES - UMR 5569, Université de Montpellier II

Report:

This report concerns the 15 shifts allocated on the BM30B beamline to run bulk Euglena samples at the As K-edge. Shifts requested in the project to perform X-ray imaging of the samples on ID22 were not allocated. EXAFS and XANES data were recorded at 10K at the As-K edge (11 869 eV) using a Si(220) monochromator at the BM30B/FAME beamline (Figs 1-3). Data were recorded in fluorescence mode using a 30 elements Ge - array detector completed by a 3 to 9 $\Delta\mu$ Ge filter to attenuate elastic scattering and Fe fluorescence from Fe-rich samples. The high flux at the sample allowed us to record good EXAFS data on very dilute samples (< 500 ppm wt. As; Fig. 2). Thanks to horizontal focusing, energy resolution was also about 0.5 eV. EXAFS and XANES data were recorded in step-scan mode after recording few quick-XANES spectra in order to check for unwanted photo-oxidation or reduction of the samples under the beam.

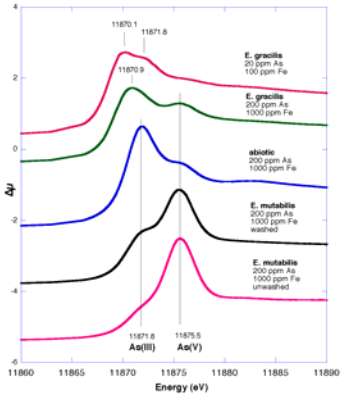

Figure 1. As-K XANES spectra of cell suspensions of *E. gracilis* and *E. mutabilis* grown in Fe^{II} and As^{III} bearing media.
In *E. gracilis*, absorption maximum at 11870.1 eV can be related to MeAsDMPS (monomethylarsenic 2,3-dimercapto-1-propane sulfonic acid) or to $As(Glu)_3$ (arsenic glutathione). Absorption maximum at 11871.8 eV can be related to As(III). Absorption maximum at 11870.9 eV can be related to MMA(III) (monomethyl arsonous acid) or to Me2AsDMPS (dimethylarsenic 2,3-dimercapto-1-propane sulfonic acid). (Smith et al. 2005)
In *E. mutabilis*, absorption maxima at 11871.8 and 11875.5 eV correspond to As(III) and As(V) respectively.

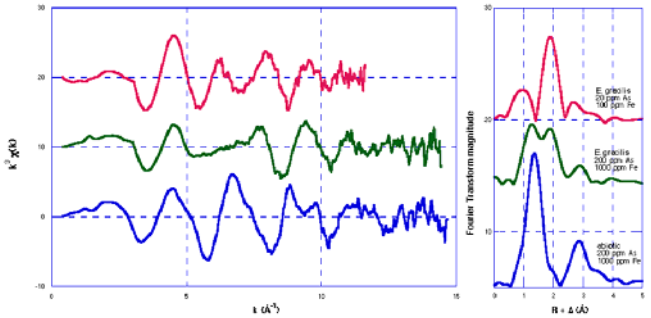

Figure 2. Comparative plot of EXAFS data on cell suspensions of E. gracilis grown in 100 ppm Fe and 20 ppm As^{III} E. gracilis grown in 1000 ppm Fe and 200 ppm As^{III}, and abiotic precipitate from the 1000 ppm Fe and 200 ppm As^{III} solution.

Preliminary shell-by-shell analysis of the EXAFS signal indicates dominant contribution of As-S bonds in *E. gracilis* grown in 20 ppm As(III) and 100ppm Fe medium, which is consistent with metabolization of arsenic as $As(Glu)_3$ and DMPS compounds. The additional presence of inorganic As(III) in *E. gracilis* grown in 200 ppm As(III) and 1000ppm Fe medium is related to the mixture with amorphous abiotic precipitate.

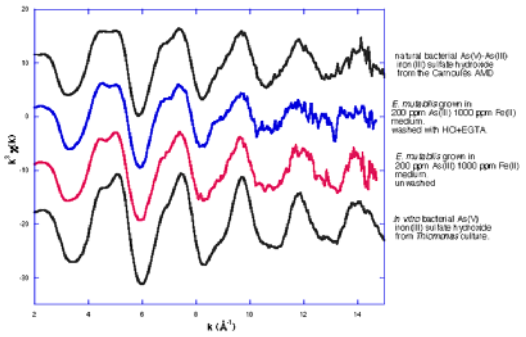

Figure 3. EXAFS data on cell suspensions of *E. mutabilis* grown in Fe^{II} and As^{III} rich media compared with EXAFS data of bacterial precipitates. The latter correspond to poorly ordered mixed As(III)-Fe(III) and As(V)-Fe(III) iron(III) sulfate oxy-hydroxides.

Similarity of the As-EXAFS spectra of *E. mutabilis* with those of bacterial Fe(III)-As(III) and Fe(III)-As(V) sulfate oxyhydroxides suggests that the major part of As(III) is co-precipitated in such mineral phases. These compounds have been already identified as products of the activity of *Acidithiobacillus ferrooxidans* and *Thiomonas* sp. (Morin et al. 2003; Duquesnes et al. 2003). These strains are abundant in the Carnoulès acid mine drainage from which the *E. mutabilis* were collected. The difficulty to separate bacteria from *E. mutabilis* cells upon the isolation procedure might explain the difference in arsenic speciation in *E. gracilis* and *E. mutabilis* samples. This result enlightens the major role of bacteria in detoxifying the Carnoulès water. Imaging arsenic speciation at the micron scale in both species would yield crucial information about the mechanisms of arsenic metabolization and sequestration.

Smith et al. (2005) *Environ. Sci. Technol.* 39, 248-254.
Morin et al. (2003) *Environ. Sci. Technol.* 37, 1705-1712.
Duquesne et al. (2003) *Appl. Environ. Microbiology* 69/10, 6165-6173.

Selenium reduction by Agrobcaterium tumefaciens

The reduction of selenite (Na_2SeO_3, IV) by strain C58 of *Agrobacterium tumefaciens* [1 , 2] follows two different and independent detoxification pathways, which are not yet characterized at the molecular level. Selenite is either reduced directly to elemental selenium (0) [3] or to dimethyl selenide (CH_3-Se-CH_3, II) and di-methyl-di-selenide (CH_3-Se-Se-CH_3, II) [2]. Metal reduction and oxidation kinetics are accessible to X-ray analyses [4, 5]. We have shown that the combination of µXANES and µXRF analyses allow the efficient monitoring of the oxidation states of Selenium in solution during microbial reduction [4], with a detection limit lower than 1ppm in cultures performed at room pressure in the laboratory.

Performing the same analyses *in situ* requires the direct contact between the live cells and the X-ray beam. X-rays are very damageable to living cells, inducing direct physical damage to organic molecules and structures, although there was no quantitative data available for micro organisms. Preliminary experiments showed that strain C58 does not survive the X-ray irradiation, which would be required to acquire 1 set of XANES or XRF spectra (less than 1 surviving cell in 10^{+8} cells, Oger et al. unpublished). The sterilizing impact of X-ray is however limited to the cylinder defined by the intersection of the X-ray beam and the sample. Therefore, providing the beam size is sufficiently small compared to the experimental volume, it might be possible to study cell driven metabolism and correct for the loss of viability. This hypothesis was tested with strain C58 to evaluate the compatibility, the sensitivity and the efficiency of XANES to study the kinetics of selenite reduction by live prokaryotes *in situ* under controlled pressure and temperature.

Experimental setup

Cells from an overnight culture of *Agrobacterium tumefaciens* strain C58 [6] were washed twice with fresh low salt LB medium (10 g yeast extract, 5 g peptone, 5 g NaCl per liter), resuspended in the same medium supplemented with 5 ppm sodium selenite (Na_2SeO_3, Sigma-Aldrich™, France) at a final density equivalent to an OD_{600} of 10. The high pressure cell of beamline BM30B was loaded with the bacterila suspension. The temperature inside the high pressure cell was raised to the optimal growth temperature of strain C58, *e.g.* 30°C, after the reference XRF and XANES spectra at t=0 were acquired.

The size of the beam was 150 µm x 300 µm (vert. x hor.), for an incident flux ca. 1-3 10^{10} ph/s. Spectra were acquired for 100s live time. The incident flux, used for normalization was measured using an ionisation chamber placed before the sample. The XANES spectra were acquired in the fluorescence mode for 1s per point (101 points) in the range 12.60-12.78 keV. µXRF and µXANES data were acquired every hour, while maintaining the DAC on the beamline.

Se concentrations in solution was derived from the transmission spectra. The redox state of Se species in solution was derived from the centroid of the normalised XANES spectra. The relative proportion of each species was determined by fitting the experimental spectrum with a linear combination of individual µXANES spectra obtained for standard Se species [4].

Kinetics of Selenite reduction by live microbes

Figure 1 summarizes the results obtained for an experiment performed at 25 MPa (Oger unpublished results). The shift of the spectrum towards lower energies indicates that selenite is reduced over the 24 hours of the experiment. This reduction is not observed if C58 cells are not added to the medium. However, no reduction of selenite was also observed for an experiment performed at 60MPa (Data not shown). The spectrum obtained at 0h is typical of selenite. Spectra acquired for intermediate incubation times clearly show a gradual replacement of selenium species in solution, with the apparition of a shoulder on the XANES spectra. After 24 hours, the XANES spectrum does not show any contribution of selenite. It

does not however correspond to elemental selenium nor to a methylated selenide species. Linear combinations of 7 different redox species of selenium showed that only two species contributed significantly to the experimental data, elemental selenium and di-methyl selenide (Oger, unpublished). By using a combination of the spectra from selenite, di-methyl selenide and selenium, we can reproduce the experimental data (Figure), and determine that for each molecule of selenium, two molecules of methylated selenide are produced.

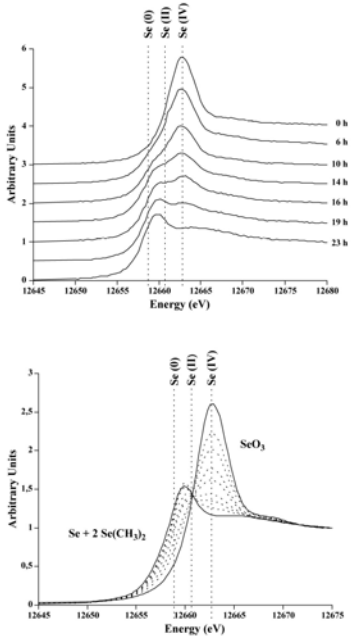

These results prove that microbiologically mediated or enzymatic reduction of selenite occurred in situ under pressure on the beamline. This constitutes the first report of the study of microbial metabolism with live bacteria by X-ray spectroscopy on a synchrotron light source.

Litterature Cited

[1] C. Mougel, B. Cournoyer, X. Nesme, Novel tellurite-amended media and specific chromosomal and Ti plasmid probes for direct analysis of soil populations of Agrobacterium biovars 1 and 2 (vol 67, pg 65, 2001), 67 (2001) 1404-1404.

[2] B. Cournoyer, S. Watanabe, A. Vivian, A tellurite-resistance genetic determinant from phytopathogenic pseudomonads encodes a thiopurine methyltransferase: evidence of a widely-conserved family of methyltransferases, BBA-Gene Struct. Expr. 1397 (1998) 161-168.

[3] C. Garbisu, T. Ishii, T. Leighton, Buchanan, Bacterial reduction of selenite to elemental selenium, Chem. Geol. 132 (1996) 199-204.

[4] P.M. Oger, I. Daniel, B. Cournoyer, A. Simionovici, In situ micro X-ray absorption near edge structure study of microbiologically reduced selenite (SeO_3^{2-}), Spectrochim. Acta B 59 (2004) 1681-1686.

[5] I.J. Pickering, R.C. Prince, D.E. Salt, G.N. George, Quantitative, chemically specific imaging of selenium transformation in plants, Proc. Natl. Acad. Sci., USA 97 (2000) 10717-10722.

[6] D. Sciaky, A.L. Montoya, M.D. Chilton, Fingerprints of *Agrobacterium* Ti plasmids, Plasmid 1 (1978) 238-253.

ESRF	**Experiment title:** Redox state and location of vanadium and chromium in magnetite and silicate glasses : implications for crystal chemistry and geochemistry of V and Cr.	**Experiment number**: CRG 30-02-724
Beamline: BM 30	**Date of experiment**: from: 4 march 2005 to: 8 march 2005	**Date of report**: 7-10-05
Shifts:12	**Local contact(s)**: J.L. Hazemann	*Received at ESRF:*

Names and affiliations of applicants (* indicates experimentalists):

Dr Laurence Galoisy* IMPMC- Univ. Paris VI

Dr Georges Calas* IMPMC- Univ. Paris VI

Dr Etienne Balan* IMPMC- Univ. Paris VI

Mr Olivier Villain* IMPMC- Univ. Paris VI

Melle Sophia Lahlil* IMPMC- Univ. Paris VI

Report:

The Cr surrounding in glasses and crystalline references was investigated using Cr K-edge XANES and EXAFS fluorescence detection. Due to the environmental impact of chromate groups in glasses, a goal was to study the redox state. We want also to determine the local structure around Cr and in various glasses, as a fonction of glass composition (alkali alumino borate, silicate and boro-silicate glasses) and synthesis conditions.
Cr K-edge XANES spectra of Cr-alum and potassium bichromate were recorded as Cr(III) and Cr(VI) references, respectively. Alum (CrIII) pre-edge splitting structure is resolved into 2 apparent compounds in good agreement with ligand-field theory, thanks to energy resolution. Bichromate spectrum is characterised by a single intense pre-edge transition (figure 1).
Glass spectra have been recorded under the same conditions. As main Cr redox states are only III and VI, Cr(VI) /total Cr can be estimated using a linear combination of the Cr-K edge pre-edge structures of the two crystalline references.
For example, a soda silicate glass sample sinthesized in air and containing 1% Cr has been studied. Its Cr(VI) /total Cr proportion has been evaluated between 40 and 45%. (figure 2).
Other samples have been studied in order to determine the influence of glass composition and synthesis conditions. Pre-edge analysis is well suited to quantify the proportion of chromate groups in multicomponent glass, for Cr total concentration down to 1000 ppm or less, and for chromate proportion as less as a few percents.

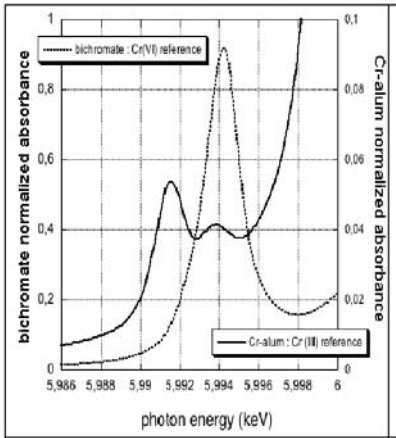

Figure 1 : Cr K-edge XANES spectra in the region of pre-edge of Cr(III) and Cr(VI) crystalline reference compounds. Absorption spectra are normalized to the atomic absorbance. Note double scale.

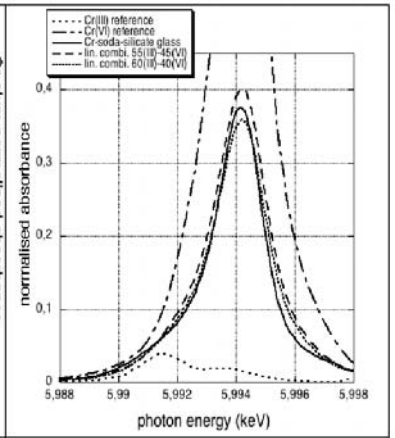

**Figure 2 : Cr K-edge XANES spectra in the region of pre-edge of Cr(III) and Cr(VI) crystalline references and Cr-soda-silicate glass. Absorption spectra are normalised to the atomic absorbance and background substracted.
Linear combinations of reference spectra indicae the relative proportion of the two oxydation states.**

ESRF	**Experiment title:** **Variations des cinétiques d'oxydoréduction du fer dans les verres et liquides silicatés à faible teneur en fer.**	**Experiment number**: 30-02-730
Beamline: BM30B	**Date of experiment**: from: 15March2005 to:21March 2005	**Date of report**:
Shifts: 15	**Local contact(s)**: Dr. Olivier PROUX, BM30B, ESRF	*Received at ESRF:*

Names and affiliations of applicants (* indicates experimentalists):

* Véronique Magnien, Physique des Minéraux et des Magmas, IPGP-CNRS, Paris

* Daniel Neuville, Physique des Minéraux et des Magmas, IPGP-CNRS, Paris

*Laurent Cormier, LMCP, Paris

*Pascal Richet, Physique des Minéraux et des Magmas, IPGP-CNRS, Paris

*Jacques Roux, Physique des Minéraux et des Magmas, IPGP-CNRS, Paris

* Matthieu Roskosz, Physique des Minéraux et des Magmas, IPGP-CNRS, Paris

Report:

The aim of our experiment was to use X-ray absorption spectroscopy to determine the kinetics of iron redox reactions in silicate glasses and melts. Especially it is interesting for us to derive information concerning implied mechanisms in order to control vitrification processes and the temperature-induced structural changes in glass or nuclear industry. XANES techniques are well adapted to answer to this goal because they they allow not only the determination of the redox coordination states of iron by resolving the pre-edge feature but also the realization of *in situ* measurements.

For this reason, we used a microfurnace set-updeveloped by Richet et al.(1993), which is made of a Pt wire with a hole which can be heated from ambient up to 2000K. A small amount of powder is placed in the hole (1 mm in diameter) and heated at different temperature stages. For each temperature stage, several XANES spectra were recorded according to time, in order to follow kinetics of oxidation reaction. Several compositions with different redox states (well characterized by chemical, Mössbauer spectroscopy and electron microprobe analyses) were investigated during these experiments, especially :

- PyroxNaFe3 : 50% mole SiO_2, 3% FeO, 21% CaO, 21% MgO, 5% Na2O
- PyroxNaFe1 : 50% mole SiO_2, 5% Na_2O, 1% FeO, 22% CaO, 22% MgO
- PyroxNaFe0.5 : 50% mole SiO_2, 5% Na_2O, 0.5% FeO, 22.25% CaO, 22.25% MgO
- And anorthite compositions (aluminosilicate)

These experiments were complementary of those carried out on ID24 in March 2004 and on FAME in May 2004. Indeed, the studied compositions were in both cases Ca, Mg – bearing iron silicates, at high temperature and near the glass transition temperature. Interesting results were obtained to understand redox mechanisms near these two temperature ranges. Iron and alumina contents could have a significant influence on redox kinetics. Our objectives were thus to compare the results obtained from different compositions.

The two first shifts were used to align the beamline and set-up the experiment according to previous experiment. Some difficulties in the loading of the sample could be encountered due to the high content of iron in our glasses, so that a very small amount of powder should be introduced within the hole in the Pt wire.

To conclude, we have observed the oxidation of these compositions from 873K to 1123K.

Results:

Some interesting and promising results could be extracted from the XANES spectra obtained at Fe K-edge. In figure 1, XANES spectra obtained at 1123 K after different time for PyroxNaFe3 illustrate our results. By comparison, the spectrum at room temperature is shown too.

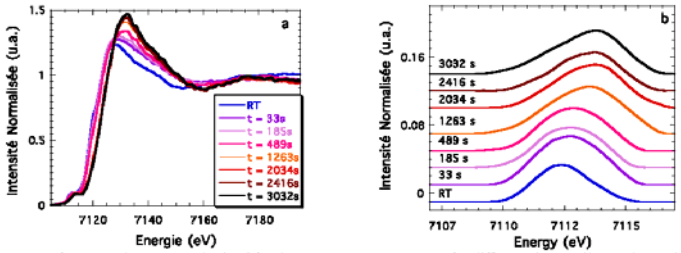

Figure 1. Left: Fe K-edge spectra obtained for the PyroxNaFe3 at 1123 K for different time until complete oxidation of Fe. Right: Zoom on the extracted pre-edge region showing the sensitivity in the position and intensity of the pre-edge, whose analysis allow the determination of iron redox and coordination state.

We observe modification of the pre-edge feature of the XANES spectra as a function of time, especially the progressive increase of a contribution at high energy (and a parallel decrease of the contribution at low energy), characterizing the oxidation state of our sample with time. Similar findings can be observed for the other samples and other temperatures. These observations indicate the evolution of redox ratios with time. Moreover slight differences between composition could be observed, indeed redox kinetics seem to be speed up by the increase of iron content.

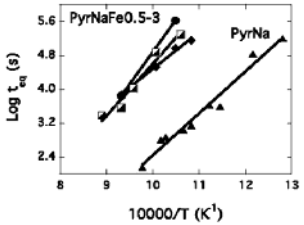

Figure 2. Time required for the oxidation process upon the temperature for various compositions.

These promising results allow to derive some estimates for the time required for the oxidation process (figure 2) and to shed light on the interpretation for the implied mechanisms. Redox kinetics seem to be significantly fast near T_g, indicating probably a divalent cation diffusion as limitating mechanism. The same conclusion was obtained for redox kinetics in composition with 10 mol% of iron from previous experiments. A comparison with previous data and results obtained by other techniques should confirm this conclusion. Besides, these results illustrate also the suitability of BM30B beamline with its large beam for the study of redox kinetics, especially near T_g.

Some additional experiments near T_g are mandatory in order to investigate other compositions. Those information should be essential to complete the understanding of redox mechanisms and the influence of composition.

ESRF

ESRF	**Experiment title:** STUDY BY XAS OF THE OXIDATION STATE AND LOCAL ENVIRONMENT OF VANADIUM SUPPORTED ON THE MESOPOROUS SILICA USED AS CATALYSTS FOR METHANE OXIDATION	**Experiment number**: 30-02-706
Beamline: BM30B	**Date of experiment**: from: 09/03/2005 to: 12/03/2005	**Date of report**: 31/08/2005
Shifts:9	**Local contact(s)**: Vivian NASSIF	*Received at ESRF:*

Names and affiliations of applicants (* indicates experimentalists):

J.M.M.Millet*,
Institut de Recherches sur la Catalyse CNRS conventionné avec l'Université Claude Bernard, Lyon I, 2

O.V.Safonova*
European Synchrotron Radiation Facility

Report:

The goal of this work was to characterize by XAS at V *K*-edge the oxidation state and local environment of vanadium in V-supported catalysts for methane oxidation to formaldehyde.

We have studied two series of samples: the former corresponds to fresh catalysts with vanadium loading varying from 0.4 wt% (V02) to 2.1 wt% (V12); the latter is V12 sample dehydrated under pure oxygen at 600°C and then hydrated again during different periods of time at room temperature in ambient air. The experiments under vacuum conditions were not seccesfull because vaccum in the cell was not good enough (only 10^{-4} torr) to reduce V12 sample. The XANES spectra obtained for the fresh catalysts are shown in Fig. 1. The spectra were analyzed by the pre-edge peak attributed to 1s→3d transition.

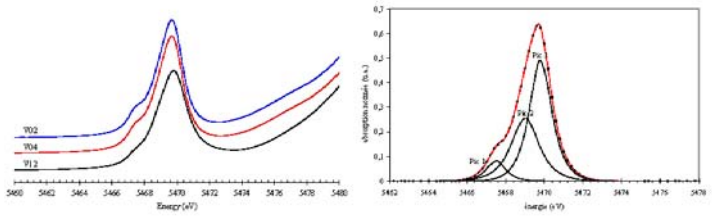

Fig.1 : V pre-edge peaks of V02,V04 and V12 samples (left) and decomposition of the pre-peak of V04 sample (right).

The V pre-edge peak was fitted using three components. The first one (Peak 3 in the Fig. 1) having maximum at 5469.8 eV was attributed to V^{5+} in square base pyramidal coordination (C_{4V} symmetry), whereas the others at 5469.0 and 5467.5 eV were attributed to V^{5+} in distorted tetrahedral coordination (C_1 symmetry) (Fig. 2). The distortion of the structure from perfect geometry (T_d) changes the distribution of the LUMO orbitals (mainly having *d* character) causing the displacement and splitting of 1s→3d transitions. The relative amount of V^{5+} in the tetrahedral coordination increase when vanadium content in the sample decrease. Tetrahedral coordination was attributed to vanadium species incorporated in the wall of the mesoporous silica. The presence of such species was indirectly confirmed by TPR experiments showing that some vanadium species were non-reducible by hydrogen even at high temperature. The relative concentration of these species evaluated from TPR data and estimated from the areas of the components in the V pre-edge peak are in a good agreement. The V^{5+} in square base pyramidal coordination has been attributed to polymeric species formed when the solid is hydrated. The existence of these species, which were already observed on silica supported vanadium catalysts, is confirmed by Raman spectroscopy. This method allowed us to observe V=O bond having characteristic vibration at 900-920 nm.

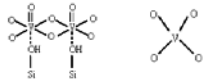

Fig.2 : Schematic representation of vanadium species, which present in the fresh solids.

The XANES spectrum of the V12 compound dehydrated at 600°C in oxygen was collected using *in situ* cell. The goal was to perform further reduction in vacuum in the same cell avoiding the risk of reoxidation. The XANES spectra of hydrated and dehydrated samples are compared in Fig. 3. The intensities of the main peak and its shoulder increase upon dehydration.

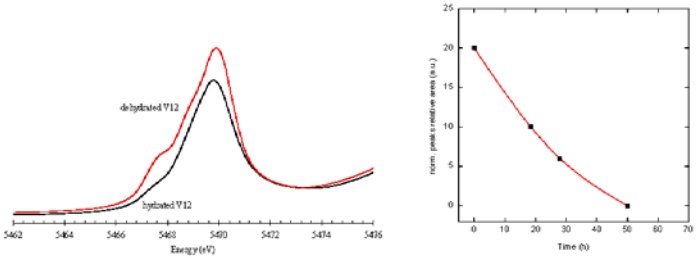

Fig.3 : XANES spectra of the V12 sample before and after dehydration (left). A variation of intensity of the peak vs time of re-hydrarion process (right).

In the same conditions Raman spectra of the dehydrated sample show that only isolated tetrahedral coordinated species present in the solid. The dispersion of vanadium upon dehydration is confirmed by TPR data; in the final state it is equal to 90%. The pre-edge peak of the dehydrated sample was also fitted using three components. The peak having maximum at 5470.0 eV is attributed to isolated vanadium species with a relatively symmetrical tetrahedral coordination (C_{3V}), whereas the two others at 5468.9 and 5467.6 eV are attributed to the vanadium species already identified in the walls of the silica support and to the species

present at the surface and also having tetrahedral coordination of low symmetry ($C_{.1}$) (Fig.4). A study by infrared spectroscopy has shown that vanadium species with a V-OH bond at 3658 cm^{-1} were present at the surface of the dehydrated compounds (Fig. 4). They could correspond to the former ones. The re-hydration of the solid at room temperature has been followed in time by recording spectra after 18h30 and 28h. The analysis was done by fitting the spectra with three components. The variation of the area of two components at 5468.9 and 5467.6 eV subtracting the contribution of the species in the wall is shown in the Fig. 3.

The experiments under vacuum conditions were not seccesfull because vaccum in the cell was not good enough (only 10^{-4} torr) to reduce V12 sample

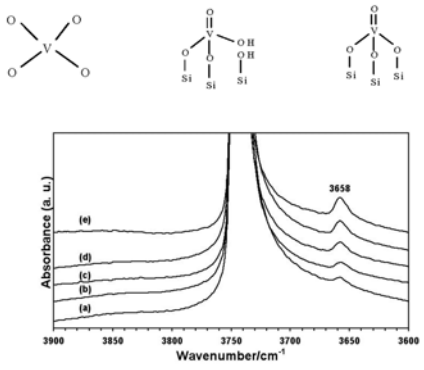

Fig.4 : Schematic representation of the species present in the dehydrated samples and the IR spectra of the samples with increasing vanadium loading (from **a** to **e**) dehydrated under dry O_2 at 550°C.

Rapport - Projet 30-02-708

L'année 2005 a été un très bon cru pour notre projet récurrent sur la spéciation des éléments traces dans le milieu naturel car, non seulement nous avons obtenu pour la première fois des spectres EXAFS de très bonne qualité au seuil du plomb, mais de plus les résultats scientifiques sont novateurs. Cette prouesse expérimentale a été rendue possible grâce à la désormais grande stabilité du spectromètre X, liée pour partie à la stabilisation de l'optique du monochromateur et à la durée de vie du faisceau X en mode uniforme (environ 60 heures).

Nous avons, en particulier, profité de la visite de Yoshio Takahashi, collègue géochimiste japonais spécialiste des nodules Fe-Mn des fonds océaniques, pour comparer la spéciation du plomb dans des nodules de sol et marins diagénétiques et hydrogènes. Les nodules océaniques étudiés ont été abondamment caractérisés au laboratoire (analyses des terres rares, diffraction des rayons X, mesures isotopiques...), et sont représentatifs des dépôts métallifères qui pavent les océans. La Figure 1 compare les spectres EXAFS de l'un d'entre eux enregistrés à SPRING8 et sur FAME, avec des temps d'acquisition comparables (10 heures). La supériorité des données qu'il est aujourd'hui possible d'acquérir sur FAME est clairement démontrée par cette étude comparative.

Pratiquement aucune différence statistiquement significative n'a été observée entre les nodules océaniques d'origine diagénétique et hydrogène (Fig. 2). Par contre, la fréquence est plus élevée que celle du spectre mesuré sur un nodule Fe-Mn de sol (PBLRi71, Fig. 3), et cette différence se reflète uniquement dans la distance Pb-O (Fig. 4), celle-ci étant plus courte dans l'échantillon de sol. L'analyse des spectres a montré que le plomb était toujours divalent, ce qui infirme l'hypothèse d'une oxydation Pb^{2+} => Pb^{4+} à la surface de l'oxyde de manganèse couplée à une réduction Mn^{4+} => Mn^{2+}. L'ordre chimique et structural dans la seconde sphère de coordination (paires Pb-Mn) est par contre semblable dans les échantillons marins et continentaux. La relaxation du site Pb dans les échantillons marins est donc limitée à la première sphère de coordination, ce qui laisse entrevoir la possibilité d'une signature cristallochimique de l'origine des nodules. L'hypothèse de paires Pb-Cl en plus des paires Pb-O dans les échantillons marins sera testée.

Les spectres du plomb adsorbé sur deux birnessites synthétiques ont été enregistrés comme références (Fig. 5). Dans les deux références, le polyèdre de coordination moyen du plomb partage des arêtes (sites de bordure des feuillets) et des sommets (sites interfoliaires à l'aplomb des sites foliaires lacunaires) avec les octaèdres de manganèse du feuillet MnO_2, mais dans des proportions qui varient avec le rapport Pb/Mn. La Figure 6 montre que le nombre de liaisons par sommets augmente avec le rapport Pb/Mn, c'est-à-dire avec le taux de recouvrement (Pb/Mn = 0.001 dans δ-MnO_2-2 et Pb/Mn = 0.05 δ-MnO_2-1). L'existence de liaisons par arêtes dans nos échantillons synthétiques était inattendue, car dans une étude récente (Villalobos et al., 2005, ES&T, 39, 569-576) seules les liaisons par sommets ont été détectées. Comme les complexes de surface à partage d'arête sont les seuls détectés dans les échantillons naturels (Fig. 4), il est important de comprendre l'origine de cette différence (effet du pH, de la force ionique?) par une étude plus systématique du système Pb-MnO_2.

En 2005, nous avons publié un article de 28 pages sur ce programme de recherche. Le résumé est copié à la fin du rapport. Les résultats obtenus à ce jour ont été présentés dans plusieurs communications orales invitées, dont quatre plénières.

Conférences plénières:

2006 Manceau A.: Probing the structure of natural nanoparticles with micrometer-sized X-ray beams. *Winter Meeting of the Mineralogical Society of Great Britain*. January 5-6, Bath, UK.

2005 Lanson B. et Manceau A.: Structure determination of natural and synthetic nanocrystalline phyllomanganates. *13th International Clay Conference*. August 21-27, Tokyo.

Manceau A.: Unlocking metal sequestration in soil nanoparticles. *13th International Clay Conference*. August 21-27, Tokyo.

Manceau A.: Illuminating the complex world of environmental materials with bright synchrotron light. *2005 UK Synchrotron Radiation User Meeting*. September 13-14, Daresbury, UK.

Conférences invitées (Keynotes)

2005 Manceau A.: Unlocking metal sequestration in soil nanoparticles. *Symposium on 'Application of Synchrotron Science to Environmental Chemistry', Canadian Chemistry Conference Annual Meeting*. May 28 - June 1. Saskatoon, Canada.

Manceau A.: Bridging the gap between fundamental and applied research in environmental science at 3rd generation synchrotrons. *Symposium on ' The Birth of a Dream: A Synchrotron Light Source in Canada. A Symposium in Honour of G. M. Bancroft', Canadian Chemistry Conference Annual Meeting*. May 28 - June 1. Saskatoon, Canada.

Manceau A.: Utilisation du rayonnement synchrotron pour l'étude de la spéciation des éléments traces (Ni, Zn, Pb...) dans le milieu naturel. *Colloque du Groupe Français des Argiles*, Paris, 18-19 Mai.

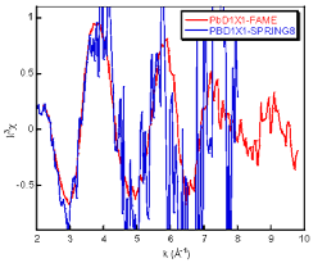

Figure 1

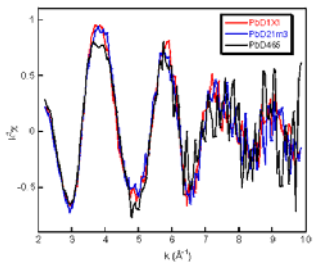

Figure 2

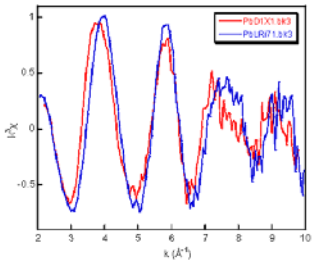

Figure 3

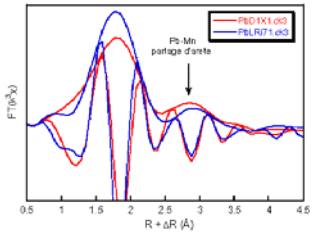

Figure 4

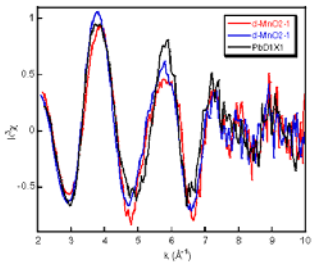

Figure 5

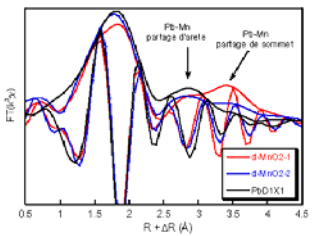

Figure 6

Geochimica et Cosmochimica Acta, Vol. 69, No. 16, pp. 4007–4034, 2005

0016-7037/05 $30.00 + .00

doi:10.1016/j.gca.2005.03.018

Natural speciation of Mn, Ni, and Zn at the micrometer scale in a clayey paddy soil using X-ray fluorescence, absorption, and diffraction

Alain Manceau,[1,*] Caterina Tommaseo,[1] Sophie Rihs,[2] Nicolas Geoffroy,[1] Daniel Chateigner,[3] Michel Schlegel,[4] Delphine Tisserand,[1] Matthew A. Marcus,[5] Nobumichi Tamura,[5] and Zueng-Sang Chen[6]

[1]Environmental Geochemistry Group, Maison des Géosciences, Univ. J. Fourier, BP 53, 38041 Grenoble Cedex 9, France
[2]Centre de Géochimie de la Surface, Université Louis Pasteur, 1 rue Blessig, 67084 Strasbourg, France
[3]CRISMAT-ENSICAEN, Bd. Maréchal Juin, 14050 Caen, France
[4]DEN/DPC/SCP, Centre d'études nucléaires de Saclay, BP 11, 91191 Gif sur Yvette, France
[5]Advanced Light Source, Lawrence Berkeley National Laboratory, One Cyclotron Road, Berkeley, CA 94720, USA
[6]Department of Agricultural Chemistry, National Taiwan University, Taipei, Taiwan

(*Received November* 11, 2004; *accepted in revised form March* 16, 2005)

Abstract—The natural speciation of Mn (0.19 g/kg), Ni (46 mg/kg), and Zn (42 mg/kg) in the argillic horizon (120 cm depth, pH = 5.6) of an Ultisol from a paddy soil in northern Taiwan was investigated by advanced X-ray synchrotron techniques. Microchemical associations were imaged by synchrotron-based X-ray microfluorescence, host minerals were identified by standard and micrometer-resolved X-ray diffraction, and the local coordination environment of Mn, Ni, and Zn was probed using extended X-ray absorption fine structure (EXAFS) spectroscopy on a powdered sample and a soil thin section, and polarized EXAFS spectroscopy on a highly textured self-supporting clay film from the <2 μm fraction of the soil. Manganese was concentrated in Fe-Mn soft mottles (44.4 g/kg) as turbostratic hexagonal birnessite and lithiophorite having Mn^{3+}/Mn^{4+} atomic ratios of ~20% and 50%, respectively. Quantitative analysis of high-order scattering paths of the EXAFS spectrum for natural and synthetic $(Al_{0.67}Li_{0.33})(Mn^{4+}_{0.68}Mn^{3+}_{0.32})O_2(OH)_2$ lithiophorite revealed that Mn^{3+} and Mn^{4+} are ordered in the $[(Mn^{4+}_{0.68}Mn^{3+}_{0.32})O_2]^{0.32-}$ layer. A structural model is proposed, in which Mn^{4+} and Mn^{3+} are ordered similarly to Al and Li in the $[(Al^{3+}_{0.67}Li^{+}_{0.33})(OH)_2]^{0.32+}$ layer, with Mn^{3+} cations being surrounded by six Mn^{4+}, and Mn^{4+} cations by three Mn^{3+} and three Mn^{4+}. Similar cation ordering in the manganese and aluminum layers likely provides a more homogeneous local balance of the excess and deficit of charges in each layer and increases the stability of lithiophorite. Ni (r = 0.70 Å) substitutes for Mn ($r(Mn^{3+})$ = 0.54 Å, $r(Mn^{3+})$ = 0.65 Å) in the manganese layer in the natural lithiophorite. In contrast, Zn (r = 0.74 Å) fills vacant sites in the gibbsitic layer of natural lithiophorite, in a similar manner as lithium (r = 0.74 Å) in synthetic lithiophorite. The partitioning of Ni and Zn between the two layers is a result of the general preference of Ni, whose size is intermediate between those of Mn^{3+} and Li^{+}, for slightly smaller sites. In contrast with nickel, which is detected only where there is lithiophorite, the Zn-lithiophorite association found in Fe-Mn mottles is not representative of the bulk soil. The combined use of X-ray diffraction, and powder and polarized EXAFS spectroscopy revealed that Zn is predominantly bound to hydroxy-Al interlayers sandwiched between 2:1 vermiculite layers in the fine soil matrix. The incorporation of Zn in the gibbsitic layer of both lithiophorite and vermiculite helps increase the stability of these minerals by providing positive charge to balance the negative charge from the 2:1 phyllosilicate layer and the $[(Mn^{4+}_{0.68}Mn^{3+}_{0.32})O_2]^{0.32-}$ layer of lithiophorite. This binding environment for zinc is probably the main mechanism by which zinc is sequestered in acidic to near-neutral aluminum-rich clayey soils.

ESRF	**Experiment title:** μ-XAS study of interaction layers between uranium-molybdenum alloys and aluminum	**Experiment number:** 30-02-713
Beamline: BM-30B	**Date of experiment:** from: 04 May 2005 to: 17 May 2005	**Date of report:** 30/08/2005
Shifts: 35	**Local contact(s):** Dr. H.PALANCHER, Dr. O.PROUX, Dr. V.NASSIF	*Received at ESRF:*

Names and affiliations of applicants (* indicates experimentalists):

Dr. H.PALANCHER[a,b]*, Dr. P.MARTIN[a]*, Dr. M.RIPERT[a]*, C.PROYE[a]*, F.MAZAUDIER[a], Dr. C.VALOT[b], Dr. J.P.PIRON[b], Dr. V.NASSIF[b,c], M.ARGOUD[c]

[(a)] CEA-Cadarache (DEN/DEC) F-13108 Saint Paul lez Durance. [(b)] CRG FAME, 6, rue J. Horowitz F-38043 Grenoble Cedex. [(c)] CEA-Grenoble, (DRFMC) F-38000 Grenoble

Report

The European Community supports the use of Low Enriched Uranium (LEU, ^{235}U<20 at.%) in fuels for research reactors such as the future Réacteur Jules Horowitz (RJH) of the CEA. This very high power reactor is expected to be operational around 2011-2012 at Cadarache (France).

But due to the decrease in ^{235}U enrichment for the conversion to LEU, new nuclear fuels have to be designed. The current choice for RJH fuel is uranium-molybdenum, in γ-phase, with 8 weight% Mo content (18 at.% UMo8). The fuel, which consists of UMo8 spherical particles surrounded by an Al alloy matrix, is pressed between two aluminium foils. Post-irradiation examinations of UMo8 [1] demonstrated its strong potentialities as fuel but they also point out its great reactivity with aluminium. This reactivity leads to the formation of an interaction layer between fuel and matrix that is suspected to cause the strong fuel plate swelling and an unacceptable mechanical behaviour.

Previous studies performed by XRD (X-ray diffraction) point out the presence in this interaction layer of binary phases (UAl_2, UAl_3, UAl_4) and ternary phases ($U_6Mo_4Al_{43}$ and UMo_2Al_{20}) [2]. However the location of Mo is not clear: Mirandou et al. suppose its insertion in binary phases to form solid solutions (U, Mo) Al_3 or (U, Mo)Al_4 when Tougait et al. report the stochiometry of UAl_4 [3] and the very limited solubility of Mo in UAl_3 (to less than at% 5 i.e. far below the 18 at % Mo content in the original UMo8 phase). The main aim of this study is to probe, by measuring EXAFS spectra at the Mo K edge (20,0 keV) in the interaction layer, the evolution of Mo environnement with:

- aluminum matrix composition (limited addition of Si in the matrix could be a solution to improve in pile behaviour of this fuel). In the following, the two different aluminium alloys, with and without Si, are respectevely writen Al6061 and AlA5.
- position from aluminum matrix (this layer is strongly inhomogenious [3]).

During these measurements, two diffusion couples have been analysed: the first with an interdiffusion layer grown between UMo/Al(A5) and UMo/Al(6061) interfaces and the second with a large interdiffusion layer UMo/Al(A5). Diffusion couples consist in Al and UMo8 foils, kept in tight contact during thermal treatment. After the thermal treatment, the samples are sectioned parallel to the diffusion direction (for SEM pictures of both samples see figure1). Note that prior to analyses on diffusion couples, EXAFS spectra at the Mo K edge were collected in the transmission mode on two samples containing pure ternary phase ($U_6Mo_4Al_{43}$ and UMo_2Al_{20}). These references were provided by H. Noël from CNRS-Rennes (LCSIM).

Considering the unique diffusion direction, incoming X-ray beam has to be microfocused in only one direction: each sample has been characterised by a 15×300 μm^2 X-ray beam. To obtain this size, an additionnal mirror (silica coated with platinum) has been used. Precise positioning of the beam on the sample was enabled by an optical microscope as illustrated on figure 2.

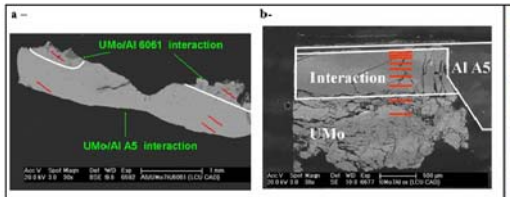

Figure 1:
SEM observations of two diffusion couples. Red lines indicate some of the areas studied by μ-EXAFS. In the first sample (a-), the interaction layer remains only. The upper side was in contact with Al alloy doped with silicon on contrary to the lower side. In the second (b-), Al alloy is silicon free.

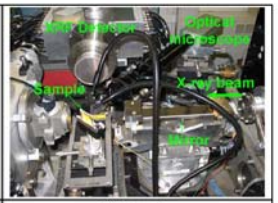

Figure 2:
Picture of the experimental set-up used for the diffusion couples characterisation in fluorescene mode. The beam is micro-focused in the vertical direction thanks an additional miror.

On the first sample, the two different areas (close to UMo/AlA5 interface and close to UMo/Al6061) were probed succesively by μ-EXAFS. As shown from figures 3 and 4, Mo environnement in the interdiffusion layer is strongly influenced by the chemical composition of Al matrix (with or without Si dopant). Howewer Mo is in both cases located in a ternary phase:

- in $U_6Mo_4Al_{43}$ in areas close to UMo/AlA5 interface,
- in UMo_2Al_{20} in areas close to UMo/Al6061 interface.

The study of the second sample (interdiffusion layer near an UMo/AlA5 interface) confirms the unique presence of Mo element in the ternary phase $U_6Mo_4Al_{43}$ whatever the distance of the probed zone from the AlA5 matrix. This last conclusion is interesting since this interdiffusion layer is known to be inhomogeneous.

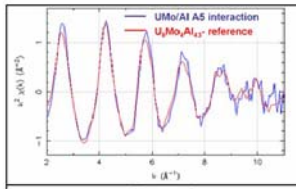

Figure 3
Comparison between spectra collected on the first sample in the aera closer to the UMo/AlA5 interface and on the pure $U_6Mo_4Al_{43}$ sample.

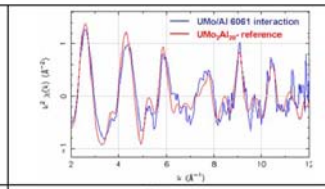

Figure 4
Comparison between spectra collected on the first sample in the aera closer to the UMo/Al6061 interface and on the pure UMo_2Al_{20} sample.

The stability and intensity of the beam available at BM30B enabled us to collect good quality EXAFS spectra (up to 12 $Å^{-1}$) even with microfocusing in the vertical direction (see figures 3 and 4). Even if further refinement of absorption data is under processing, original results have already been obtained about Mo environnement in the interdiffusion layer.

Based on the instrumental developments carried out at BM30B beamline (avalaibility of a 10×10 μm^2 beam), we intend to confirm by μ-EXAFS on the fuel itself, the possible systematic presence of Mo in ternary phases in the interdiffusion layer.

Acknowledgement
M.Mezouar is gratefully acknowledged by the beam-line staff and the users for the loan of the KB miror.

References

[1] M. K. Meyer *et al.*, *Journal of Nuclear Materials* (2002) 304, 221-236.
[2] M. I. Mirandou *et al.*, *Journal of Nuclear Materials* (2003) 323, 29-35.
[3] O. Tougait, H. Noël, *Intermetallics* (2004) 12, 219-223.
[4] H. Noël, O. Tougait, (2005) *personal communication.*

ESRF	**Experiment title:** A XAFS spectroscopy study of local environment around gold in high T/P aqueous sulfide and chloride solutions: Implications for the mechanisms of gold deposits formation	**Experiment number:** 30 02 720
Beamline: BM30B	**Date of experiment:** from: 3 November 2003 to: 11 November 2003	**Date of report:** 8 September 2005
Shifts: 18	**Local contact(s):** Jean-Louis Hazemann, BM30B (FAME), ESRF	*Received at ESRF:*

Names and affiliations of applicants (* indicates experimentalists):

* **Boris Tagirov** (complete please)
* **Jean-Louis Hazemann** & ***Olivier Proux**, Laboratoire de Cristallographie, ESRF-CNRS, Grenoble
* **Jacques Schott** & ***Gleb Pokrovski**, Laboratoire des Mécanismes & Transferts en Géologie, LMTG, Toulouse

Report:

Experimental. The dissolution and atomic structure of gold in chloride and sulfide aqueous solutions were examined by XAFS spectroscopy at Au L_3-edge at temperatures from 200 to 450°C and pressures to 600 bar, using an X-ray cell recently developed at the Laboratoire de Cristallographie[1]. This cell allows simultaneous measurement of the absolute concentration of the absorbing element in the fluid (from edge-step height in transmission mode, fluid density and absorption cross-section of the element), and atomic environment around the absorber (from analysis of XANES and EXAFS spectra in fluorescence and/or transmission mode)[2]. An improved cell design used in the present experiment utilizes two mobile pistons equipped with Viton joints and inserted into a glassy-carbon tube with low absorption coefficient for X-rays. This construction has already been successfully applied in our recent Sb XAFS study to 500°C[3].

Results from the chloride system. Two experiments were performed in the system 0.035m $HAu^{(III)}Cl_4$-0.5m NaCl-0.01m HCl±Au(metal) at 600 bar as a function of temperature and time. It was found that below 100°C, the XAFS spectra are consistent with the plane-square $Au^{(III)}Cl_4^-$ complex reported in previous low-temperature XAFS and Raman studies[4,5]. At higher temperature, there is a fast decrease of Au concentration accompanied by the reduction of Au(III) to metallic gold. This behavior is also observed in our previous experiment on the same system using a sapphire cell. Batch-reactor solubility studies indicate, however, that above 200°C, $AuCl_4^-$ in the presence of metallic gold should convert to $AuCl_2^-$ and attain concentrations 10 times higher than measured in our experiments[6]. This discrepancy might be attributed to a reaction of Au(III) with the carbon cell walls. Another possibility could be the beam-induced reduction of $AuCl_2^-$ into Au° (e.g., ref. 4).

Results from the sulfur system. Four experiments were performed in NaOH solutions, one in pure water, and one in the presence of H_2SO_4 by allowing a foil of metallic gold and a desired mass of sulfur crystals to react with corresponding solutions at high temperature. Dissolved sulfur concentrations ranged from 0.1 to 4 mol/kg. As show thermodynamic equilibrium calculations[7], at neutral to basic pH (4-8), the reaction of sulfur with NaOH-H_2O above 200°C produces sulfide (H_2S, HS^-) and sulfate ($NaSO_4^-$, HSO_4^-, SO_4^{2-}) species. At acid pH (<3) above 300-400°C, however, SO_2 becomes the dominant species. In all experiments below 400°C, dissolved Au concentrations derived from the absorption edge jump attain a steady state within a few hours (Fig. A & B). The dissolved sulfur concentrations, estimated from the before-edge absorption in transmission mode (sulfur is the major contributor to the absorption below the Au L_3 edge in our solutions), are in agreement with predicted sulfur solubilities within better that 30% of the value. In some S-rich experiments at 400 and 450°C, a drop of dissolved sulfur and gold concentrations with time was observed. This is likely due to precipitation of some amount of sulfur in colder parts of the cell close to the Viton rings and fluorescence window.

Steady-state Au contents measured in our experiments in the system S-NaOH at neutral pH in a wide range of S concentrations are in excellent agreement (within 0.2 log units) with the predicted equilibrium concentrations using the thermodynamic properties of $Au(HS)_2^-$ (ref. 8). Fluorescence spectra recorded on these solutions are in perfect agreement with the dominant presence of this complex in which Au is linearly coordinated with 2±0.2 sulfur atoms at 2.29±0.01 Å over the wide temperature range (Fig. C & D).

A very similar Au 1st shell environment is found in the system S-H_2O (N_{Au-S}=2.2±0.3, R_{Au-S}=2.29 Å at 300 and 400°C, experiment 7). However, some subtle differences in the 2nd shell are detected (Fig. D). The derived structural parameters are inconsistent with the neutral mono-sulfide complex AuSH° which has been widely believed the dominant Au species in S-bearing acid solutions[8]. Moreover, the measured Au solubilities are 1 to 2 orders of magnitude higher than those predicted using the AuSH° thermodynamic properties (Fig. B). These findings strongly suggest that Au is likely to be complexed with other sulfur ligands like SO_2 in these acid solutions by forming species with linear S-Au-S arrangement like $Au(SO_3)_2^{3-}$, similar to the well-known thiosulfate $Au(S_2O_3)_2^{3-}$ complex stable at low temperatures[9]. This unexpected result may have important implications for Au transport by high-temperature magmatic fluids (< 450-500°C) in which SO_2 largely dominates over H_2S.

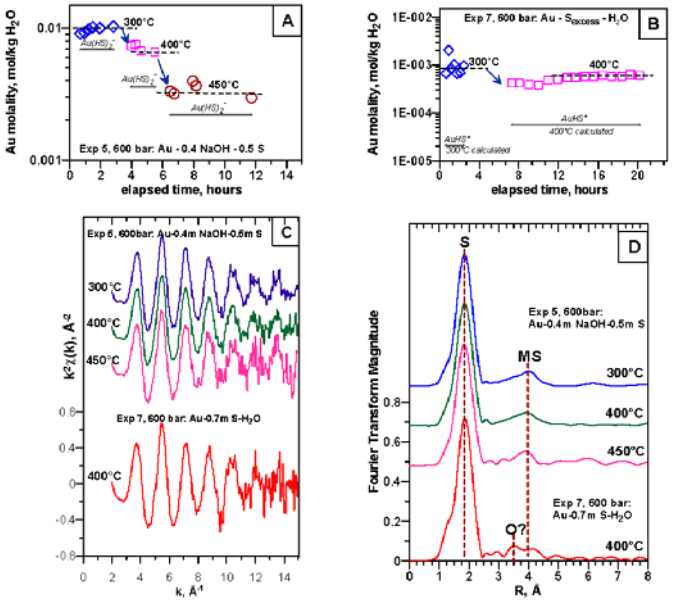

Fig. A & B. Gold concentrations derived from absorption-edge height in transmission mode as a function of time and temparature in two XAFS experiments. Each simbol corresponds to a XAFS scan; arrows indicate temperature changes during the run. Horisontal grey bars denote calculated Au concentrations at each temperature using the thermodynamic properties of the major AuHS and $Au(HS)_2^-$ complexes and sulfur species. Uncertaities associated with these calculations are at least ±0.3 log units.
Fig. C & D. Typical fluorescence EXAFS spectra and their corresponding FT's at indicated conditions. Note a good quality of the spectra to at least 10-12 $Å^{-1}$. MS denote multiple scattering withing the linear S-Au-S cluster.

Conclusions & perspectives. To our knowledge, this experiment is the first quantitative measurement of gold solubility and structure of Au-sulfide species at hydrothermal conditions using *in situ* XAFS spectroscopy. At near-neutral to basic pH, our data are in excellent agreement with numerous batch-reactor solubility studies and are fully consistent with the dominant formation of the $Au(SH)_2^-$ complex at least between 200 and 450°C. At acid pH, however, our results indicate the formation of new species presumably with sulfite (SO_2). Condidering both the poorly quantified chemical speciation and low kinetics of sulfur equilibration in acid solition, more measurements on Au and its analogs (Ag, Cu) by XAFS/batch-reactor, and sulfur species by Raman spectroscopy will be performed in these systems.

References

1. Testemale D. et al. (2005) Rev. Sci. Instrum. 76, 43905; **2.** Pokrovski G.S. et al. (2005) Chem. Geology 217, 127; **3.** Pokrovski G.S. et al. (2005) GCA 69, A734; **4.** Berrodier I. et al. (2004) GCA 68, 3019; **5.** Murphy P.J. et al. (2000) GCA 64, 479; **6.** Gammons C.H. & Willams-Jones A.E. (1997) GCA 61, 1971; **7.** SUPCRT 96; **8.** Tagirov B.R. et al. (2005) GCA 69, 2119; **9.** Bryce R.A. et al. (2003) J. Phys. Chem. A 107, 2516.

ESRF	**Experiment title:** Arsenic toxicity: Cellular mechanisms of arsenic transfer and resistance: effect of Fe magnetic nanoparticles	**Experiment number:** 30 02 740
Beamline: BM30b	**Date of experiment:** from: 29 June 2005 to: 4 Jully 2005	**Date of report:** 26/09/05
Shifts: 12	**Local contact(s):** Hervé Palanché (e-mail: palanche@esrf.fr)	*Received at ESRF:*

Names and affiliations of applicants (* indicates experimentalists):

ROSE jérôme[1]*, AUFFAN Mélanie[1]*, CHAURAND Perrine[1]*, Dr. Pr BOTTA Alain [2], Dr. Pr. BERGE-LEFRANC jean-louis[2], Pr JOLIVET Jean-Pierre[3], Dr. CHANEAC Corinne[3]

1. Géosciences de l'environnement – CEREGE UMR 6635 CNRS-Université Paul Cézanne Aix-Marseille III, Europole Méditerranéen de l'Arbois BP 80 13545 Aix en Provence Cedex 04, France.
2. Laboratoire de Biogénotoxicologie et, Mutagenèse Environnementale, IFR PMSE 112, Faculté de médecine, Univ. de la Méditerranée, 27 Bd jean Moulin, 13385 Marseille cedex
3. C.N.R.S. - UMR 7574, Chimie de la Matiere Condensee, Université Pierre et Marie Curie, 4 Place Jussieu, 75252 Paris Cedex

Report:

Aim of the project

Arsenic is a toxic metalloid largely studied worldwide. Its toxicity is known to be related to its oxidation state and speciation. In cellular media, arsenic shows a strong affinity to thiol functions, which play an important role on As biocellular transformations and cancerogenic effects. Serious health effects due to high rates of arsenic in drinking water, amplified the interest in minerals such as iron oxide which can immobilize arsenic species on their surfaces and so decrease their toxicity. Recently, Nano-Maghemites (iron oxide nanoparticles with a diameter <10nm), are studied for biomedical purposes (MRI contrast agents, drug delivery or cell engineering). These nanoparticles are very attractive because approximately 50% of their atoms are at the surface that increases significantly their surface energy, reactivity and affinity with adsorbates.

In that context, our project aimed to assess the synergetic effects of Nano-maghemites and As on their mechanisms of transfer and toxicity for human cells (fibroblasts). Since the interaction between Fe and As is strong and the surface developed by nanoparticles is high, it can be postulated that Nano-maghemites can decrease the transfer of As onto fibroblasts and consequently lower As toxicity. On the other hand Fe nanoparticles can be internalized coated or not with arsenic and induce toxic effects.

The aim of this XAS experiment was (1) to determine whether or not Nano-maghemites can fix As initially present in the extra and/or intracellular media and (2) to study the at the atomic scale the As/Nano-maghemites surface interactions (As adsorption, presence of competitive anions, surface passivation…).ADDINADDIN

Experiment

The experiment was conducted on BM-30b beamline 'FAME' from 29th June to 4th July 2005. During the measurement of the XAS spectra the samples (under liquid or lyophilized forms) were cooled at the liquid Helium temperature (4 K) in a cryostat. This procedure allowed to improve spectrum quality by minimizing radiation damage and by decreasing thermal motions of atoms. Moreover, the use of a cryostat, allowed to keep the As in the same oxidation state during the experiment which is necessary in our experiment.

The sample analysed, contained 27 mg/L of Nano-maghemites coated with DMSA (2,3-dimercaptosuccinic acid) and 30 µM of As_2O_3, which were injected in the fibroblasts media. The coating with DMSA was used to enhance the colloidal stability of Nano-maghemites at physiological conditions. This sample was analysed in fluorescence mode in two times: (1) the cellular part and (2) the nutritive cell solution. Thirteen organic and inorganic As references compounds at different valence and local atomic environment were also analyzed (As_2O_3, As_2O_5, As_2S_3, phenylarsine, arsanilic acid, arsenopyrite…). For each reference, 3 to 6 scans were performed in transmission mode. At the end of the aquisition the signal/noise ratio of the XANES and EXAFS spectra was extremely good.

First results

We studied the impact of the sample freeze drying process on the As speciation. This point is of high importance in order to confirm that no modification of the As speciation could be generated by the sample preparation. Figure 1 shows the EXAFS and the corresponding Fourier Transform of the sample containing cells initially freeze dried or not. No modification of the As oxidation state due to the freeze drying process is observed. Then, in the continuation of the XAS experiment, the samples and references compounds were analyzed under lyophilized form.

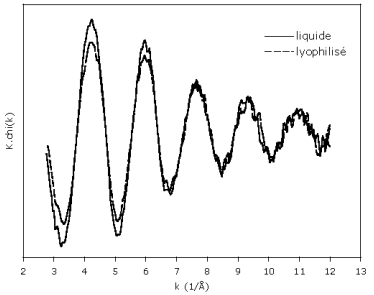

Figure 1 : EXAFS spectra of the fresh and freeze dried cell samples

In order to determine the effects of Nano-maghemites on the As behaviour in contact with fibroblasts, we compared the As oxydation state and local atomic environment in the intra- and extra-cellular medium versus reference compounds (figure 2).

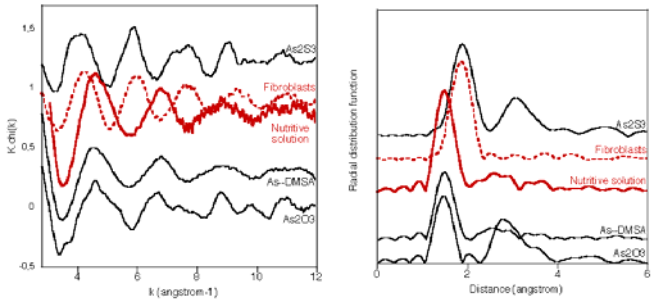

Figure 2 : EXAFS and Fourier Transform of As in the intra- (fibroblasts) and extra-cellular medium (nutritive solution) compared with reference compounds.

The figure 2 shows that the arsenic speciation in the intra- and extra-cellular medium is different:

- In the intracellular part: the speciation of As which is internalized by fibroblasts is similar to As speciation in As_2S_3. Due to these spectra and to the XANES results, we can suppose that an important part of the intra-cellular As is trivalent and link to sulfidric groups (glutathione, cysteine, dithiols from proteins…). It doesn't seem that As is linked to the Nano-maghemites surface but these hypothesis have to be confirmed by the EXAFS modelisations which are in progress.
- In the extracellular solution: there are a lot of similarities between the As speciation in the extra-cellular medium and As which is linked to DMSA coated Nano-maghemites (called "As-DMSA"). The XANES results show that As is trivalent in the extra-cellular medium with oxygen atoms in the first coordination sphere. EXAFS modeling are in progress.

These preliminary results need to be confirm, but it seems that Nano-maghemites are not internalized by cells and that they adsorb As on their surface via DMSA.

ESRF	**Experiment title:** Speciation of copper in vapours and brines under magmatic-hydrothermal conditions	**Experiment number:** ME-1137
Beamline: BM30B (FAME)	**Date of experiment:** from: 20 July 2005 to: 26 July 2005	**Date of report:**
Shifts: 24	**Local contact(s):** Jean-Louis Hazemann	*Received at ESRF:*

Names and affiliations of applicants (* indicates experimentalists):

Dr. Olivier PROUX*, CNRS
Dr Joël BRUGGER*, SA Museum/Adelaide University
Dr. Barbara ETSCHMANN*, CSIRO
Dr. Jean-Louis HAZEMANN*, CNRS/ESRF
Dr Weihua LIU*, CSIRO/SA Museum
Dr. Gleb S. POKROVSKI, CNRS
Dr. Denis TESTEMALE*, SNBL

Report:

Introduction: Magmatic-hydrothermal ore deposits contain most of the world's Cu, Au, Pb, Zn and Ag resources. The long-term goal of this project is to measure experimentally the speciation and solubility of metals in hydrothermal fluids and metal partitioning between solid, fluid and vapour at temperatures and pressures typical for the formation of natural ore deposits (350-550°C; 500-3000 bars) in H_2O-NaCl-H_2S-CO_2 fluids. In particular, we wish to address a major new paradigm in hydrothermal geochemistry: analyses of single fluid inclusions from magmatic-hydrothermal ore deposits (e.g., Porphyry Copper deposits) show that metals such as copper are actually enriched in a low-density "vapour" phase coexisting with a hypersaline brine. Traditional models –and available thermodynamic models- assume that metals strongly partition into the brine under these conditions. Understanding the role of vapour in these systems has the potential to revolutionise our understanding of the formation of some of the world's richest and biggest ore deposits. The present experiment aimed to:

- Determine the speciation of copper in hypersaline brines under magmatic hydrothermal conditions.
- Measure directly the partitioning of copper between liquid and vapour phases.
- Investigate the change in speciation of copper in HCl-NaCl-H_2O solutions as a function of density.
- Test the capability of the CNRS cell for in-situ solubility studies of copper minerals.

Results: Fluorescence and transmission Copper (8979 eV) *K*-edge XANES and EXAFS spectra of Cu(I) in acidic chloride solution were measured with the X-ray cell developed at the Laboratoire de Cristallographie. Despite the synchrotron working in 16 bunch mode with a maximum current of 90 mA, we were able to collect excellent XANES and EXAFS spectra at temperatures to 500°C and pressures to 700 bars for Cu concentrations ranging from 0.05 to 0.3 m.

Speciation experiments. A series of 6 solutions containing Cu(I) and varying salt concentrations were heated under isobaric conditions to 425-500°C: (i) 3.5 m NaCl, 700 b, 30-500 °C; (ii) 0.1 m NaCl, 350 b, 30-425 °C; (iii) 1.15 m NaCl, 450-360 b, 450 °C; (iv) 14 m NaCl, 600 b, 200-500 °C; (v) 6 m NaCl, 500 b, 30-450 °C; (vi) 15.6 m LiCl, 600 b, 25-400 °C. The most graphic experiment was without a doubt (vi), in which XANES spectra show that the geometry of the Cu(I) complex changes from predominantly tetrahedral ($CuCl_4^{3-}$) at room temperature, to trigonal planar to linear at 400°C (Fig. 1). This set of spectra is very similar to the one obtained at SNBL (see experiment report ME-998) under isothermal conditions (150°C), varying the salt concentration from 17 m LiCl to 1.5 m LiCl.

Liquid-vapour partitioning experiments. Two experiments were conducted to measure directly the partitioning of Cu(I) between vapour and brine at 400°C. The solutions were pressurised, then heated to 400°C; the pressure was then released slowly until phase separation occurred. We were able to analyse the low density "vapour" phase, but due to the relatively large "dead" volume between the piston and the cell wall, the brine could not be analysed. EXAFS spectra were acquired at different pressures corresponding to increasing amount of vapour in the system.

Copper solubility in supercritical fluids of varying density. One experiment successfully measured CuCl(s) in a H_2O-HCl solution at 420°C, at pressures between 400 and 290°C (Fig. 2). Under these conditions the fluid remains one phase (supercritical); however, the density of the solution changes from 0.42 to 0.20 g/cm^3. Results indicate a dramatic decrease in copper solubility, accompanied by subtle changes in speciation as recorded by EXAFS.

Figure 1: Cu Speciation: 15.6 m LiCl

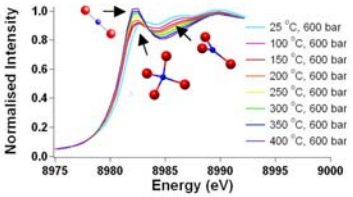

Figure 2: Cu Solubility, 420 °C

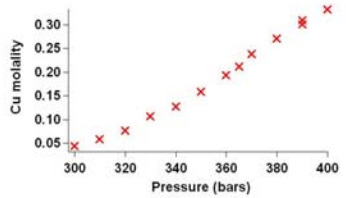

Conclusions and recommandations

We successfully obtained the first copper XANES and EXAFS data in supercritical fluids, and conducted the first in-situ copper solublity experiment in low density fluids.

1. We now have a complete, high quality XANES/EXAFS dataset on Cu(I) chloride solutions from 25°C to 500°C.
2. Detailed analysis of EXAFS data is made difficult by the complexity of the speciation in these solutions, which always contain a mixture of species, often with different geometries. Successful EXAFS analysis requires the integration of all available XANES, EXAFS, solubility and UV-Vis spectroscopic data. Preliminary results look good!
3. The solubility study shows that the amount of Cu in solution decreases significantly with decreasing pressure in the supercritical phase; under favourable conditions, a drop in pressure of 100 bars can result in the precipitation of 90% of the dissolved copper; the low density fluids can still carry a significant amount of copper. Hence, pressure may have a more significant role in the formation of ore deposits than previously assumed.
4. The present geometry of the piston prevented successful measurement of the partitioning of copper between brine and vapour. This can be overcome by current developments devoted to minimizing the dead-volume by high precision machining of the glassy carbon cell. However, the current dataset suggests that although low density "vapour" can carry significant amounts of copper, chloride complexes cannot explain the *preferential* partitioning of copper into the vapour phase. Therefore, the focus of the next study will be in studying additional ligands, such as bisulfide.

ESRF

ESRF	**Experiment title: High-pressure investigation of the lead-free relaxor ferroelectric $BaTi_{0.65}Zr_{0.35}O_3$**	**Experiment number**: 30 02 733
Beamline: BM 30B	**Date of experiment**: from: 13/07/2005 to: 18/07/2005	**Date of report**: 30/08/2005
Shifts: 15	**Local contact(s)**: Hervé Palancher	*Received at ESRF:* *31/08/2005*

Names and affiliations of applicants (* indicates experimentalists):

F. Hippert*, J. Kreisel*, C. Laulhé*

LMGP, ENSPG

P. Bouvier*

LEPMI, ENSIEG

W. Crichton*

ESRF

Report :

The dielectric permittivity of relaxor ferroelectrics shows a large, frequency-dependent maximum as a function of temperature, which is not related to a structural phase transition as it is the case in classical ferroelectrics. Relaxors are not yet fully understood, but it is generally admitted that they present an intrinsic nano-scaled local structure which consists of polar nano-regions in a somewhat different "matrix". In the past, the usual approach towards the understanding of relaxor ferroelectrics was mainly through their chemical composition- or temperature-dependent behaviour. We could recently show that the parameter high-pressure is also an appropriate variable in elucidating relaxor ferroelectrics [1].

The aim of the experiment was to study the pressure-induced evolution of the local order around Zr atoms through EXAFS measurements at the Zr K edge (18 keV), in the relaxor $BaTi_{0.65}Zr_{0.35}O_3$. $BaZrO_3$ was measured as well, as a reference compound. Previous Raman results indicated important changes of the $BaTi_{0.65}Zr_{0.35}O_3$ local structure at 5.7 and 15.1 GPa [2].

The EXAFS experiments were performed in the transmission mode. The pressure was applied with the BM29 Paris-Edinburgh press. 5 mm diameter anvils and gaskets from ID 27 were used.
The samples consisted of 5%-diluted $BaTi_{0.65}Zr_{0.35}O_3$ and $BaZrO_3$ powders in the LiF pressure-transmitting medium, pressed into 1.5mm diameter micro-pellets. The transmission was about 6% at energies above the Zr K-edge energy.
A CCD camera was placed close to the transmitted beam, in order to collect the diffraction rings from the sample and the pressure-transmitting medium. The applied pressure was deduced from the LiF cell parameter [3]. The photograph below presents the experimental set-up.

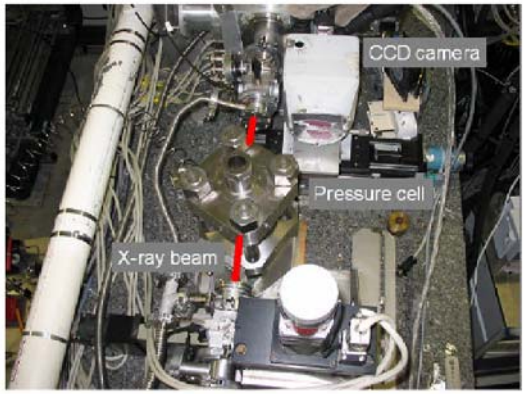

$BaTi_{0.65}Zr_{0.35}O_3$ and $BaZrO_3$ powders were studied on increasing pressure on 12 intervals up to 15.5 GPa. The acquisition time was about 40 mn per spectrum. A total of 4 spectra per sample and pressure was necessary to obtain satisfactory statistics.

Typical EXAFS oscillations are represented below for $BaTi_{0.65}Zr_{0.35}O_3$, illustrating the high-quality of the data (fig. 1).
Fourier transforms are also represented on fig.2, at selected pressures.

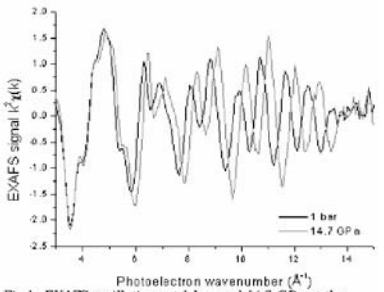

Fig.1: EXAFS oscillations at 1 bar and 14.7 GPa at the Zr K-edge, in $BaTi_{0.65}Zr_{0.35}O_3$ at room temperature.

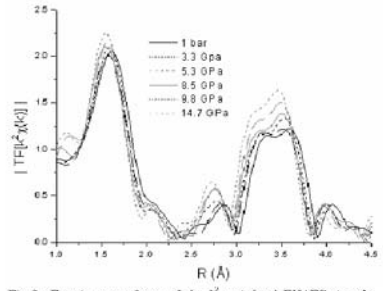

Fig.2: Fourier transform of the k²-weighted EXAFS signals for $BaTi_{0.65}Zr_{0.35}O_3$ at various pressures up to 14.7 GPa at 300 K.

First we observe that the application of pressure clearly modifies the EXAFS signal, especially its amplitude. This can be due to the evolution of either the bonds strength, or static disorders. The clearest change occurs near 5 GPa, as expected from the previous Raman results [2]. A detailed analysis of the EXAFS oscillations is in progress.

[1] J.Kreisel *et al.*, Phys. Rev. B **63** 174106 (2001), **65** 172101(2002), **68** 14113 (2004), Phys. Rev. Lett. **90** 25601 (2004)
[2] J. Kreisel, P. Bouvier, M. Maglione, et al., Phys. Rev. B **69**, 092104 (2004).
[3] T. Yagi, J. Phys. Chem. Sol. **39**, 563 (1978).

ESRF

ESRF	**Experiment title:** Zinc speciation in the hyperaccumulating plant *Arabidopsis halleri*	**Experiment number:** 30 02 692
Beamline: BM 30B	**Date of experiment:** from 14 to 19 April 2005, and from 26 to 30 August 2005	**Date of report:** October, 10, 2005
Shifts: 24	**Local contact(s):** Olivier Proux	*Received at ESRF:*

Names and affiliations of applicants (* indicates experimentalists):
Géraldine Sarret* , Marie-Pierre Isaure* and Nicolas Geoffroy*
LGIT, Maison des Géosciences, Univ. Joseph Fourier, BP 53, 38041 Grenoble Cedex

Report:

Introduction

Certain plant species have the ability to survive and reproduce on soils containing high concentrations of metals, and to store large amounts of metals in their aerial parts (more than 10000 mg kg^{-1} dry weight for Zn). These plants present a great interest for phytoremediation, a soft method in which plants are used for the cleanup of metal-polluted soils. The project aimed at better understanding the molecular mechanisms underlying the immobilization of zinc as non-toxic forms in the Zn and Cd hyperaccumulator *Arabidopsis halleri*. This species is a good model since its genome is simple and very close to *A. thaliana*, the well known genetic model for higher plants, so the molecular tools developed for *A. thaliana* (genetic map, gene ships, …) can be transferred to *A. halleri*. In a previous experiment, we used Zn K-edge EXAFS spectroscopy to identify the major form of zinc in *A. halleri* and in the non-tolerant and non- hyperaccumulating species *A. lyrata* (Sarret *et al.*, 2002). We concluded that Zn occurred as Zn malate in *A. halleri*, and as Zn phosphate in *A. lyrata*. There was no influence of the plant origin and of the concentration of Zn in the nutrient solution. However, the EXAFS spectra were recorded on freeze-dried leaves. This treatment may induce some artifacts, therefore these analyses had to be repeated on frozen hydrated samples.

More recently, we showed that the base of the trichomes (epidermal hairs) of both species was highly enriched in Zn and other metals. However, this compartment accounted for a minor proportion of total Zn present in the leaves, especially for *A. halleri* (Sarret *et al.*, in preparation)

Zn tolerance and Zn hyperaccumulation traits are genetically independent. Therefore, an interspecific crossing between these two species yielded a first generation of non accumulating and slightly tolerant plants (F1 progeny), and second generation of plants presenting new phenotypes, such as tolerant and non-hyperaccumulator, or moderately tolerant and hyperaccumulator (F2 progeny). This original material allows the study of the two traits, independently.

The objectives of this study were to (1) check that previous results obtained on freeze-dried samples of *A. halleri* and *A. lyrata* were valid, (2) determine the chemical form of Zn in the trichomes, and (3) evaluate the relationship between the genetic traits and the mode of Zn sequestration by studying plants of the F2 progeny.

Materials and Methods

Plants were grown for three weeks on Zn-contaminated compost (treatment 1), and *A. halleri* plants were collected on a smelter-impacted soil containing about 2% weight Zn (treatment 1). Plant leaves (young and mature) were ground and pressed as pellets in liquid nitrogen, and transferred into a Helium cryostat. Trichomes could not be isolated from hydrated leaves, therefore they were collected on freeze-dried leaves, ground and pressed as pellets. Zn reference compounds included various solutions containing Zn nitrate and an organic acid, amino-acid or protein, or a mixture of these ligands were prepared. All spectra were recorded at 20°K, using a Canberra 30-element detector.

Results

First, we analyzed Zn reference compounds in solution in order to test the sensitivity of EXAFS for these complexes (Figure 1). Zn oxalate has a characteristic spectrum. This complex in solution has the same structure as the solid-state complex, with two oxalate chelating the metal in the equatorial plane, and two axial water molecules. Zn histidine also has a characteristic spectrum owing to multiple scattering in the imidazole ring (Krämer et al., 1996).

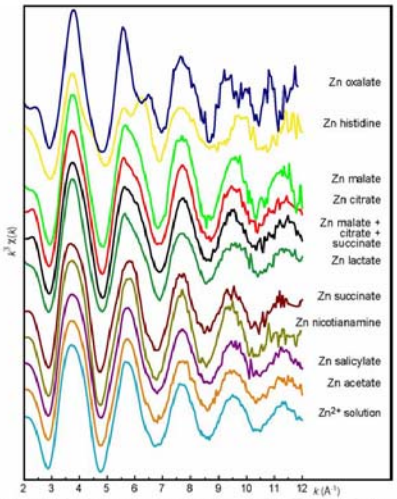

Figure 1: Zn K-edge EXAFS spectra of reference compounds in solution. The pH of all solutions is 5.5. The Zn/ligand ratio is 1/10 for all references except Zn acetate (1/2), Zn nicotianamine and Zn oxalate (1/4), and Zn salicylate (1/5).

The other spectra can be divided in two groups: Zn malate to Zn lactate spectra (group 1) and Zn succinate to Zn acetate spectra (group 2). The great spectral similarity within each group suggests that in the absence of complementary information, it may be difficult to distinguish these ligands in unknown samples. Some of the

spectra of group 2 are close to Zn^{2+} spectrum, which suggests a weak interaction bteween Zn and the ligand. To compensate the relatively weak sensitivity of EXAFS for Zn complexes in solution, the concentration of organic acids was measured in the plant samples by ionic chromatography.

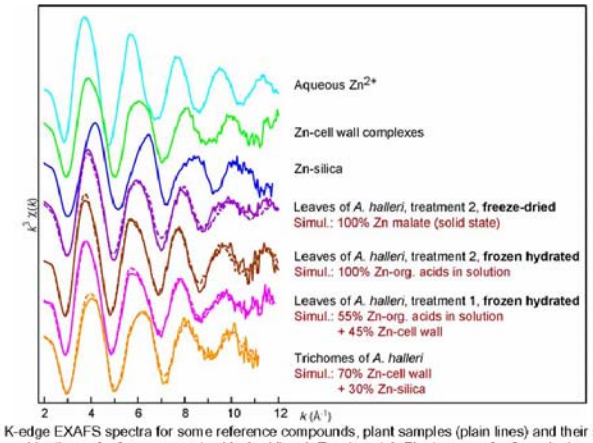

Figure 2: Zn K-edge EXAFS spectra for some reference compounds, plant samples (plain lines) and their simulations using linear combinations of reference spectra (dashed lines). Treatment 1: Plants grown for 3 weeks in a compost contaminated with $ZnSO_4$, and contained 9000 mg kg^{-1} d. w. Zn in their shoots. Treatment 2: Plants were collected in a smelter-impacted soil, and the contaminated, and contained 15 400 mg kg^{-1} d. w. Zn in their shoots.

Figure 2 shows significant differences between the spectra for freeze-dried and frozen hydrated leaves of *A. halleri* from the contaminated soil (treatment 2). There was no difference between young and mature leaves. The best simulation for the frozen hydrated sample was obtained with a mixture of Zn-organic acids in solution including malate, citrate and succinate. Chemical analyses showed that malate was the most concentrated organic acid (Zn/malate molar ratio > 1), and that citrate was present in minor amount (other ligands were not measured). This is consistent with a sequestration of the metal in the vacuolar compartment, which is rich in simple organic acids. Based on these concentrations and on the complexation constants, and supposing that the species are all present in the vacuoles at a pH of 5.5, we calculated Zn speciation in solution using *PhreeqC* software. Second to this calculation, Zn is present as 55% Zn citrate, 20% Zn^{2+} and 25% Zn malate.

Figure 2 shows significant differences between *A. halleri* collected in a contaminated soil (treatment 2) and grown on Zn-amended compost (treatment 1). For the latter sample, the best simulation was obtained with a combination of Zn-organic acid complexes in solution and Zn complexed with isolated cell walls. This suggests the presence of Zn in the vacuoles and in the apoplasm. TEM-EDX observations are planned to confirm this hypothesis.

This difference in the mode of sequestration of Zn may arise form the differences in the duration of exposure to Zn, from the interference of other metallic contaminants for the treatment 2, or from genetic differences between the plants. In order to test the first hypothesis, which seems the most plausible, we plan to compare plants at various durations of exposure.

The spectrum for frozen hydrated leaves of *A. lyrata* and of the F2 plants differed from *A. halleri* spectra (not shown). Data treatment and simulations are under way for these samples.

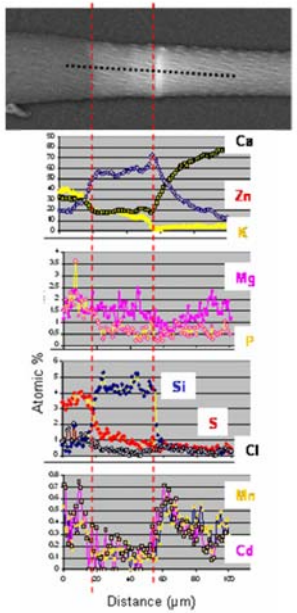

Figure 3: Profile of elements near the Zn-richest region of the trichome. Phosphorus is almost absent.

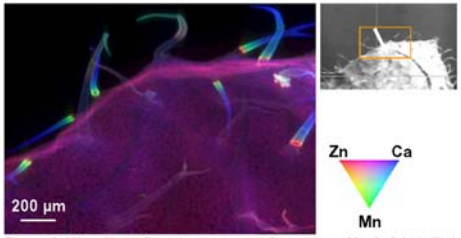

Figure 4: Micro X-ray fluorescence map of a portion of leaf of *A. halleri*. Some of the trichomes present localized Zn enrichments in the form of a ring, which suggests an association with the cell wall and cuticle.

Concerning the trichomes of *A. halleri*, two simulations of equivalent quality were obtained, one with Zn phosphate and one with Zn-cell wall and Zn-silica. The first one was rejected since phosphorus was not detected by SEM-EDX (Fig. 3). The second one is consistent with the localization of Zn in the external part of the trichomes observed by micro-X-ray fluroescence (Fig. 4).

Similar metal accumulations were observed in the trichomes of the two species, so this phenomenon is not related to the tolerance and hyperaccumulation.

Conclusions

Working on frozen hydrated samples is essential to limit artifacts on these types of samples. The combination of bulk EXAFS spectroscopy and micro-imaging techniques including micro-X-ray fluroescence and SEM-EDX revealled very powerfull to study the mechanisms responsible for Zn tolerance and hyperaccumulation in plants.

References

Kramer U, Cotter-Howells JD, Charnock JM, Baker AJM, Andrew C, Smith J (1996) Free histidine as a metal chelator in plants that accumulate nickel. Nature 379: 635-638

Sarret G, Saumitou-Laprade P, Bert V, Proux O, Hazemann JL, Traverse A, Marcus MAM, Manceau A (2002). Plant Physiol. 130: 1815-1826

Scientific production related to this experiment

Sarret G., Willems, G., Manceau A., Marcus M.A., Saumitou-Laprade P., 2005, Relationships between zinc tolerance and hyperaccumulation and zinc localization and speciation in *Arabidopsis halleri, 8th International Conference on the Biogeochemistry of Trace Elements (ICOBTE)*, 3-7 April 2005, Adelaïde, Australia

Sarret G., Isaure M.P., Marcus M.A.M., Saumitou-Laprade P., and Willems G., Relationships between Zn chemical form and Zn tolerance and accumulation traits: an EXAFS study of *Arabidopsis halleri* and *Arabidopsis lyrata* interspecific crosses. *In preparation.*

ESRF-report

Proposal Category and Count Number: **30-02-699**

Title : ***Copper complexes as probe for surface molecular patterning in mesostructured silica.***

B. Albela , L . Bonneviot, S. Abry and S. Calmettes

Introduction

All the experiments have been performed at the copper K edge with a Si(220) monochromator as planed. Our machine time scheduled in march has been delayed late in the summer (31 of august, 1,2 and 3 of October). This explains a late and only preliminary analysis of our data. Furthermore, it was a first contact of our laboratory with ESRF. Only one of us (LB) had previous experience on other synchrotron facilities in XAFS studies. Two PhD students have been initiated to XAFS on BM30B, S. Abry and S. Calmettes, which should be a key technique for their thesis work. In addition, this first contact on this particular line has been very precious to realize all constrains that should be taken into account to design an *in situ* and low temperature measurements cell in both transmission and fluorescence mode.

Experimental goal

Our study concerned copper at the oxidation state 2 and used as a probe for adsorption sites on nanostructured silica of high surface area (900 m^2/g). The originality of our study relies on the partial hydrophobization of the silica internal surface according to a new method developed in our laboratory and called molecular stencil patterning. This method is designed to create hydrophilic nano-island isolated one to another where adsorption may operate. Tetraamminecopper (II) is adsorbed at 25°C. The absence of the nitrate counterion in the silica is consistent with a strong adsorption as hydroxide precipitate, surface silicate or isolated adsorbed complexes. The isolated adsorption site would be characterized by the absence of Cu-O-Cu correlations as expected in hydroxides or silicates and by the formation of one or two Cu-O-Si bridges, only. Ideally, it would be a neutral diamminedisilanolatocopper(II) surface complex, $[Cu(NH_3)_2(SiO)_2]$. The site isolation do not occur on a genuine silica surface leading to surface copper silicate with a mixture of copper and silicon in the second coordination shell but should operate on a modified silica as such as ours. However, chemical analyses reveal a nitrogen to copper smaller than 2 and EPR signals that were difficult to interpret. The second shell analysis of the EXAFS signal should help us to solve the problem.

XAFS measurements

12 samples and four references were investigated for this study during the first three days. In this first series. The samples were design with a varying level of hydrophibization to modulate the isolation effect. The measurements were performed at room temperature on pellets of the sample diluted in boronitride, BN and finely grounded in a mortar. The references were chosen to get pure oxygen or oxygen-nitrogen mixture of first copper coordination sphere, $CuSO_4.5H_2O$ for $CuO_4(O_{TT})_2$, $[Cu(en)_2].2NO_3$, $CuN_4(O_{TT})_2$, $[Cu(DPA)].2NO_3$, $CuN_3(O_{TT})_2$, where O_{TT} stands for ligand position stretched or squeezed by the Jahn-Teller effect. We need to have a silicate as a reference (dioptase or chrysocolla) that will be investigated in the next runs.

All measurements were collected in an energy range large enough for a pre-edge baseline extraction and, in the EXAFS range up to a value of 16 in k space. Detection was taken in fluorescence and transmission modes on the sample and simultaneously on a copper metal foil in transmission mode. Four to seven spectra were taken for each sample depending on the concentration of copper to get a satisfying signal to noise ratio.

We have observe that all EXAFS signals vanish between k = 13 to 14. The preliminary EXAFS analysis clearly shows that a satisfying second coordination shell analysis is possible on the transmission signal for most of the cases and in the all cases on fluorescence signals. A more detailed analysis will allow us to discriminate copper to silicon in the second shell.

The supplementary day of machine time has been devoted to start the study on copper complexes grafted on partially hydrophobized silicas described above. Here, the copper is not adsorbed directly in the hydrophilic “hole”. The organic polyamine ligand is gafted first acting as an anchor between copper and the surface. 6 samples were investigated. The preliminary study reveals that Cu-O-Cu and Cu-O-Si contributions are barely detectable showing that site isolation has operated and that that copper does not “see” the silica surface despite the short length of the anchor (3 carbon chain). A thorough analysis is necessary to definitively conclude on these points.

Conclusion

This first experience of our team on the BM30B line for XAFS measurements has been very positive. Two students are now familiar with the usual operating conditions. The feasibility of our experiment is fully confirmed. A design of an *in situ* cell is now on progress. The preliminary analysis suggest some improvements on the first series of samples. The supplementary day has been used to start another very promising set of samples of copper complexes grafted in our nanostructured and organically modified silicas, our bio-inspired heterogeneous catalysts.

ESRF	**Experiment title:** Uranium speciation in eucaryotic and procaryotic cells	**Experiment number:** 30-02-726
Beamline: BM 30B	**Date of experiment:** from: 14-09-2005 to: 20-09-2005	**Date of report:** 28-09-2005
Shifts:	**Local contact(s):** Jean-Louis Hazemann	*Received at ESRF:*

Names and affiliations of applicants (* indicates experimentalists):

Marie CARRIERE*
Barbara GOUGET*
Céline THIEBAULT*
Sarah MILGRAM*
Laure AVOSCAN*

CEA/DSM/DRECAM/LPS
CEA Saclay
Bât 637
F-91191 Gif sur Yvette, France

Aims of the experiment and scientific background

Uranium is a naturally occuring heavy metal. Its extensive use in the nuclear cycle and for military applications has focused attention on its health effects and on its potential ecotoxicological impact. It is now established that speciation has a great influence in U dissemination in the biosphere and in its toxicity. Moreover, some bacteria are able to metabolize it and certainly to modifiy its chemical form. Due to their rapid growing and their ubiquity, they represent an important source of U dissemination in the biosphere. U dissemination leads to three types of possible animal and human exposure: either ingestion or inhalation or directly through a wound. After an acute exposure, U rapidly transits from the site of contamination to the blood, which distribute it in the body to target organs, namely kidneys and bones.

The main goal of the experiment was to determine U speciation after accumulation either in **bacteria** and in animal cells. For this purpose, we exposed either *Ralstonia metallidurans* CH34 bacterial strain (procaryotic cells), or NRK-52E (**kidney**, rat) and ROS (**bone**, rat) eucaryotic cells to two U(VI) chemical forms: U(VI)-bicarbonate and U(VI)-citrate. Quantification of metal uptake was monitored by ICP-MS analyses. Our results proved the ability of bacteria and animal cells to ad- or absorb large amounts of U. Moreover, electron microscopy observations and nuclear microprobe analyses of exposed rat renal cells revealed the existence of two U physical/chemical forms: on the one hand some dense precipitates are visible, and on the other hand soluble U is also present in cell cytoplasm. The second aim of our experiment was thus to precisely identify these two chemical forms, and to compare it to U chemical form in bacterial/eucaryotic cell exposure media.

X-ray absorption spectroscopy (EXAFS) of lyophilized cells at the U L_{III}-edge was performed on BM30B.

Experimental method

NRK52E (rat, renal proximal tubule) and ROS (rat, osteoblasts-like) cultured cells were continuously grown at 37 °C, 5% CO_2 in DMEM (Dulbecco's Modified Eagle's Medium) cell culture medium supplemented with 10% (v/v) fetal calf serum. Cells were washed twice with serum free cell culture medium, and exposed either to 300-600 µM U(VI)-bicarbonate or to 150-300 µM U(VI)-citrate diluted in serum free culture medium. After a 24 h incubation period, cells were washed twice with 10 mM $NaHCO_3$ and scrapped from their support. After centrifugation, the pellet was frozen and then lyophilized by highering temperature from –10 °C to 20 °C in 3h under a 0.37 mbar vacuum. The samples were pressed as 5-mm diameter pellets. EXAFS spectra were recorded at U L_{III}-edge in fluorescence mode (samples) or by transmission (references) using a 30 elements solid state Ge detector (Canberra). The monochromator was a Si(220) double crystal.

As no sample evolution was detected during the measurement, acquisitions were conducted at room temperature. At least 6 spectra for each sample were recorded and averaged to improve the statistics. The EXAFS oscillations were isolated from the raw, averaged data by removal of the pre-edge background, approximated by a first-order polynomial, followed by μ_0-removal *via* spline fitting techniques (SEDEM and Athena). Curve-fitting amplitudes and phases will be calculated in a second step.

Results

Bacteria:

U is known to precipitate on phosphate residues of Gram-positive cell wall components. Moreover, bacterial strains known as dissimilatory metal-reducing bacteria (DMRB) reduce U(VI) to the less mobile uraninite (UO_2). *Ralstonia metallidurans* CH34 was shown to resist U concentration up to 8 mM and to accumulate nearly 30% of the initial dose.

XANES and EXAFS spectra of bacteria exposed to U(VI)-bicarbonate and U(VI)-citrate are shown in figure 1.

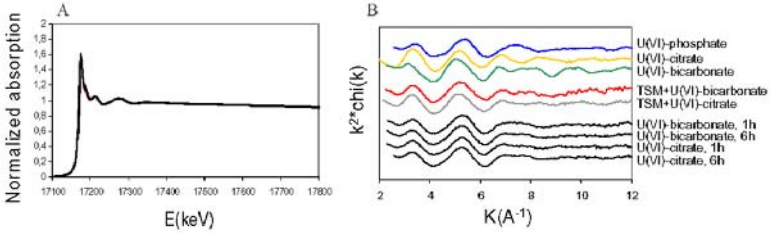

Fig. 1. U L_{III}-edge XANES spectra (A) and the corresponding k^2-weighted EXAFS oscillations (B) of Ralstonia metallidurans CH34 bacterial strain exposed to 1 mM U(VI)-bicarbonate or 1 mM U(VI)-citrate (black) compared to 1 mM U(VI)-bicarbonate (red) and –citrate (grey) diluted in TSM bacteria culture medium and to U(VI)-bicarbonate (green), -citrate(yellow) and –phosphate (blue) standards.

As shown in figure 1, whatever the exposure U(VI) chemical speciation, EXAFS spectra are closely resembling, and present strong similarities with exposure media (TSM+U(VI)-bicarbonate and TSM+U(VI)-citrate). U(VI) speciation in these two exposure media is similar, certainly a combination of U(VI)-phosphate and another form of U. Working with a defined culture medium, it is probable the a second speciation of uranium is U(VI)-sulfate complex.

Animal cells:

It was previously reported that, after exposure to U(VI)-bicarbonate and intracellular accumulation, U(VI) precipitated in a cell compartment called lysosome. X-analysis revealed the presence of U and P, suggesting that the precipitate was U(VI)-phosphate. We also showed that U(VI)-citrate is more toxic than U(VI)-bicarbonate, either to NRK-52E (kidney) and ROS (bone) cells. Assimilation pathways of these two U(VI) chemical forms could thus be different.

EXAFS spectra of NRK-52E and ROS cells exposed to U(VI)-bicarbonate and U(VI)-citrate are shown in figure 2.

In the case of ROS cells, whatever the composition of exposure medium, U(VI) concentration and length of exposure period, the spectra are very near and the local structure of U resemble that of U(VI)-bicarbonate.

Analysis of NRK-52E cells exposed to 300 µM U(VI)-bicarbonate during 24 h leads to a spectrum which might be a combination of U(VI)-bicarbonate and U(VI)-phosphate spectra. On the contrary, the local order of U in NRK-52E cells exposed to 600 µM U(VI)-bicarbonate during 24 h is similar to the one of U(VI)-phosphate. This data confirms the evolution of U local structure in NRK-52E cells as a function of U concentration and exposure duration. As expected, U(VI) has been metabolized by cells and precipitated as a U(VI)-phosphate mineral.

The results should be confirmed after modelling of the Fourier transforms obtained from these data.

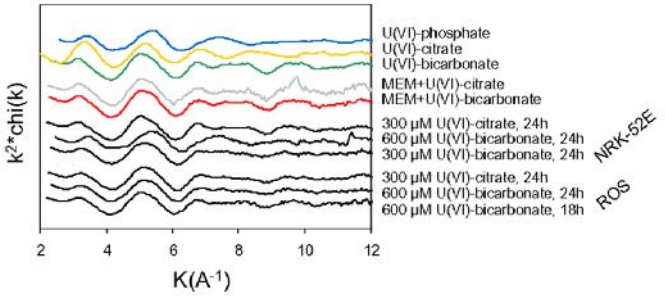

Fig. 2. U L_{III}-edge k^2-weighted EXAFS oscillations of NRK-52E and ROS cells exposed to 300 or 600 µM U(VI)-bicarbonate or -citrate (black) compared to 600 µM U(VI)-bicarbonate (red) and 300 µM U(VI)-citrate (grey) diluted in MEM cell culture medium and to U(VI)-bicarbonate (green), -citrate(yellow) and –phosphate (blue) standards.

Conclusions and perspectives

Fitting of the measured data using a structural model of shells has not been processed yet. However, the first results obtained from XANES spectra and examination of EXAFS oscillations are promising. They should be confirmed by analysis of more samples ranging the whole course of U intoxication for both cell lines. To conclude on bacterial analysis, the spectra of certain standards have to be added to our database (U-sulfate at least). As U local structure in bacteria seem to be the same after 1h and 6h exposure, it would be valuable to analyse kinetics of U accumulation/transformation for shorter exposure periods as bacterial metabolization of U might be much more rapid than expected.

Bibliography

- G. Sarret, L. Avoscan, M. Carrière, R. Collins, N. Geoffroy, F. Carrot, J. Covès and B. Gouget. Chemical forms of selenium in the metal-resistant bacterium Ralstonia Metallidurans CH34 exposed to selenite and selenate. *Applied and Environmental Microbiology*, 71(5): 2331-2337, 2005.
- M. Carrière, L. Avoscan, R. Collins, F. Carrot, H. Khodja, E. Ansoborlo, B. Gouget. Influence of uranium speciation on normal rat kidney (NRK-52^E) proximal cell cytotoxicity. *Chemical Research in Toxicology* 17: 446-52, 2004.
- M. Carrière, H. Khodja, L. Avoscan, F. Carrot, B. Gouget. Uranium (VI) complexation in cell culture medium: influence of speciation on Normal Rat Kidney (NRK-52^E) cell accumulation. *Radiochimica Acta*, 93, 2005, in press.
- M. Carrière, B. Gouget, H. Khodja, L. Avoscan, F. Carrot, R. Gobin, JM. Verbavatz, JP. Gallien. Cellular distribution of uranium after acute exposure of epithelial renal cells: SEM, TEM and µPIXE. *Nuclear Instruments and methods in Physic Research B*, 231: 268-273, 2005.

ESRF	**Experiment title:** XAS study of chromium in advanced nuclear fuel	**Experiment number:** ME-1304
Beamline: BM-30B	**Date of experiment:** from: 04 September 2005 to: 06 September 2005	**Date of report:** 03/10/2005
Shifts: 6	**Local contact(s):** Dr. H. PALANCHER, Dr. O. PROUX	*Received at ESRF:*

Names and affiliations of applicants (* indicates experimentalists):

*Dr. H. PALANCHER[a,b], *Dr P. MARTIN[a], *Dr G. CARLOT[a], *A. PIERAGNOLI[a], Dr C. SABATHIER[a], P. GARCIA[a], Dr C. VALOT[a]

[(a)] CEA-Cadarache (DEN/DEC) F-13108 Saint Paul lez Durance. [(b)] CRG FAME, ESRF, F-38043 Grenoble Cedex.

Report

The behaviour of nuclear fuels at high burn-up is mainly limited by the release of fission products. In these measurements, we study one possible solution to improve this behaviour: the low UO_2 doping by chromium. Indeed, it is reasoned that by promoting UO_2 grain growth, the diffusion length for fission products to reach grain boundaries increases, thus presumably reducing fission product release.
However, the presence of foreign elements in the fuel matrix is liable to increase the diffusion kinetics of fission products. To fully understand any influence of the doping agent on the diffusion kinetics of fission products, it is crucial to know in which crystallographic phase chromium atoms are present. The knowledge of how these phases change with temperature is also required.
The aim of these measurements was to investigate by XAS the evolution with temperature of both the local environment and the oxidation state of Cr atoms in doped UO_2.

In our study, pellets were prepared from an UO_2 powder mixed with Cr_2O_3 (0.2 %wt) and sintered at 1700°C during 4 hours. Scanning electron microscopy analyses of the samples confirm the expected UO_2 grain growth: the average grain size was about 50 µm (compared with the 10 µm measured on undoped UO_2). X-ray diffraction patterns collected on each pellet do not reveal the presence of any other phase than that of UO_2.

In this report, we focus on the comparative study of two samples. The first is "as fabricated" but the second has undergone an additional thermal treatment: annealing at 1750°C for 4 hours.
To carry out an efficient XANES analysis at the chromium K edge of both UO_2 samples doped with Cr, absorption spectra were also collected on reference compounds Cr_2O_3 and Cr metal. Figure 1 illustrates the result of this study. A quantitative study is ongoing, but it already appears that the XANES spectra collected on fuels can not simply be interpreted as a linear combination of the spectra representative of metallic chromium and chromium oxide. The hypothesis whereby chromium is soluble in the UO_2 lattice will further be evaluated through XANES spectra simulations.
However it must noted that the XANES technique failed in differentiating the environment or oxidation state of chromium atoms in the two studied samples

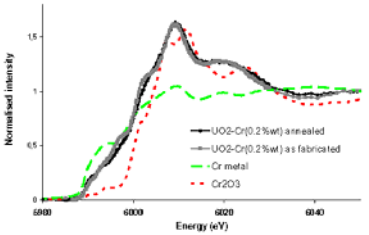

Figure 1: XANES spectra at the chromium K edge collected on two UO_2 samples doped with Cr.
(dashed lines indicate XANES signal measured on reference compounds Cr_2O_3 and Cr metal).

EXAFS spectra were then collected up to 10 $Å^{-1}$ on the two doped UO_2 samples at the chromium K-absorption edge (cf. figure 2-a). These are significantly different underlining the influence of temperature on Cr local environment in UO_2. When considering the magnitude of the Fourier Transform of the EXAFS spectra (cf. figure 2-b), it appears that annealing caused an inversion of the magnitude of the first and second shells.
In both samples, the first shell seems to consist of oxygen atoms. A preliminary analysis leads to Cr-O distances of about 2.0 Å in the "as fabricated" sample; this value corresponds to the shortest distance between Cr and O atoms in Cr_2O_3 (1.96 Å). Even if further analysis is required, the Cr-O bond length appears shorter in the annealed sample (about 1.7 Å).
In the annealed sample, the second shell is very probably due to chromium atoms: the refined distance (2.65 Å) is consistent the Cr-Cr bond length in chromium metal (in this material the two shortest Cr-Cr distances are 2.50 Å and 2.88 Å).

Conclusion:
EXAFS appears to be a key technique in the characterization of the local Cr environment in Cr doped UO_2. Leenears et al. (*Journal of Nuclear Materials* 317, 62 (2003)) have reported the presence of large chromium precipitates (3µm) in the fuel. The use of a micro-focused X-ray beam (with a typical size of 15×15 µm²) should enable us to probe areas where these precipitates are not present: the collected EXAFS spectra would then be only representative of chromium in the UO_2 matrix. This additional study should:

- give us an additional insight into the homogeneity of the local environnement of chromium atoms in the UO_2 matrix,
- confirm the interpretation of the results of this analysis carried out with a 200×300 µm² X-ray beam.

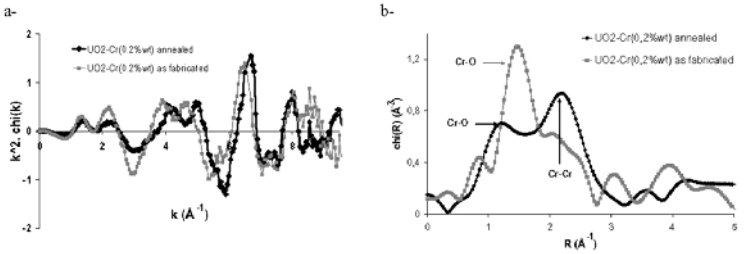

Figure 2: Comparison of the environnement Cr elements in two UO_2 samples. Figure 2-a shows the EXAFS spectra collected on both samples at the chromiun K edge (a-) and their Fourier transforms (b-). Note that in this last figure, no phase correction has been applied.

ESRF	**Experiment title: Electronic properties of Na_xCoO_2 and its hydrated analogue**	**Experiment number**: BLC-2324
Beamline: FAME	**Date of experiment** from: **07/10/2005** to: **10/10/2005**	**Date of report**: 09/11/2005
Shifts: 6	**Local contact(s)**: J.-L. Hazemann & O. Proux	*Received at ESRF:*

Names and affiliations of applicants (* indicates experimentalists):

Philippe Leininger*

Laboratoire de Chimie Physique – Matière et Rayonnement, Université Pierre et Marie Curie, Paris

Jean-Pascal Rueff*

Synchrotron SOLEIL, Saint-Aubin / Laboratoire de Chimie Physique – Matière et Rayonnement, Paris

Report:

The recent discovery of superconductivity in the hydrated bilayer cobaltate $Na_xCoO_2.yH_2O$ (NCOH) [1] has motivated an increasingly large number of experiments to investigate their properties. Despite this wealth of information, several questions remain un-answered or are subjected to debate, such as the origin of superconductivity or the role of water molecules. The parent compound has a hexagonal structure (space group 194 $P6_3/mmc$) consisting of two dimensional Co-O layers which form a triangular lattice and involve renewed properties compared to the Cu-O square lattice in cuprates. The hydration of the parent compound increases the *c* axis and the distance between the CoO planes which are considered as playing an important role in the superconducting properties.

In this experiment, we have investigated the electronic properties of the CoO planes in NCOH and in unhydrated (NCO) single-crystals by x-ray absorption spectroscopy (XAS) at the Co K edge. This high-energy probe is selective of the cobalt properties and provides bulk data, a crucial aspect in these materials highly sensitive to humidity. The incident energy was selected by a double crystal Si(220) monochromator[2] which gives a total energy resolution of 450 meV. The spot size was 280 × 150 μm^2 at the sample position. The sample was fixed between two kapton sheets, glued on a plaque with a hole and put on a sample holder. The measurements were carried out on both samples at low temperature (20K), using a liquid helium cryostat, in order to keep them hydrated (unhydrated). The spectra were measured in reflection geometry along two polarization directions by turning the sample holder by 80 degrees in the horizontal plane, starting from the polarization (e) quasi perpendicular to the *c* axis (in-plane polarization) to the polarization parallel to the *c* axis (out-of-plane polarization).

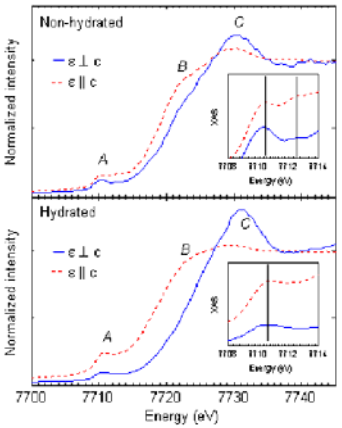

Figure.1: Polarization-dependent XAS spectra in the NCOH and NCO compounds. The polarization vector e is set either perpendicular or parallel to the c axis. The inset represents a detailed view of the pre-peak region.

When the polarization in turned from in-plane to out-of-plane directions (Fig. 1), the intensity of peak *C* decreases in contrast to peak B, indicating that these mainly correspond to *1s* ? $4p_{x,y}$ (in-plane) and *1s* ? $4p_z$ (out-of-plane) transitions, respectively. The relative spectral change between the two polarization directions in the hydrated compound with respect to the non-hydrated one was compared to calculated XAS spectra within a LMTO method[3]. The underlying calculated density of states indicates a decrease between the CoO planes hybridization when the compound is hydrated, consecutively to the elongation of the *c* axis. The Co K pre-edge region (cf. inset in Fig. 1), which principally results from quadrupolar *1s* ? *3d* transitions (though with admixture of dipolar character because of the trigonal distortion of the Co octahedral site), shows two peaks in the non-hydrated compound related to the crystal field split *3d* states. The splitting is in good agreement with previously reported value[4]. In the hydrated compound, only the lowest *3d* split state is visible. In NCOH, the crystal field splitting was estimated at 4.5 eV[4]. The second structure, expected at higher energy compared to NCO, is likely masked in the tail of dipolar-like white line. Finally, we observe a shift of the XAS spectrum in the hydrated compound by about 1 eV to higher energy compared to the non-hydrated counterpart, which reflects the Co valence increase when the compound is hydrated.

The extended x-ray absorption fine structure, measured during the same run of experiment, is currently being analyzed. It will provide information about the inter-atomic distances and the local structure of the Co site in these compounds.

References

[1] K. Takada *et al.*, Nature **53**, 422 (2003).
[2] O. Proux *et al.*, Physica Scripta. **T115**, 970-973, (2005).
[3] Ph. Leininger *et al.*, in preparation (2005).
[4] A. Chainani *et al.*, Phys. Rev. B **69**, 180508(R) (2004).